SLAC TRANS - 92

PHOTOPRODUCTION OF NEUTRAL VECTOR ρ^{o} AND ϕ MESONS IN THE FORWARD DIRECTION AT VARIOUS ATOMIC NUCLEI

by

Ulrich Becker

Translated by L.B. Kapp [March 1969] from the German *Photoproduktion der neutralen Vektor-Mesonen* ρ^{o} *und* ϕ *in Vorwärtsrichtung an verschiedenen Atomkernen*. Doctoral dissertation submitted by Ulrich Becker from Dortmund. Hamburg (1968).

TRANSLATED FOR

STANFORD LINEAR ACCELERATOR CENTER

PHOTOPRODUCTION OF NEUTRAL VECTOR ρ^{o} AND ϕ MESONS IN THE FORWARD DIRECTION AT VARIOUS ATOMIC NUCLEI

Ulrich Becker

Doctoral thesis presented by the author at the Faculty of Mathematics and Natural Science, Hamburg University, in 1968. Approved by the Faculty at the request of Professor Dr.P.Stähelin, February 7, 1968. Dean: Professor Dr. R. Nast

A b s t r a c t

The reactions $\gamma + A \longrightarrow \rho^{o} + A$ and $\gamma + A \longrightarrow \phi + A$ are investigated for gamma energies of 2.7 - 4.5 GeV and 4.0 - 6.2 GeV in the region of small angles of production relative to the γ beam, $\delta < 6^{o}$, on the target materials A = Be, C, Al, Cu, Ag, Pb.

The dependence of the differential effective cross section on the nucleus A indicates the coherence; the diffractive character of the particle production is shown by the dependence of the momentum transfer + on the various elements. The measurements at various momenta p permit the inference that the total effective cross section is constant. This contradicts the one-pion-exchange model; on the other hand the diffraction-dissociation model describes the

measurements well.

Throughout the region measured the effective cross section can be described consistently within the limits of experimental error by the formula:

$$\frac{d^2\sigma}{d\Omega\, dm} = C \cdot F_{TA}(R,t,\sigma_{VN}) \cdot f_T(R,t,\sigma_{VN}) \cdot f(p) \cdot 2m \cdot R(m)$$

The functions F_{TA} and f_T are derived from the diffraction-dissociation model. They contain the total effective cross section σ_{VN} for ρ^0 or ϕ mesons on nucleon as a parameter. F_{TA} gives, for a constant momentum transfer, the relative dependence on the nuclear radius R, while for constant R f_T gives the change in t. The momentum dependence f(p) is taken from the model of S.M. Berman and S.D. Drell. R(m) represents the mass distribution of J.D. Jackson, multiplied by $(m_0/m)^4$. In agreement with the values found for the process $\pi + p \longrightarrow \rho^0 + n$, the mass m_0 and width Γ_0 of the ρ^0 meson were found to be

$$m_0 = 765 \pm 5 \quad MeV/c^2$$
$$\Gamma_0 = 130 \pm 5 \quad MeV/c^2$$

The relative behavior of the effective cross section on different nuclei A yields information on the reactions $\rho^0 + N \longrightarrow \rho^0 + N$ and $\phi + N \longrightarrow \phi + N$. The following total effective cross sections can be derived using the model of S.D. Drell and J.S. Trefil

$$\sigma_{\rho N} = (31.3 \pm 2.3)\ mb$$
$$\sigma_{\phi N} = (13.3 \pm 3.4)\ mb$$

The values are in agreement with the predictions of the quark model.

The coupling coefficients of the vector dominance model can be determined using this effective cross section. In the nomenclature of M. Gell-Mann they are :

$$\frac{\gamma_\rho^2}{4\pi} = 0.44 \pm 0.07$$

$$\frac{\gamma_\phi^2}{4\pi} = 7.8 \pm 1.7$$

The ρ^0 coupling constant is in agreement with the values derived by other methods. Comparison values for the ϕ coupling constant are expected in the near future.

*****

LIST OF CONTENTS

*****

1. INTRODUCTION

In order to explain the nuclear forces, H. Yukawa[1] in 1935 postulated the existence of the π-meson as a quantum of the strong interaction field. It was demonstrated in the cosmic radiation in 1946 by Lattes, Occhialini and Powell[2]. The idea that the nuclear forces depend on the emission and absorption of π-mesons involves the assumption that the nucleon has an internal structure. R. Hofstadter[3] used electron scattering experiments to demonstrate the existence of a nucleon structure as regards electromagnetic interactions, and this expresses itself in the form factor.

In order to explain this internal charge distribution, R. Sachs[4] made the hypothesis that the nucleon consists of an inner nucleus with spin 1/2 and a π meson field with 1π, 2π and 3π states with definite probabilities. By considering the anomalous magnetic moment he came to the conclusion that the 1π contribution must be small. W.G.Holladay[5] showed that this model can only be upheld on the assumption of a strong pion-pion interaction in the L=1 state.

The first detailed calculations for the $\pi - \pi$ interactions were carried out by R.W. Frazer and J.R. Fulco[6] by means of dispersion relations.

They were able to describe correctly the isovector component of the form factors which were experimentally available by explaining the anomalous behavior of the π form factor as vector-meson resonance of mass $\sqrt{12\, m_\pi^2}$. Later calculations[7] yielded a mass of $\sqrt{22.4\, m_\pi^2} = 660$ MeV/c. The first experimental value of this resonance - later called a ρ-meson - was given by I. Derado[8] as $\sqrt{22\, m_\pi^2}$. Numerous more recent measurements have, however, indicated higher masses, but they have confirmed unanimously the predicted quantum numbers as

Isospin	I = 1
Spin	J = 1
Parity	P = -1
G-parity	G = +1

The neutral ρ^o meson has a special position insofar as together with the ω and ϕ mesons it has the same quantum numbers $J^P = 1^-$ as the photon. The interpretation of the form factors suggested that vector mesons play a dominant role in the coupling of photons to hadrons. The idea of a vector meson dominance in the electromagnetic interactions of hadrons was consequently further developed by J.J. Sakurai and M. Gell-Mann, D. Sharp, W.G. Wagner[9] as far as the theory of N.M. Kroll, T.D. Lee, B. Zumino and H.Joos[10] where the electromagnetic current operator $J_\mu(x)$ for hadrons is expressed directly as a linear combination of the phenomenological fields F^V_μ of the vector mesons $(V = \rho^o, \omega, \phi)$ with the coupling constant γ_V and masses m_V

$$J_\mu(x) = -\frac{1}{2}\left[\frac{m_\rho^2}{\gamma_\rho^2} F_\mu^\rho(x) + \frac{m_\omega^2}{\gamma_\omega^2} F_\mu^\omega(x) + \frac{m_\phi^2}{\gamma_\phi^2} F_\mu^\phi(x)\right]$$

This relation represents the kernel of the vector dominance model.

While the quantum numbers of the ρ^o meson can be regarded as determined, the most recent measurements of its mass and width show relatively large variations. In particular the production process appears to play a part. While the reaction

$$\pi^- + p \rightarrow \rho^o + n$$

gives typically the mass $m_o = 770\,MeV/c^2$ and the width $\Gamma_o = 140\ MeV/c^2$ (ref. 11), the corresponding values for the photoproduction $\gamma + p \rightarrow \rho^o + p$ are about $m_o \simeq 728 - 750\ MeV/c^2$ and $\Gamma_o = 150\ MeV/c^2$ (refs. 14-17).

P. Söding[12] has explained this mass shift in hydrogen as being due to the interference of the π-pairs from ρ^o decay with π-pairs produced nonresonantly in the p state. On the other hand M. Ross and L. Stodolsky[13] obtained in the "photon dissociation model" a factor $(m_o/m)^4$ from the coupling of a γ quantum to a ρ^o meson of mass m, and this deforms the mass distribution and causes a shift of about 15 MeV/c^2.

The photoproduction of ρ^o mesons was measured on the Cambridge electron accelerator with a bubble chamber[14] and a counter system[15], and on the German electron synchrotron using a bubble chamber[16] and spark chambers[17] for γ-energies up to 5.8 GeV.

Of the proposed production mechanisms

a) one pion exchange

b) diffraction

it appears that the diffraction model gives the best predictions.

It has been shown in the work of S.D.Drell, J.S. Trefil[18] and M.Ross and L.Stodolsky[13] that if a homogeneous density distribution of nucleons in the nucleus is assumed, measurements of photoproduction in the forward direction in complex nuclei allow inferences of the free path length of the ρ^o meson in the nucleus to be made, and hence of the total effective cross-section $\sigma_{\rho N}$ for ρ^o mesons on nucleons. (Since the extremely short lifetime of the ρ^o meson allows only a path of a few nuclear diameters, it can practically only undergo interactions in the nucleus in which it is produced. Using the data of L.J. Lanzerotti et al.[15] S.D. Drell and J.S. Trefil[18] found

$$\sigma_{\rho N} \quad = \quad 66 - 94 \text{ mb};$$

a result that does not agree well with the predictions of symmetry schemes like $SU(6)_w$ (ref. 19):

$$\sigma_{\rho N} \quad \simeq \quad \sigma_{\pi N} \quad \simeq \quad 30 \text{ mb}$$

In the present situation it seemed interesting to investigate the photoproduction of $\pi^+ - \pi^-$ pairs with reference to

a) determination of mass and width of the ρ^0 meson,

b) investigation of the production mechanism,

c) measurement of the total absorption cross section of ρ^0 mesons on nucleons, and

d) further resonances in the mass range 350-1200 MeV/c^2 $(0^+, 1^-, 2^+ \ldots)$.

It seemed also that an exact measurement of ρ^0 photoproduction was necessary in order to measure the branching ratio

$$BR = \frac{\Gamma(\rho^0 \rightarrow e^+ e^-)}{\Gamma(\rho^0 \rightarrow \pi^+ \pi^-)}$$

in a further experiment[20].

An experiment was carried out early in 1967 on the German electron synchrotron in conjunction with Columbia University in order to investigate the photoproduction of ρ^{o} mesons in the energy range of 2.4 - 6.0 GeV at small forward angles (0 - 6^{o}) on various target materials (Be, C, Al, Cu, Ag, Pb). This experiment will be described below.

2. THEORETICAL ASPECTS AND MODELS

There are three basic models which describe ρ^{o} photoproduction in the forward direction, i.e. for very small momentum transfer t at the target.

2.1 One particle exchange (OPE) model

H. Joos and G. Kramer[21] considered the photoproduction from the point of view of the peripheral model and calculated the matrix elements of the one particle exchange (OPE) according to the graph Figure 2a for $x = \pi^{o}, \eta, \sigma$.

While the contributions of π^{o} and η to the effective cross section for momentum transfer at the nucleus vanish as $t \rightarrow 0$, the σ exchange yields a finite value because of the spin 0 and parity $P = +1$ of σ. The photoproduction involving exchange of a $J^{P} = 0^{+}$ particle would indicate production by diffraction, however the existence of the σ meson is very questionable.

Assuming roughly equal coupling constants the contribution of η is small because of its large mass ($m_\eta^2 \simeq 16\ m_\pi^2$) and the problem reduces to π^0 exchange. On the hypothesis that the energy of the incident gamma quantum k is large in comparison with the mass of the ρ^0 meson m_o, S.M. Berman and S.D. Drell[22] give the effective cross section in the laboratory system as

$$\left.\frac{d\sigma}{d\Omega}\right|_{\delta\to 0^\circ} \approx \frac{3}{8}\left(\frac{g^2_{\pi NN}}{4\pi}\right)\frac{1}{24}\left(\frac{g^2_{\gamma\pi\rho}}{4\pi}\right)\left(\frac{m_o}{M}\right)^2\left(\frac{m_o}{m_\pi}\right)^4\frac{1}{k^2} \qquad (1.1)$$

where $g_{\pi nn}$, $g_{\gamma\pi\rho}$ are the vertex coupling constants and M is the nucleon mass. The $1/k^2$ fall-off of the differential effective cross section is characteristic. According to the optical theorem it is expected that the total effective cross section should fall off as $1/k$ as the energy increases.

2.2 Diffraction model

Figure 1a shows the ladder graphs for the π-nucleon diffraction scattering according to the multiperipheral model of D. Amati, S. Fubini and A. Stanghellini[23] (A.F.S.). The (p-p) scattering is described analogously insofar as the uppermost branch is replaced by N*(3/2, 3/2) with the corresponding coupling constants. S.M. Berman and S.D. Drell[22] calculate in this way the ratio of the effective cross sections for $(\pi - \rho)$ and (p-p) scattering in good agreement with the quotients of the measured values.

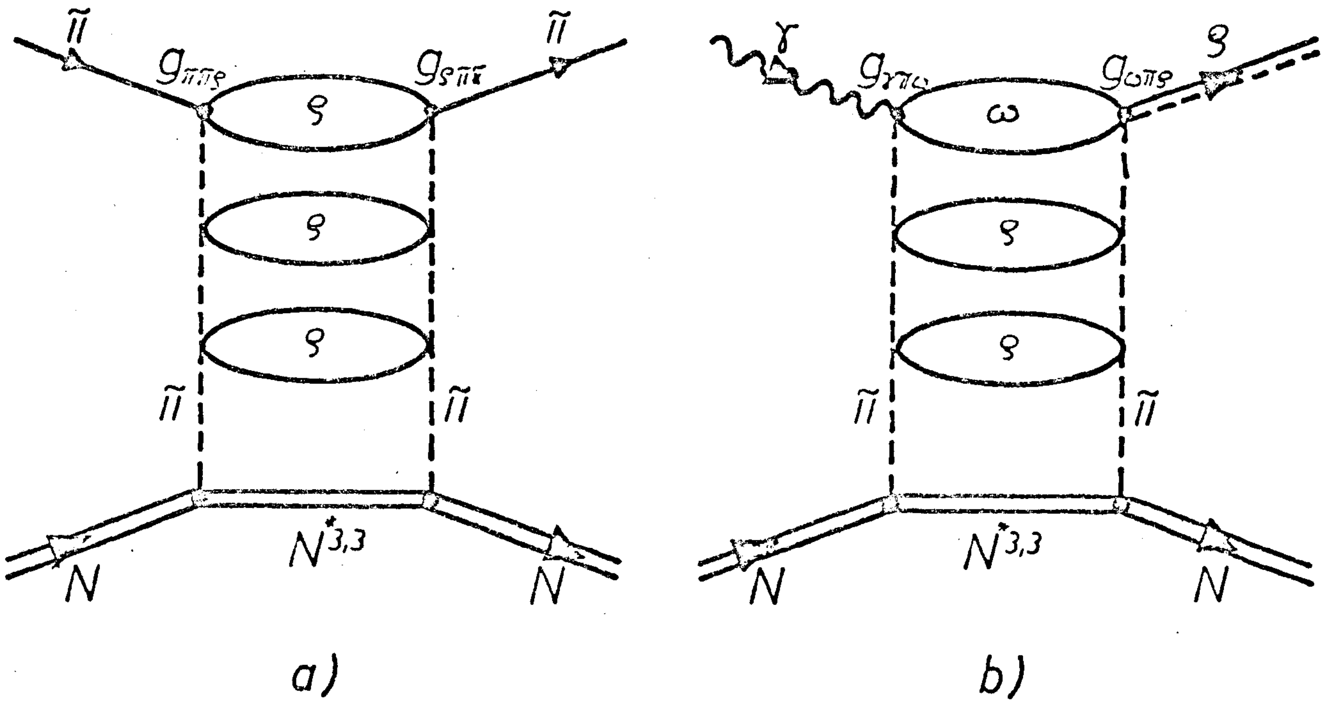

<u>Figure 1.</u> Graphs for the multiperipheral model

Because of the equality of the quantum numbers of γ quantum and ρ^{o} meson they apply the same reasoning - by analogy - to the ρ^{o} photoproduction for high energies and small momentum transfer (Figure 1b) and obtain

$$\frac{d\sigma}{d\Omega}\Bigg|^{Diffr}_{\substack{\gamma\to\rho \\ \delta\to 0^\circ}} = \frac{1+\cos^2\delta}{32}\,\frac{\left(\frac{g^2_{\gamma\pi\omega}}{4\pi}\right)\left(\frac{g^2_{\rho\pi\omega}}{4\pi}\right)}{\left(\frac{12\Gamma_0}{m_0}\right)^2}\,\frac{|\vec{p}_\rho|}{E_\rho}\,\frac{d\sigma}{d\Omega}\Bigg|^{Diffr}_{\substack{\rho\to\rho \\ \delta\to 0^\circ}} \qquad (1.2)$$

where $\vec{p}_\rho$, E_ρ are momentum and energy of the ρ^o meson, δ is the angle between $\vec{k}$ and $\vec{p}_\rho$, Γ_o is the width of the ρ^o meson, and $g_{\gamma\pi\omega}$, $g_{\rho\pi\omega}$ are coupling constants.

The dependence of the photoproduction cross section on energy and production angle - so long as the latter remains small - is basically the same as in (π-p) scattering. This differential cross section increases roughly as k^2, while the OPE model requires $1/k$, so that it is possible to distinguish clearly between the two production mechanisms by measuring the energy dependence of the cross section.

The prediction of the decay angle distribution of $\rho^o \longrightarrow \pi^+ + \pi^-$ is independent of the model for exact forward production. The transverse polarization of the γ quantum is transferred to the ρ^o meson with spin 1. The angular distribution of the decay pions is hence[32]:

$$W(\theta_\pi^*) = \frac{1-\bar{\beta}^2\cos^2\theta_\pi^*}{4\pi(1-\bar{\beta}^2/3)} \xrightarrow[\bar{\beta}\to 1]{} \frac{3}{8\pi}\sin^2\theta_\pi^* \qquad (1.3)$$

θ_π^* denotes the angle between the π^+ and the γ-beam direction in the rest system of the ρ^o, which has the velocity $\bar{\beta}.c$ in the laboratory system. One expects in particular in the vector-dominance model of a conservation of helicity also for angles $\delta \neq 0^o$. The angular distribution (1.3) should then be considered with reference to the ρ^o momentum.

In what follows two studies on the diffraction production of ρ^o mesons will be considered, since they are closely connected with the experiment described here.

2.3 Diffraction-dissociation model[24]

By way of explanation of the name, it may be recalled that a particle of mass M and momentum $\vec{p}$ dissociates into components without change of quantum number, as for example:

$$d \to p + n$$
$$\pi \to 3\,\pi$$
$$\gamma \to \rho^{o}, \omega, \phi .$$

These transitions are not possible in free space because of energy and momentum conservation, but the energy and momentum conservation can be satisfied by a longitudinal momentum transer Δ

$$\Delta \geqslant \frac{M^{*2} - M^{2}}{2|\vec{p}|} \tag{1.4}$$

This can, for example, be given up in a diffraction scattering of the dissociated system of mass M^* to an arbitrary nucleon or nucleus.

For high momenta $\vec{p}$ a relatively small momentum transfer is therefore sufficient to make the dissociated system "materialize". Figure 2b shows the diagram for dissociation production. M. Ross and L. Stodolsky introduce a phenomenological γ- ρ coupling, for which the constant $g_{\gamma\rho}$ is connected with the γ_ρ defined by Gel-Mann[9] by

$$g^{2}_{\gamma\rho} = \frac{\alpha \cdot \pi}{\gamma_\rho^{2}} \qquad \alpha = \frac{1}{137}$$

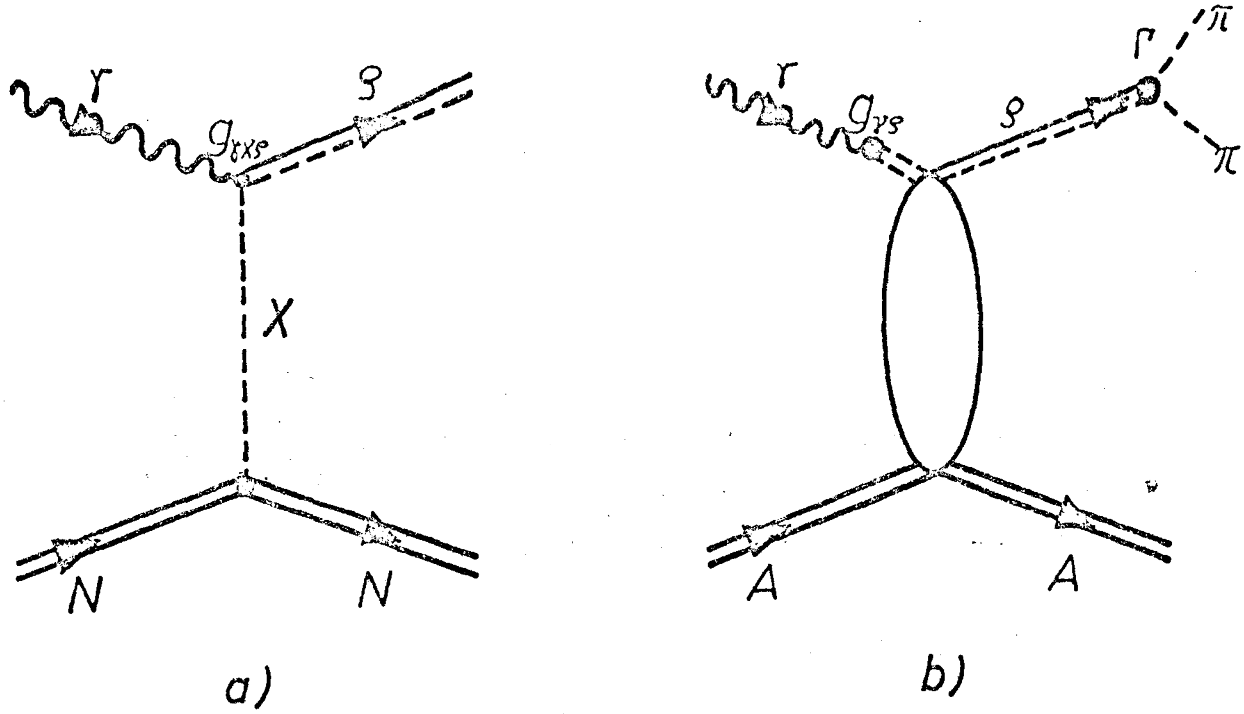

<u>Figure 2</u>. a) Graph for the OPE model and

b) Diagram of the diffraction dissociation model

This coupling combines the γ quantum with the dissociation components of a ρ^o. After the diffraction scattering, which likewise does not change any quantum numbers, the ρ^o is a real particle distributed around the central mass m_o with width Γ_o.

We shall attempt to make the form of the cross section plausible* since the polarization remains constant during diffraction scattering the spin averaging of the initial and the summation over the final spin states is trivial.

* The necessity arises from the use of the nonrelativistic Breit-Wigner mass distribution in the work of M.Ross and L.Stodolsky which was quoted (ref.13).

The diagram of Figure 2b is treated in the manner of the Feynman graphs but uses the propagators of the Klein-Gordon equation for the inner lines of the spin 1 states.

The dissociated system has the propagator

$$\frac{1}{k^2 - m^2 + i\varepsilon}$$

where $k^2 = 0$ is chosen, since a real photon is incident. Correspondingly for the emergent ρ^o meson

$$\frac{1}{m^2 - m_o^2 + im_o \cdot \Gamma} \qquad (p^2 = m^2)$$

The meson is treated as an unstable particle which has a mass m distributed around the mean m_o with half value width Γ. Since the decay $\rho^o \longrightarrow \pi^+ + \pi^-$ is 99% predominant, the partial decay width is given by $\Gamma_{\pi\pi} \simeq \Gamma$

Using the vertex coupling constants $m_o^2 g_{\gamma\rho}$ and $(m_o\Gamma)^{\frac{1}{2}}$ one obtains for the amplitude of the photo-production of a ρ^o meson in the mass interval $(m, m + dm)$:

$$A(m) \sim g_{\gamma\rho} \frac{m_o^2}{-m^2} A_{\rho\to\rho} \frac{(m_o\Gamma)^{1/2}}{m^2 - m_o^2 + i m_o\Gamma}$$

$A_{\rho' \to \rho}$ is the amplitude of the diffraction scattering of the dissociation state ρ' into a ρ^o meson. In this model this amplitude is approximated by that of the scattering of a real ρ^o meson by a nucleus: $A_{\rho \to \rho}$ and thus has the cross section

$$\frac{d^2\sigma(\gamma+A\to\rho^o+A)}{d\Omega\, dm^2} = g_{\gamma\rho}^2 \left(\frac{m_o}{m}\right)^4 \frac{d\sigma(\rho+A\to\rho+A)}{d\Omega}\ \frac{1}{\pi}\ \frac{m_o \cdot \Gamma}{(m_o^2-m^2)^2+m_o^2\Gamma^2} \qquad (1.5)$$

It can be shown that on integrating over all masses:

$$\frac{d\sigma(\gamma+A\to\rho^o+A)}{d\Omega} = g_{\gamma\rho}^2\ \frac{d\sigma(\rho+A\to\rho+A)}{d\Omega} \qquad (1.6)$$

Integration over $d\Omega$ yields

$$\sigma(\gamma+A\to\rho^o+A) = g_{\gamma\rho}^2 \cdot \sigma_{elastic}\ (\rho+A\to\rho+A)$$

If it is assumed that the elastic ρ^o scattering amplitude in the forward direction ($\delta \simeq 0^o$) is mostly imaginary, it follows on applying the optical theorem that

$$\left.\frac{d\sigma(\gamma+A\to\rho^o+A)}{d\Omega}\right|_{\delta=0^o} = g_{\gamma\rho}^2 \left(\frac{k}{4\pi}\right)^2 \cdot \sigma_{tot}^2\ (\rho+A) \qquad (1.7)$$

This relation gives the possibility of determining the coupling constants $g_{\gamma\rho}$, insofar as it is possible to determine $\sigma_{tot}^2(\rho + A)$.

2.4 Model of the diffraction scattering at a nucleus A

Instead of calculating the ladder graphs (Figure 1b), S.D. Drell, J.S. Trefil[18] and M. Ross, L. Stodolsky[13] use a simpler model of the diffraction scattering at complex nuclei A. Here the nucleus is treated as a purely absorbing medium of nucleon density $\rho(r)$. Using the asymptotic scattered wave expansion in the collision parameter b it is possible[26] with the aid of the optical theorem to obtain the total effective cross section for diffraction scattering of pions and protons at a nucleus A:

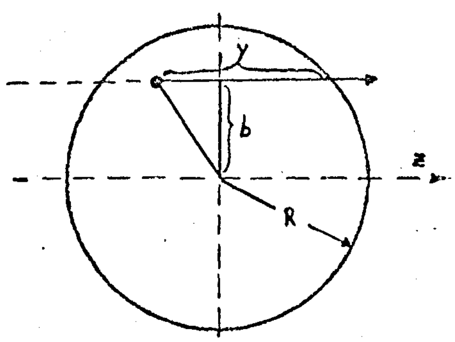

$$\sigma_{tot}(A) = 4\pi \int_0^\infty b\, db \left\{ 1 + e^{-\sigma \int_0^\infty \rho(y,b)\, dy} \right\} \quad (1.8)$$

The question can now be asked: which total cross section σ for the incident particle must be inserted in (1.8) in order to describe in the best way the A-dependence of σ_{tot}? Using the simplest form of the density distribution

$$\rho(r) = \begin{cases} \rho_0 & \text{for} \quad r < R = r_0 A^{1/3} \\ 0 & \text{otherwise} \end{cases}$$

M. Ross, L. Stodolsky and S.D. Drell, J.S. Trefil using the experimental data of M.I. Longo, B.J. Moyer[27] find for pion scattering, and G.Belletini et al.[28] for proton scattering on different elements A

$$\sigma_{\pi p} \approx 30 \text{ mb} \quad \text{at momenta} \quad P_{\pi} = 3 \text{ GeV/c}$$
$$\sigma_{pp} \approx 40 \text{ mb} \quad\quad P_{p} = 19.\text{GeV/c}$$

This agrees well with the directly measured values of S.J. Lindenbaum[30] and justifies the model.

The result is hardly different if a modified Gaussian distribution is assumed for the density function $\rho(r)$. This intensitivity of the results to the special form of $\rho(r)$ is, according to R. Serber[31], to be expected for small momentum transfers.

2.5 Total ρ^0-nucleon cross section

In contrast to the diffraction scattering of π, p considered above when these relationships are applied to ρ^0 photoproduction one must take account of the existence of the minimum momentum transfer

$$\Delta_{min} = \frac{m_0^2}{2|\vec{p}|}$$

For sufficiently small momentum transfers Δ which satisfy the coherence conditions $\Delta \cdot R \ll 1$ let $\langle f \rangle \cdot e^{i\Delta z}$ be the forward production amplitude at a nucleon. Corresponding to the length of path y of the ρ^0 in the nucleus it is attenuated according to

$$e^{-0.5 \cdot \sigma_{\rho N} \cdot \rho \cdot y}.$$

Because of the coherence one integrates over the whole nuclear volume and all collision parameters and obtains the forward amplitude g_T for the photoproduction and reabsorption of transverse ρ^0 mesons in a nucleus A of radius R:

$$g_T(R,\Delta,\sigma_{\rho N}) = 2\pi \langle f \rangle \int_0^\infty b\, db \int_{-\infty}^{\infty} e^{i\Delta z} \cdot e^{-\frac{\sigma_{\rho N}}{2}\int_z^\infty \rho(y,b)\, dy} \cdot \rho(z,b)\, dz \qquad (1.9)$$

Because of the insensitivity to the special form of $\rho(r)$, let it be assumed again that it has the simplest form of a homogeneous density in a sphere of radius $R = r_0 \cdot A^{1/3}$. The integral (1.9) can then be evaluated analytically with the result

$$g_T(R,\Delta,\sigma_{\rho N}) = \frac{2\pi \langle f \rangle}{\sigma_{\rho N}\cdot\rho/2 + i\Delta} \left\{ e^{i\Delta R}\left(\frac{R}{i\Delta} + \frac{1}{\Delta^2}\right) - \frac{1}{\Delta^2} + \frac{1}{(\sigma_{\rho N}\cdot\rho + i\Delta)^2} + e^{-(\sigma_{\rho N}\cdot\rho + i\Delta)R}\left(\frac{R}{\sigma_{\rho N}\cdot\rho + i\Delta} + \frac{1}{(\sigma_{\rho N}\cdot\rho + i\Delta)^2}\right)\right\} \qquad (1.0)$$

Since

$$\left.\frac{d\sigma}{d\Omega}\right|^{\delta\to 0^\circ} \sim \left| g_T(R,\Delta,\sigma_{\rho N})\right|^2$$

by measuring the photoproduction cross section at various nuclei A it is possible to determine the total ρ^{o}-nucleon cross section $\sigma_{\rho N}$. Like the amplitude $\langle f \rangle$ it is to be understood as being averaged over protons and neutrons.

3. EXPERIMENTAL SETUP

The following considerations played a major part in the design of the experimental system:

a) The theoretical models which make the clearest predictions refer to the region of small momentum transfer, which means ρ^{o} production at very small angles and high energies.

b) The decay angle distribution for the ρ^{o} gives preference to decay symmetrical with respect to $\vec{p}_{\rho}$.

For the investigation of forward ρ^{o} production therefore it seemed best to use a detector for symmetrical π pairs. The wide angle electron pair spectrometer[33] already has the required properties.

Figure 3 shows the experimental arrangement, Figure 4 the reflection symmetrical magnetic double spectrometer employed. The gamma beam produced at an internal target of the synchrotron hits the experimental target after collimation and purification. The $\pi^+ - \pi^-$ pairs are deflected from the gamma beam by the dipole magnets MD and analysed with respect to momentum and angle of production by the further dipole magnets MB and MA. Eight scintillation counters detect the particle pair in coincidence, and the pairs are sorted according to momentum, production angle and particle type by six hodoscopes, four threshold Čerenkov counters and two shower counters.

3.1 Gamma beam

An internally rotating target consisting of 0.2 mm thick tantalum foil is immersed in the beam of electrons generated in the synchrotron at the maximum energy point. The beam of bremsstrahlung produced in this way leaves the machine tangentially through a thin tantalum window. At 11.6 m from the target it is limited in cross section and direction by the first collimator, consisting of a lead slab of 30 cm length with an aperture of 10 x 10 mm, and at 18.3 m it is limited by a second collimator with an aperture of 15 mm x 15 mm.

The collimators were carefully adjusted using polaroid photographs of the beam. Two horizontally deflecting magnets of 12.5 and 25.0 KG.m and a vertically deflecting magnet of 20.0 KG.m clear the beam of charged particles, and the latter magnet prevents any background asymmetry in the horizontal measuring system. About 35 m from the machine target the γ-beam hits the experimental target, with a cross-sectional area of $2.5 \times 2.5\ cm^2$. After leaving MD the beam is led through a vacuum tube shielded with lead and heavy concrete to the quantameter.

The intensity behavior of the bremsstrahlung in relation to time has a bell-shaped distribution of 400-500 µs half-value width, which involves an energy deviation of at most 0.2%.

3.2 Intensity measurement

The total energy of the γ beam passing through the target is measured by a gas-filled quantameter, differing in a few details[35] from the Wilson type[34]. The number of "effective quanta" Q_{eff} is directly proportional to the total charge Q collected by the quantameter according to :

$$Q_{eff} = \frac{1}{k_{max}} \int_0^{k_{max}} k \cdot N(k)\, dk = \frac{K \cdot Q}{k_{max}}$$

The calibration constant K was found by a comparative measurement using a Faraday cage in an external electron beam from the synchrotron to be:

$$K = (3.35 \pm 0.1) \cdot 10^{-15} \frac{GeV}{A \cdot s}.$$

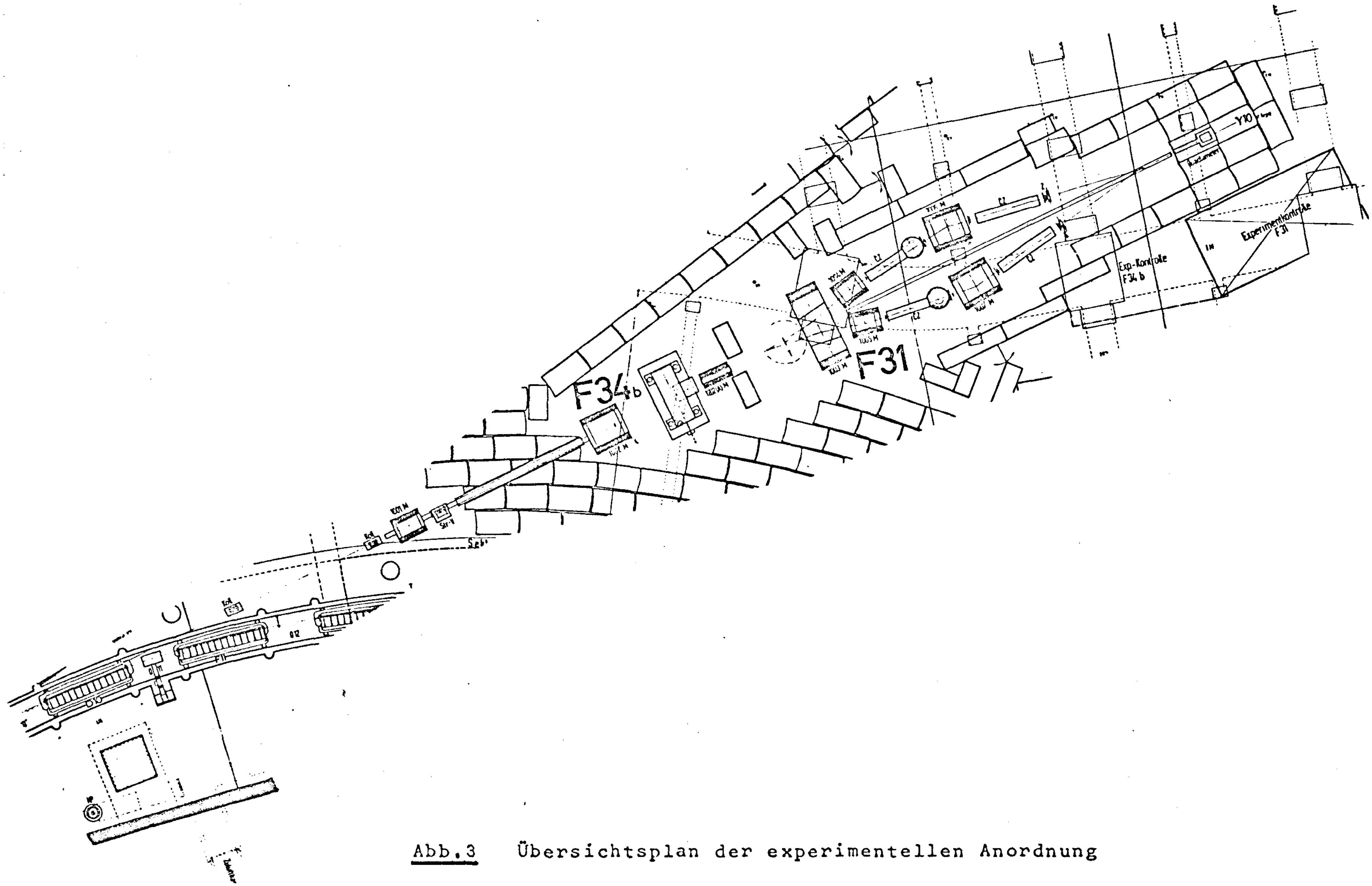

Abb.3 Übersichtsplan der experimentellen Anordnung

Figure 3. Overall plan of the experimental system

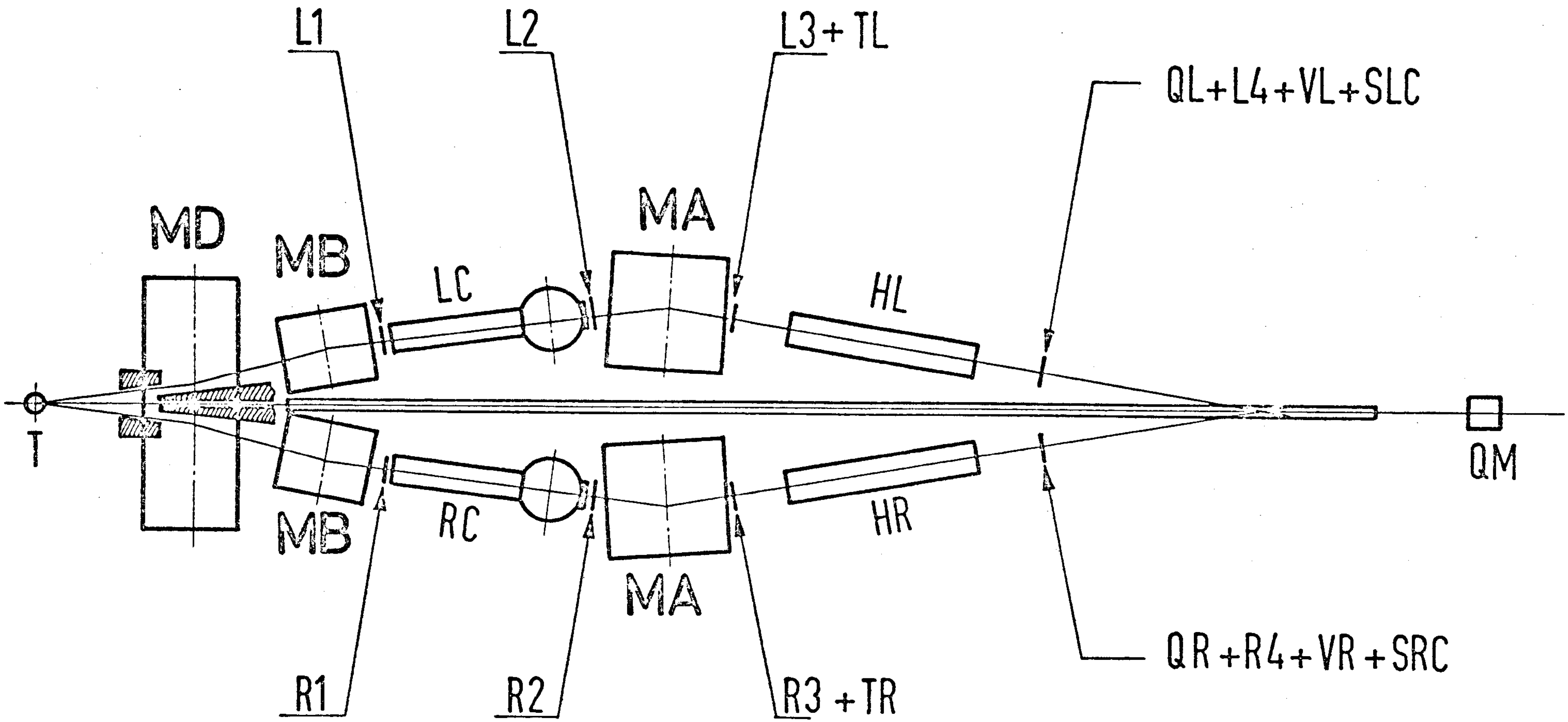

Abb.4 Schematischer Aufbau des Paarspektrometers

Figure 4. Schematic construction of the pair spectrometer

The quantity of charge yielded by the quantameter was summed up by an integrator with a long time constancy of 0.5 %. The average intensity was 2×10^{10} Q_{eff}/sec for a duty cycle of .02 - .04.

The quantameter indication was checked by a telescope consisting of five scintillation counters connected in coincidence each of 10×3 cm^2 directed at a 2 mm copper target 2 m in front of the quantameter and at 30° to the beam axis. This confirmed the quantameter indication to within 10% and showed that by suppressing electronically all pulses 2 μs before and 2 μs after the maximum of the machine pulse only some fraction 10^{-4} of the beam was lost.

3.3 Targets used

Table 3.1 gives the targets used and their degrees of purity.

Table 3.1

Material	Be	C	Al	Cu	Ag	Pb
Purity (%)	99.9	99.8	96.7	99.9	99.99	99.9
Thickness (mm)	15.1	29.98	4.98	1.03	1.01	1.02
Thickness (g/cm^2)	2.405	5.057	1.363	.910	1.056	.987

By giving the thickness in (g/cm^2) the contribution of other admixtures can be allowed for on the assumption of a contribution to the counting rate proportional to $A^{1.5}$. The largest correction for Al amounts to +2.4%. The targets have a surface area of 12 x 12 cm^2 and can be moved along the spectrometer axis on a calibrated optical bench.

3.4 Magnetic spectrometer

Figure 4 shows the spectrometer consisting of the dipole magnets (MD, MA, MB).

Charged particles leaving the target with a nominal momentum p_o are deflected by MD through an angle of $15^o - \theta_o$. Here θ_o is the vertically projected angle between the particle momentum and the direction of the γ-beam. The nominal angle θ_o is adjusted by moving the target on the optical bench. At a distance of 2.18 m further down the beam from the center of MD two magnets MB with field volumes of 102.9 x 30.3 x 10.6 cm^3 deflect back particles of nominal momentum p_o by a constant amount -8^o toward the beam. The target position and the field of MD are in each case so chosen that the nominal trajectories are the same, from the exit of MD onward for all spectrometer configurations (p_o, θ_o). This includes the important special case where at $\theta_o = 15^o$ the MD, which is common to both particles is turned off and the spectrometer arms can have different nominal momentum configurations. The magnets MA with the field volume 130.0 x 48.8 x 16.6 cm^3 deflect particles with p_o about -17.47^o back toward the beam.

A screened channel consisting of lead and heavy metal in the interior of MD isolates the γ beam and prevents particles with too small an angle of production from entering the spectrometer. Two lead blocks which are moveably mounted on pneumatic stands screen off particles with too large an angle. The positions of the inner and outer screening were varied with the angle θ_o, but in such a way that there was at least 5 cm distance between the extreme trajectories. The magnet MD can produce a maximum field of 18 KG in an effective volume of 100 x 150 x 27 cm^3 where stray field and saturation effects are important. The field behavior in one quarter of this space was measured by a Hall probe in the form of a spatial grid of 2 cm side, and the symmetry of the field with respect to the horizontal and vertical mid-planes was tested at several pairs of symmetrical points. The excitation curve was found at characteristic points and the absolute accuracy of the Hall probe measurements was confirmed by the proton resonance method. The field in the utilized volume was thus known to within $\leq 0.1\%$. The field distributions of the MB and MA magnets were measured in the DESY magnet laboratory with an accuracy of $\leq 0.03\%$.

The important features of this system are:

a) The acceptance of the system is determined exclusively by the triggerable counters R2-4, L2-4. Stray radiation from screening edges gave no measurable contribution to the coincidence counting rate.

b) The dipole magnets MD and MB together with the screening in MD effect a large reduction in the low energy background. The counters of the spectrometer have no direct line of sight on the target. The highest instantaneous counting rate was <4 MHz in R2, L2.

c) For angles $\theta < 15^{\circ}$ the dispersion of MD was reversed by the subsequent magnets MB and MA and overcompensated, so that a $(p.\theta)$ focus occurs in the horizontal plane, and this lies exactly in the Q-hodoscope when the target is so positioned as to make $\theta_o = 7^{\circ}$.

The recombination of trajectories with the same $p.\Theta$ effects a large acceptance with good resolution in t. For a fixed spectrometer adjustment the acceptance of each arm is

$$\frac{\Delta p}{p} = \pm\ 0.18 \quad \frac{\Delta\Theta}{\Theta} = \pm\ 0.14 \quad \Delta\phi = \pm\ 8 \text{ mrad.}$$

The resolution for particle pairs is :

$$\frac{\Delta m}{m} = \pm\ 0.15 \qquad \frac{\Delta t}{t} = \pm\ 0.10$$

3.5 Triggerable counter

A particle pair was registered when there was a simultaneous response from the triggerable counters L1-4, R1-4. Their dimensions were:

L1,R1	32.0 x 9.9 cm^2
L2,R2	33.0 x 13.7 cm^2
L3,R3	33.0 x 14.9 cm^2
L4,R4	43.1 x 18.1 cm^2.

In order to keep down multiple scattering and nuclear absorption they consisted of 0.3 cm thick Pilot-Y scintillator material, which has a good light transmission length of 2 to 3 m. Curved strips of Plexiglass of equal length carried the light from the longer edges of the scintillators to selected RCA 7746 photomultipliers with high amplification and low noise level. These light guides have the advantage that the time of arrival of the pulse depends only slightly on the point at which the particle makes its transit. All counters exhibited a response probability of $\geq$ 99.9% in a 1 GeV/c electron test beam of 2 x 2 cm^2, over the whole of the sensitive area. The last four dynodes were supplied from separate power sources in order to avoid saturation effects at high counting rates.

Identification of electrons was carried out by the threshold gas Čerenkov counters LC, RC, HL, HR in addition to the shower counters SRC, SLC. The former are described in detail elsewhere[36].

3.6 Hodoscope

The relatively large spectrometer acceptance is divided up by 3 hodoscope pairs TR, TL. QR, QL, VR, VL in order to obtain a better kinematic resolution of each event.

The V hodoscopes consist of two horizontal elements which are mounted behind the triggerable counters R4, L4, The Q,T hodoscopes have 5 vertical elements each and are situated behind R4, L4, and R3, L3 respectively. The surfaces of the hodoscopes were chosen 2 cm longer in each direction than the triggerable counters, so as not to introduce any aperture limitation.

While the V hodoscopes measure the azimuthal angle ϕ and hence the coplanarity of an event the T hodoscopes determine the angle θ between the particle in the horizontal plane and the γ-beam and the Q hodoscopes measure the product $p.\theta$ for the adjustment $\theta_o^+ = \theta_o^- = 7^o$.

The particles in each arm are thus determined to within

$$\frac{\Delta p}{p} = \pm .2\ \% \qquad \frac{\Delta\theta}{\theta} = \pm\ 3\ \% \qquad \Delta\phi = \pm\ 4\ \text{mrad},$$

thus giving the resolutions

$$\frac{\Delta m}{m} = \pm\ 1.5\ \% \qquad \frac{\Delta t}{t} = \pm\ 2\ \%$$

for each particle pair.

3.7 Electronics

The logical combination of the counter signals is indicated by the block diagram of the electronics in Figure 5a. The units used allow a maximum pulse frequency of 125 MHz. The counters R4 and L4 which define the acceptance are brought into coincidence with the other counters R2, R3; L2, L3 of each spectrometer arm in the units C, B; E,D. BC and DE give the number of accepted particles in each arm. The coincidence A between BC and DE indicates particle pairs within 8 ns. In order to suppress accidental coincidences in A the resolution is successively reduced to 10, 8, 7, 6, 5 ns in the units X1, X2, X3, Y1, Y2, in which counters in each arm responding to very short signals are again brought into coincidence with the 10 ns-wide output signal of A. Only the coincidence M from these five units is counted as a particle pair. This system of staggered resolution widths τ allows an accurate check on accidental coincidences, and, compared with delayed coincidences, is relatively independent of any structure in the intensity vs. time curve. The true counting rate can be found by extrapolation to $\tau \longrightarrow 0$.

A further system of electronics consisting of 100 MHz units (Figure 5b) served as an independent check, and was also used for the identification of electron pairs. The coincidences L and R indicate particle transits in the left and right spectrometer arms; Z0 registers all pairs occurring within a 16 ns period. Z1 and Z2 indicate the events for which both the threshold Čerenkov counters RC, LC or both the shower counters SRC, SLC have responded. Z1Z2 and Z3Z4 indicate electron pairs with resolving times of 12 and 16 ns respectively, which is sufficient for the low rate occurring.

The individual counting rates of the triggerable counter and the duty ratio of the machine pulse were continuously checked in order to keep dead time losses < 4%. The intensity of the gamma beam was so chosen that the rates for coincides A -- M did not differ by more than 4%. In addition to using photography of the beam, the symmetry of the γ-beam could be checked via the individual counting rates for electrons in the two arms. The long-term stability of the electronics system was regularly tested with a test pulse generator and found to be constant to within 0.3 ns.

The resolution curves for coincidences with electron pairs ($\beta \simeq 1$) were tested at longer intervals (Figure 6). Figure 5c shows the electronics of the time of flight system. Coincidences R234 and L234 also represent particle transits through the right and left spectrometer arms respectively, while FO determines simultaneity to within 100 ns. When FO responds the unit TOF converts the time difference of the signals from the units R4 and L4 into a signal proportional to amplitude, using the overlap principle, and this signal is registered by the multichannel.

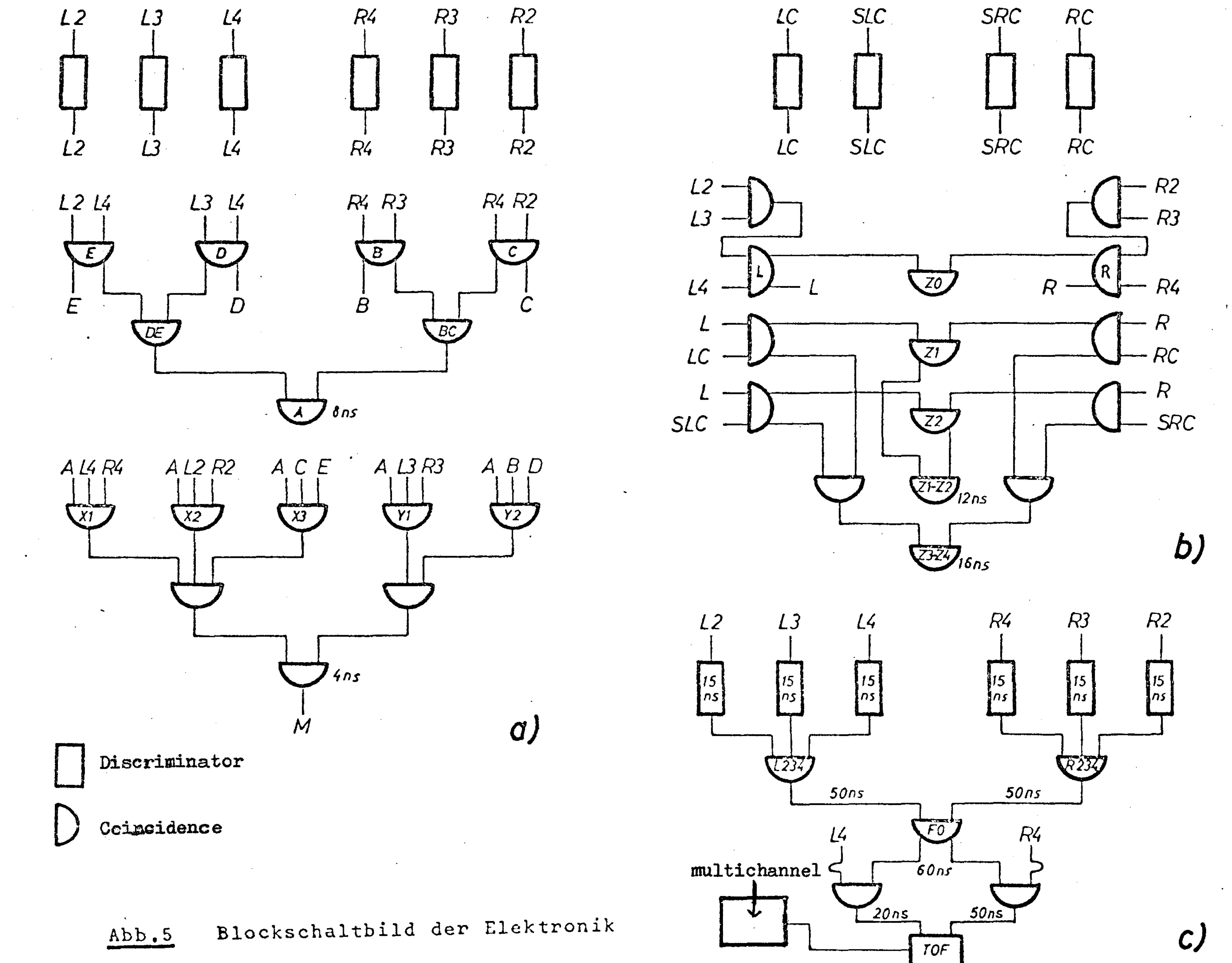

Abb.5 Blockschaltbild der Elektronik

Figure 5. Block diagram of electronics

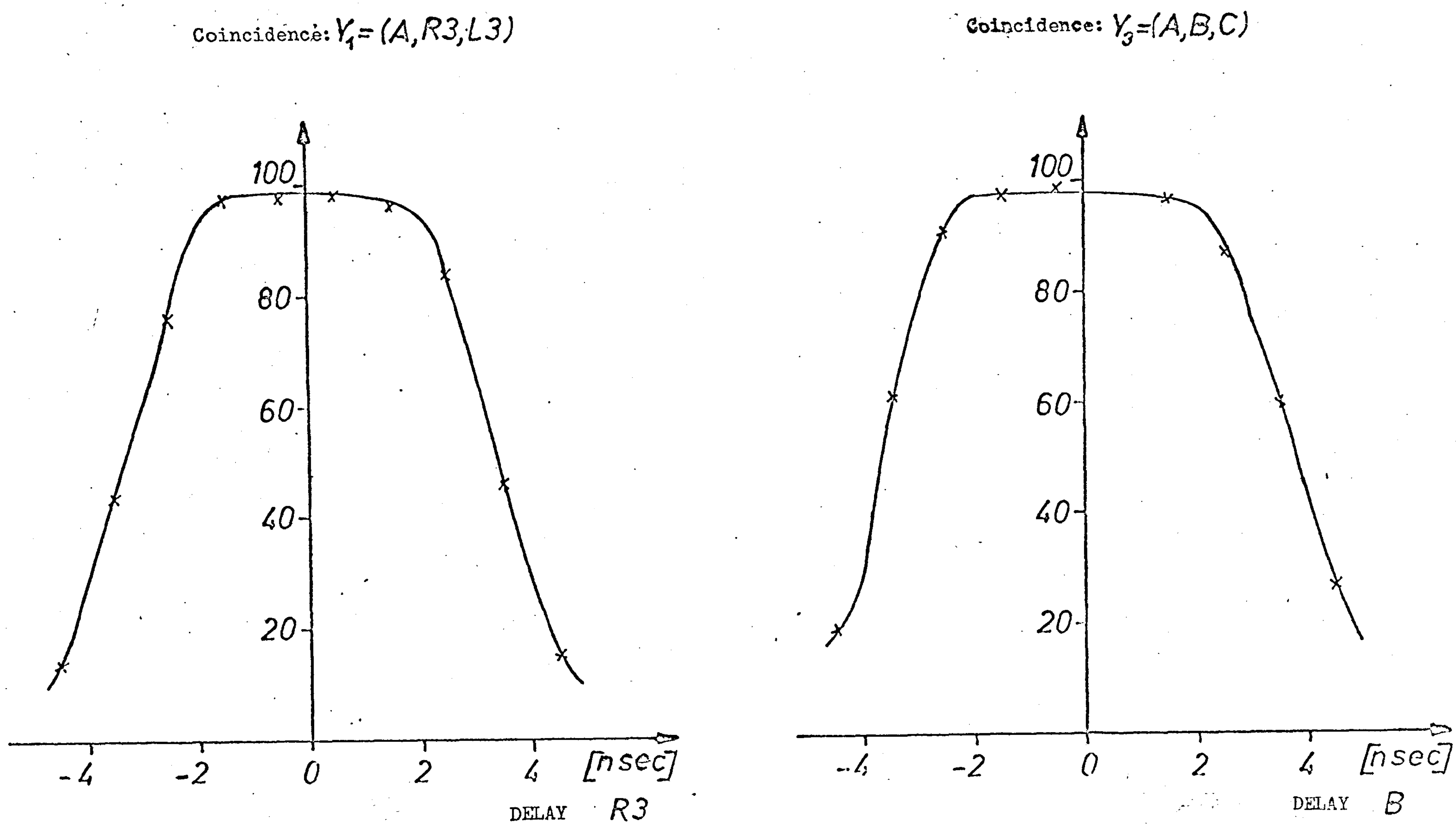

Abb.6 Im Experiment gemessene Auflösungskurven der Koinzidenzen Y1 und Y3.

Figure 6. Resolution curves for coincidences Y1 and Y3 measured in the experiment

3.8 D a t a - s t o r a g e

The hodoscope counters yield the more exact kinematic relationships of each event. Since the 6 hodoscopes can indicate 2500 states, this information is stored on a magnetic tape and subsequently analysed on an IBM 7044 computer.

The transfer of an event to magnetic tape occurs in the following manner (see Figure 7a).

The signal m defining a pair is brought into coincidence with each of the 24 hodoscope counters. Each counter which responds emits a coincidence signal which is stored in the flip-flop register as "1". The signal M is transferred as M' after delay to the event counter and initiates the read out sequence. The control unit makes the inputs to the system insensitive by means of a veto signal during the read-out time. The 6-channel multiplexer scans successively the 96 storage locations in groups of 6 "information bits", which are each written as one "character" by the step tape unit. After 16 steps the contents of the intermediate store are transferred to tape; the store is cleared and the input veto removed, so that the next event can be registered.

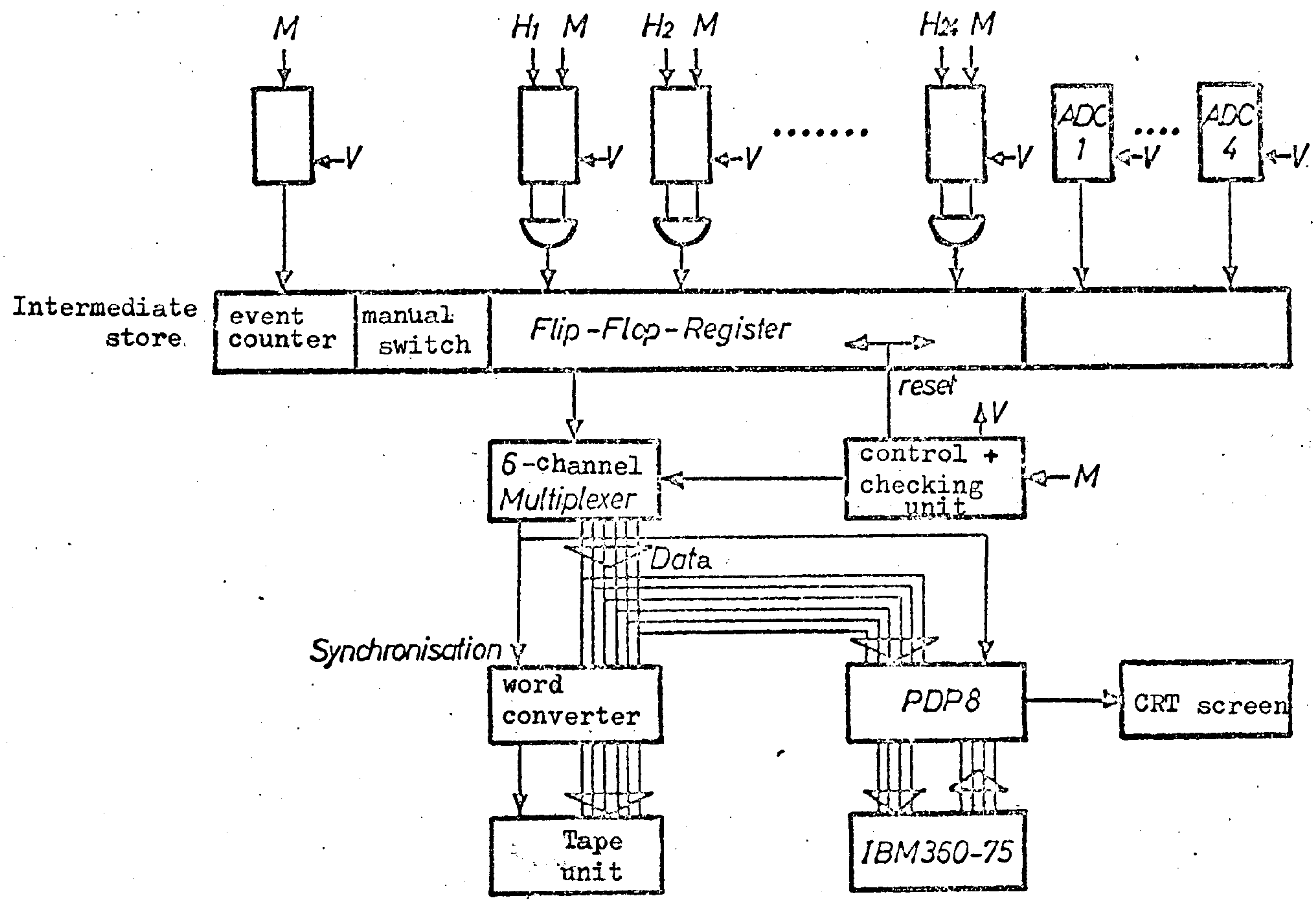

Abb.7a) Blockschaltbild des Daten-Erfassungssystems

Figure 7a: Block diagram of the data acquistion system

Event no.		Numerical code		Hodoscope combination								ADC			
1	4	S1	S7	VL1	TL1	QL1	TR1	QR1							
2	8	S2	S8	VL2	TL2	QL2	TR2	QR2							
4	1	S3	S9	VR1	TL3	QL3	TR3	QR3							
8	2	S4	S10	VR2	TL4	QL4	TR4	QR4							
1	4	S5			TL5	QL5	TR5	QR5							
2	8	S6		M_{ee}											

Figure 7b: Information storage on magnetic tape

Abb.7b) Informationsspeicherung auf Magnetband

Since the IBM 7044 computer requires internally a block of information - a "word" of 6 x 6 "bits", but an event consists of 6 x 16 "bits", the word converter transforms 3 events into 8 IBM words[29].

Figure 7b shows how the information referring to this event appears when written on tape. The first two "characters" contain the event number as a binary number, the following two contain the manually set numerical code, which indicates to which series of measurements the event belongs.

The hodoscope combination comes in columns 5-9, the information Mee = 1 indicates an electron pair. The data tapes written in this way are read with the aid of the program "Readun" which sorts the good events in the computer according to hodoscope combinations and e^+e^- or $\pi^+\pi^-$ pairs, and the contents so gathered are written on a library tape. The event distribution in all six hodoscopes is printed out for each experimental run in order to test their functioning. Events in which one hodoscope registered no transits or more than one transit are printed out. The resolution curves for all 24 counters could be found simultaneously by delaying the signal M and evaluated by the computer.

The subcomputing unit PDP 8 is connected in parallel with the tape unit. This can likewise store events and analyse them with the aid of the main computing system IBM 7044 (later IBM 360-75)[41].

4. TESTS OF THE APPARATUS AND CORRECTIONS

4.1 Experimental tests

a) In order to test the magnetic transport equations, both spectrometer arms were measured using a current-carrying wire ("floating wire" method). The nominal trajectories were verified to within 0.5% which is also the resolution limit of this method of measurement.

b) The correctness of the spectrometer calculation was demonstrated in the large angle electron pair production experiment[33] by verifying the counting rate and likewise the distribution of pair events in the hodoscopes.

c) In order to investigate the effect of multiple scattering and nuclear absorption of Pi-mesons, two 4 cm thick Plexiglass plates were placed in the beam path. These correspond to the total interaction material of the spectrometer, or 1.5 cm Al at the location of the triggerable counters R3 L3 and R4 L4. For a spectrometer adjustment of $\theta_o = 15^o$, p_o = 1400 MeV/c the mean decrease in the counting rate ($\simeq$ 10%) corresponded roughly to the calculations, which gave 11.7%.

d) Figure 8 shows the counting rate for a fixed spectrometer adjustment at $\theta_o = 15^o$, $p_o = 1400$ MeV/c as a function of target thickness in carbon, The linear increase indicates that multiple processes play no part in the target.

e) Figures 9a, b, c, show spectra of the relative time of flight difference of two particles leaving the target with spectrometer adjustment for the ρ^o mass, but different momenta. The temporal resolution of the triggerable counter is very good: for L4 against R4 in Figure 9a, c, it is 2.5 ns FWHM and for L3 against R3 in Figure 9b it is 2.0 ns FWHM, which can be explained as due to the smaller size of the counter and the lower target distance (10.10 against 14.8 m).

The spectra yield four experimental checks.

1) The resolution of the main trigger M of $\tau = 4$ ns causes no loss of counting rate.

2) The accidental coincidences shown in the relatively bad sequence of Figure 13b do not exhibit any structure.

3) The admixtures of unequal particle pairs e.g. p^+, π^- which should occur at the points marked $\overset{p}{\longmapsto}$ are obviously small and do not fire the main trigger.

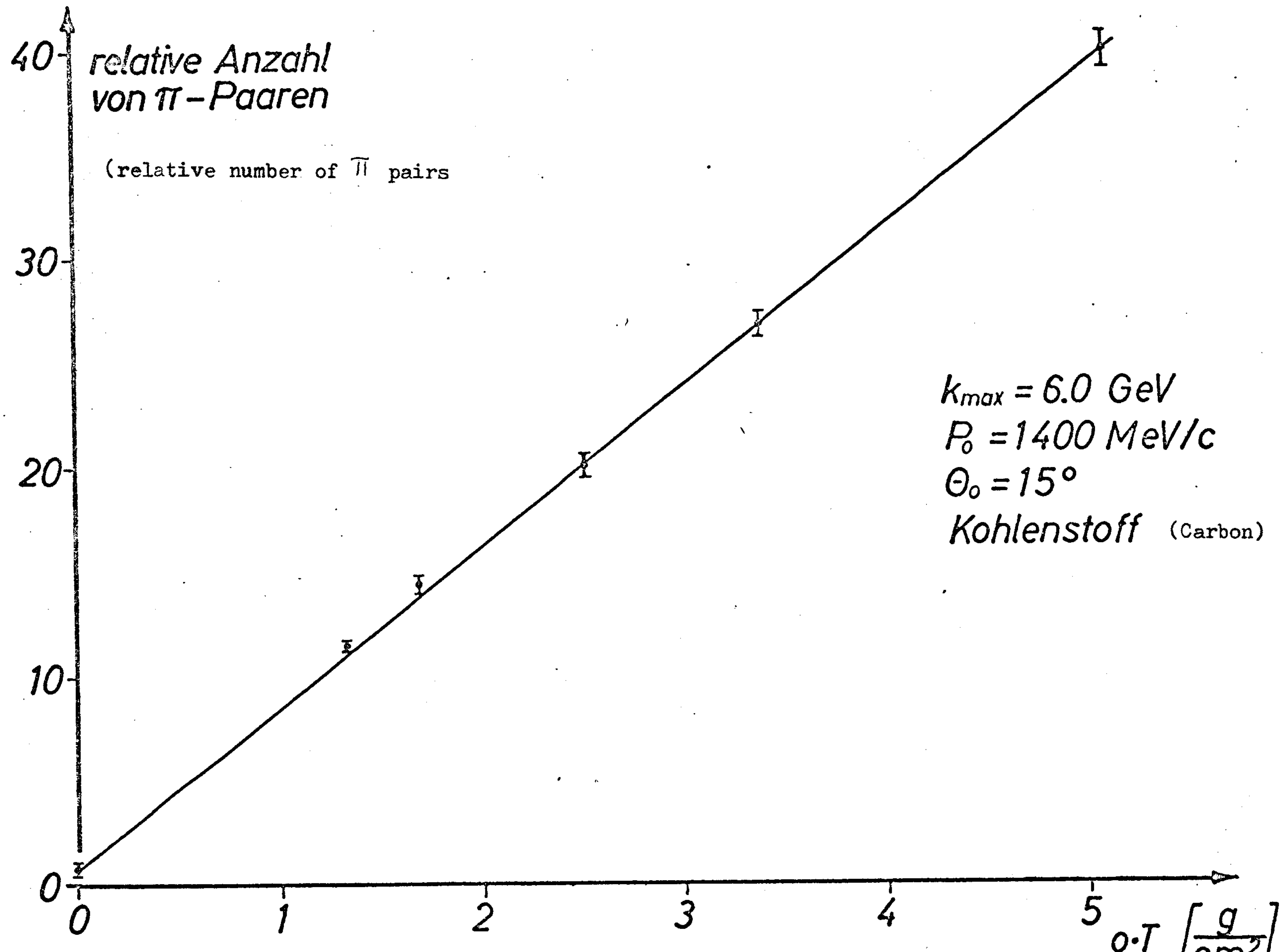

Abb.8 Zählrate als Funktion der Targetdicke

Figure 8. Counting rate as function of target thickness

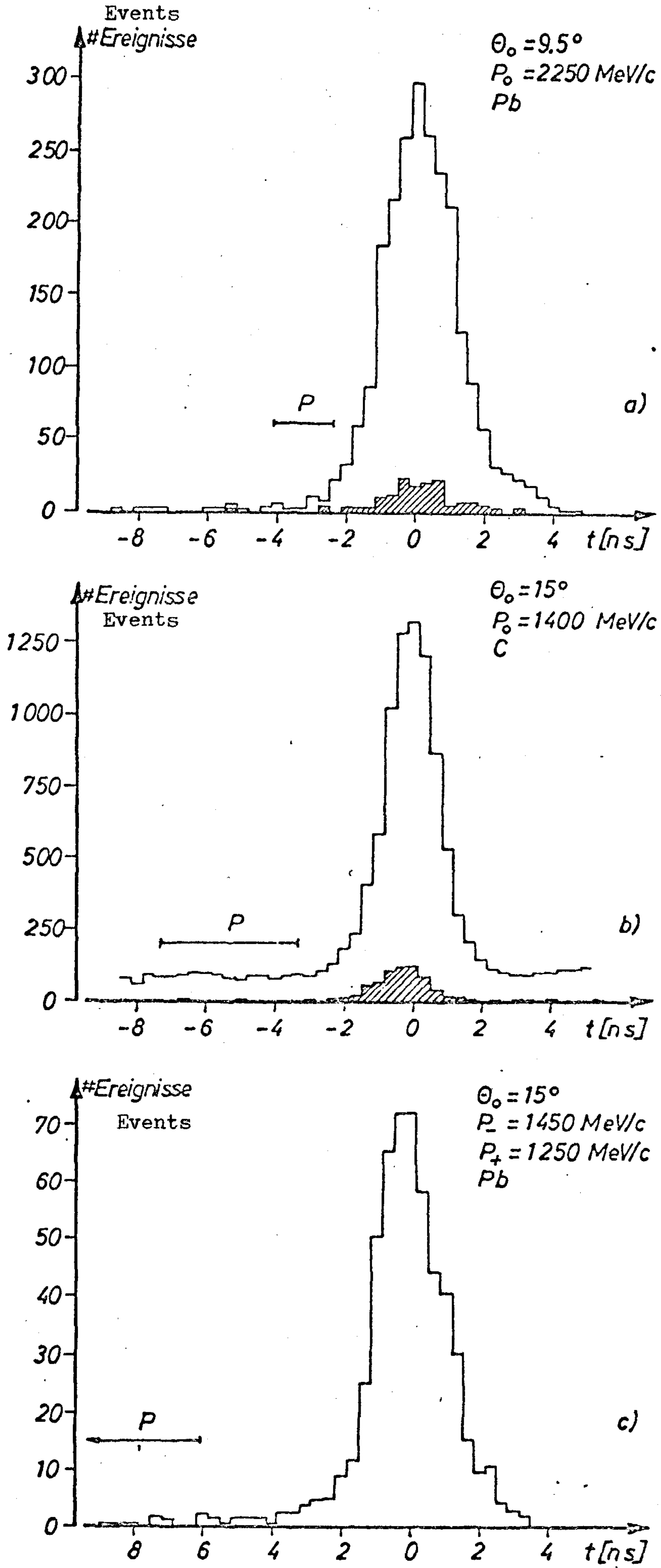

Figure 9. Time of flight measurements

Abb.9 Flugzeitmessungen

4) The no-target events, which are shown hatched exhibit the same behavior as the normal events.

4.2 Corrections

Each individual measurement was corrected for:

Dead time of electronics	DE	4%
Accidental coincidences	AC	3%
No target rate, normalized	NR	4%
Beam loss in target	BM	6%
Nuclear absorption	NA	12%

by replacing the measured quantameter charge QM' by :

$$QM = QM' \frac{(1-DE)}{(1-AC)(1-NR)} \cdot \frac{(1 + BM)}{(1 + NA)} \qquad (4.1)$$

The counting rate losses due to discriminator dead time can be calculated from the instantaneous individual counting rates. The mean counting rates of the triggerable counters were measured several times in each experimental run. Division by the duty ratio gives the instantaneous rates. The duty ratio ($\simeq$ 0.3) was calculated from the duration of the γ beam measured on the oscillograph making an approximate allowance for the synchrotron fine structure.

The contribution of accidental coincidences was eliminated by extrapolating to $\tau = 0$ the counting rates of those coincidences M, $\longrightarrow$, Zo, which were staggered by their resolution times τ. This gives as the 'true' counting rate the component which is common to all coincidences (independent of resolution). The results were confirmed by the time of flight measurements described previously (4.1.e). The normalized no target rate is the ratio of the rate without target to the rate with target corrected by DE and AC. It is itself small and therefore requires no correction for dead time or accidental coincidences.

On average the effective intensity in the target is that attenuated by about half the target thickness. The beam absorption in a half target thickness for different materials was estimated with the aid of the total photo absorption cross section of E. Malamud and J.K. Walker[43].

These losses depend on photoelectron production since a part of the electrons/positrons do not reach the quantameter. When the magnet MD is switched on the loses are roughly twice as great. The absolute value of the loss (6%) and its dependence on the field of MD were confirmed by a comparison measurement between the quantameter and a thin-walled ionization chamber placed in front of the target.

The attenuation of a pion flux I in a material of atomic weight A and thickness T (g/cm^2) is given approximately by :

$$I(T,A) \approx I_0 \cdot e^{-N_A \cdot \overline{\sigma_{\pi N}} \cdot A^{2/3} \cdot T}$$

where N_A is Loschmidt's number.

---

* Translator's note: Avogadro's number ?

The mean cross section $\overline{\sigma_{\pi N}}$ for π^+ or π^- in the energy range $1 < E_\pi < 3$ GeV/c^2 which was of interest in this experiment was put at $\overline{\sigma_{\pi N}} = 31$ mb, where it was assumed that 25% of the elastic scattering ($\overline{\sigma_{\pi N el.}} \simeq 9$ mb) remains in the spectrometer[26].

The absorption coefficients are summed as

$$\alpha = \sum_i N_{Ai} \, \overline{\sigma_{\pi N}} \, A_i^{2/3} T_i$$

for all material layers i penetrated by the particle as it passes through the spectrometer. The absorption probabilities in the double spectrometer are independent for the two pions so that the loss is

$$NA = 1 - (e^{-\alpha})^2$$

The spectrometer causes a loss of 8.1% with an additional contribution according to the target used. Corrections for multiple scattering and pion decay have already been allowed for in the acceptance program.

The dead time of the tape unit was found to be constant at 0.3 sec. It could be allowed for exactly by considering the ratio of the number of main triggering events M to the number of registered events. The dead time loss was about 5-12%. Non-identifiable events, i.e. those in which a hodoscope did not respond to all (< 2%), or in which more than one element responded (< 7%) should very probably, on the basis of the time of flight spectra, be regarded as true $\pi^+ \pi^-$ pairs; they are allowed for in the correction factor (usable events/total number of events). The systematic error in the measurement is composed of the uncertainties in the following quantities:

Number of γ quanta:	quantameter	3%
	brems-spectrum	1%
Acceptance calculation		4%
Absorption correction		3%
Radiation loss		0.5%
Dead time		1%
Accidental coincidences		2%
The root of the sum of squares of these errors is		6.5%

5. FUNDAMENTALS OF DATA ANALYSIS

5.1 Kinematics

The reaction

$$\gamma + A \rightarrow \rho^{o} + A$$
$$\hookrightarrow \pi^{+} + \pi^{-} \qquad (5.1)$$

contains, with the momentum and two angles apiece for each reaction partner, 12 kinematic parameters.Of these we know:

2 from a knowledge of the direction of the γ-beam, and

3 from the assumption that the target nucleus is stationary

4 further unknowns can be eliminated by using momentum and energy conservation.

Consequently at least three other quantities must be measured in order to fix the reaction (5.1).

This can be done in the manner of "missing mass" spectroscopy, in which further parameters of the incident particle and the recoil particle can be determined. In this experiment the direct detection of the ρ^{o} by measuring the decay pions was used. The apparatus described in the previous chapter allows the determination of the angles and momentum of each member of a pair within the acceptance centered on the nominal value.

The kinematic invariants of the process (5.1) are in squared form:

The total energy : $s = (\hat{k} + p_T)^2 = 2m_T + 2m_T k$ (5.2)

Momentum transfer: $t = (\hat{k} - p)^2 = m^2 - 2k(E - |\vec{p}|\cos\delta)$ (5.3)

where m is the invariant mass of the 2 pion system:

$$m^2 = (p_+ + p_-)^2 = 2m_\pi^2 + 2(E_+E_- - |\vec{p}_+||\vec{p}_-|\cos(\theta_+ + \theta_-)) \quad (5.4)$$

$\hat{k}$, p_T, p four-vectors of γ, target nucleus and 2π-system

m_T mass of the target nucleus

k energy/momentum of γ quantum

E, $\vec{p}$ energy/momentum of 2π system

δ angle $(\vec{k}, \vec{p})$

$E_\pm$, $\vec{p}_\pm$ energy/momentum of $\pi^\pm$

$(\theta_+ + \theta_-)$ angular aperture of pair.

For a nearly symmetrical pair: $\theta_+ \simeq \theta_- \simeq \theta$, $|\vec{p}_+| \simeq |\vec{p}_-| \simeq p_\pi$

and for $\delta \simeq 0^\circ$ the approximations

$$t \simeq -\left(\frac{m^2}{2|\vec{p}|}\right)^2 - \vec{p}^{\,2}\delta^2 \quad (5.5)$$

$$m^2 \simeq 4\, m_\pi^2 + 4\, p_\pi^2 \sin^2\theta \quad (5.6)$$

apply.

The last relation offers two simple possibilities for taking mass spectra with a symmetric double spectrometer, namely:

1) To vary $|\vec{p}_+|, |\vec{p}_-|$ at constant $(\theta_+ + \theta_-)$ or

2) To vary $(\theta_+ + \theta_-)$ at constant $|\vec{p}_+|, |\vec{p}_-|$.

Figure 10a gives an overall sketch with some acceptance windows in the p-θ plane. The window is valid for one arm of the spectrometer, the other has mirror symmetry in the p-axis. Iso-mass lines are drawn in in accordance with (5.6) for the case in which particles of these masses (in MeV/c^2) decay in symmetrical π pairs. They are crossed in method 2) by a horizontal line (shown dashed).

Since the incident γ-beam consists of a continuous spectrum of photons of the form $1/k \ f(k,k_o)$ (see Figure 10, curve a[37]) in method 1) above, the ratio of nominal momentum/maximum energy k_o would change with the spectrometer adjustment and allow various inelastic components.

For this reason and particularly because of the strong p-dependence of the cross-section which is expected, method 2) was used.

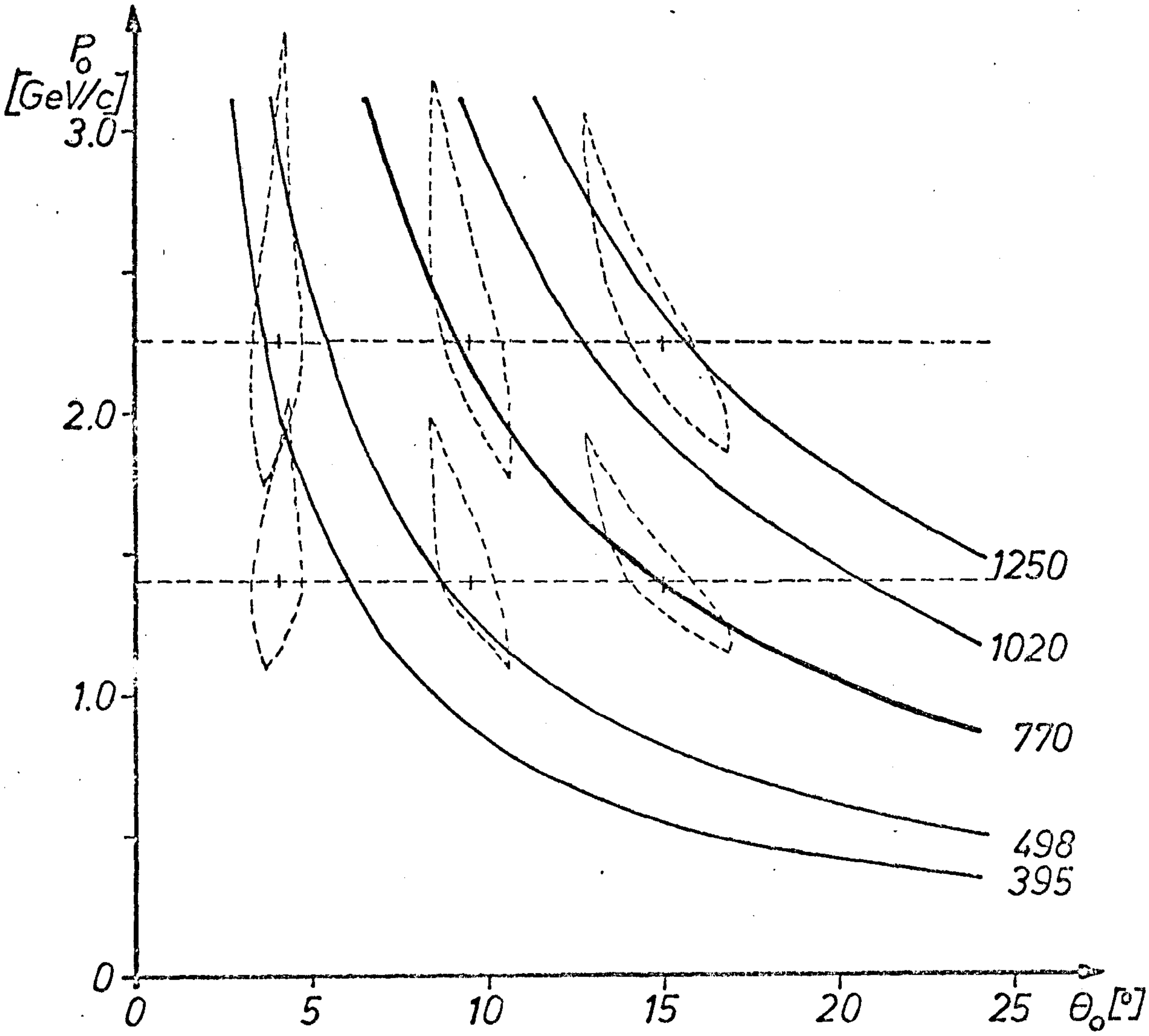

Abb.10a) Spektrometerfenster

Figure 10a. Spectrometer windows

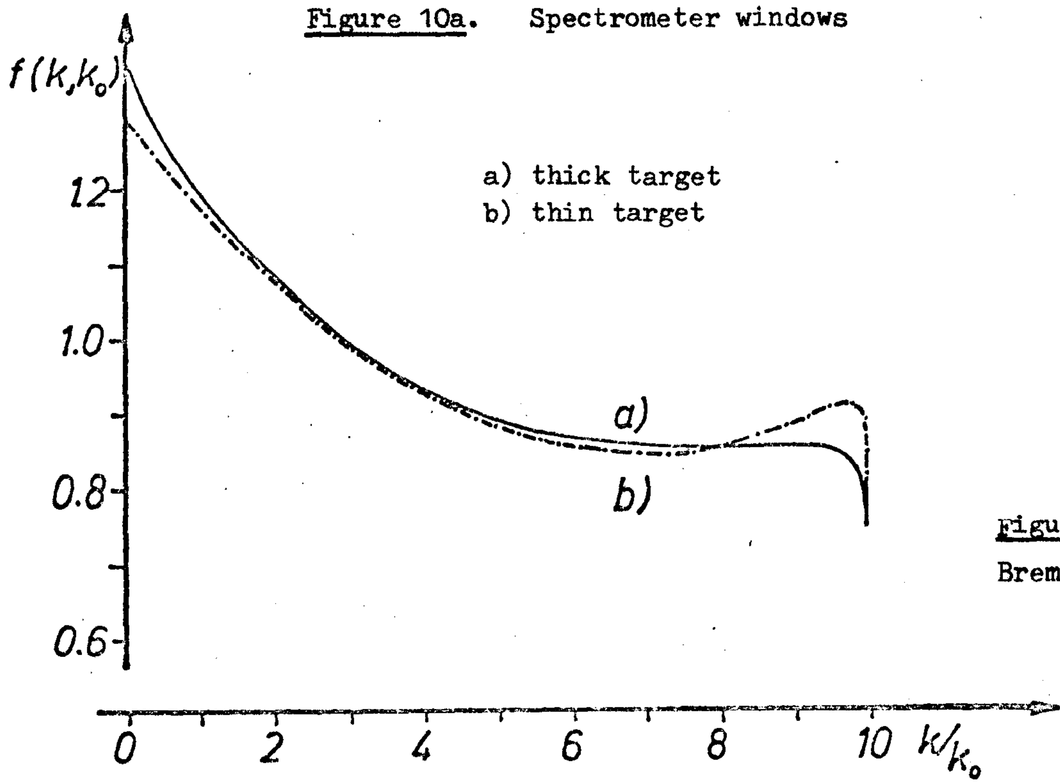

Figure 10b

Brems-spectrum

Abb.10b) Bremsspektrum

5.2 Resonance analysis

According to J.D. Jackson[38] there exists a relation between the differential cross section $d\sigma_s(m)$ of a stable particle of mass m and the cross section $d\sigma$ for a resonance

$$d\sigma = d\sigma_s(m) \frac{1}{\pi} \frac{m_o \Gamma(m)}{(m_o^2-m^2)^2+m_o^2 \Gamma^2(m)} \qquad (5.7)$$

Here m_o is the mass of the resonance and $\Gamma(m)$ its width, which has for a spin J = 1 resonance the form:

$$\Gamma(m) = \Gamma_o \frac{m_o}{m} \left[\frac{m^2-4m_\pi^2}{m_o^2-4m_\pi^2}\right]^{3/2} \qquad (5.8)$$

By applying the diffraction-dissociation model to the photoproduction of ρ^o mesons, M. Ross and L. Stodolsky[13] obtain a factor m_o^2/m^2 from the $\gamma-\rho$ vertex. Hence one obtains a relation between the differential cross sections of the stable particles and the resonance

$$\left.\frac{d^2\sigma}{d\Omega dm^2}\right|_{Photo} = \left.\frac{d\sigma_s(m)}{d\Omega}\right|_{Photo} \frac{1}{\pi} \left(\frac{m_o}{m}\right)^4 \frac{m_o \Gamma(m)}{(m_o^2-m^2)^2+m_o^2\Gamma^2(m)}$$

(5.9)

If one uses $dm^2 = 2\,m.dm$ then:

$$\left.\frac{d^2\sigma}{d\Omega dm}\right|_{Photo} = \left.\frac{d\sigma_s(m)}{d\Omega}\right|_{Photo} \cdot 2m \cdot R(m)$$

where
$$R(m) = \frac{1}{\pi} \left(\frac{m_o}{m}\right)^4 \frac{m_o\Gamma(m)}{(m_o{}^2-m^2)^2+m_o{}^2\Gamma^2(m)} \tag{5.10}$$

gives the mass distribution of the hypothetical stable particles, and these taken together describe the resonance. In other words: the observed mass distribution of the $\pi^+ \pi^-$ system depends not only on the specific properties of the resonance ρ^o but also on the production process, which yields, on assuming the diffraction-dissociation model, the factor $(m_o/m)^4$ with the mass distribution for an isolated resonance given by J.D.Jackson.

The effect of this factor can be seen from Figure 11. Curve a) represents the function $2m.R(m)$, while b) does not contain the factor $(m_o/m)^4$.

5.3 Formula for the cross-section

Both the OPE model in eq. 1.1 and the diffraction model of S.M.Berman and S.D. Drell[22] in eq. (1.2) predict the dependence of the differential cross section on the product momentum. The momentum dependence is up to a factor (p_ρ /E) the same as in diffraction scattering of π mesons at $\delta \longrightarrow 0^o$

$$\frac{d\sigma}{d\Omega}\Big|^{\delta=0^o} \sim f(p) = p^2 \cdot f'(p)$$

The component which is weakly dependent on momentum is obtained using the optical theorem from the relative change in the total π -N cross section

$$f'(p_\rho) \approx \frac{p_\rho}{E_\rho} \frac{\sigma^2_{\pi N}(p_\pi = p_\rho)}{\sigma^2_{\pi N}(p_\pi = 20\ GeV/c)} \qquad (5.11)$$

Curve a) in Figure 12 was obtained using the data for the total π -N cross section of A. Citron et al.[40]. For comparison curve b) shows the prediction of the OPE model. Only the relative behavior is of interest, the absolute value was established - somewhat arbitrarily - from the estimates of S.M. Berman and S.D.Drell[22] for H_2.

Starting from equation (1.2) one could then go on to try to describe the momentum transfer dependence of the ρ^o production cross section by the"optical model with constant density" as in π -N scattering. In this case the target nucleus is considered as a homogeneous "gray" sphere of radius $R = r_o \cdot A^{1/3}$. Considered semiclassically only partial waves with $1 \leq p.R$ can be scattered. For each of these waves there is the same constant density $a_l = a > 0$, real. For all waves with $1 > pR$ we have $a_l = 0$. The scattering amplitude is then purely imaginary, i.e. there is no direct elastic scattering apart from shadows of the inelastic processes (diffraction scattering).

One obtains the well known relation for the diffraction picture: (J_1 is the Bessel function of first order)

$$\frac{d\sigma}{d|t|} = (1-a)^2 \cdot \pi R^4 \left[\frac{J_1(R \cdot \sqrt{-t})}{R \cdot \sqrt{-t}} \right]^2 \qquad (5.12)$$

which for small values of

$$|t| < .8 \ (\mathrm{GeV}/c)^2 / A^{2/3}$$

becomes approximately

$$\frac{d\sigma}{d|t|} = (1-a)^2 \cdot \frac{\pi \cdot R^4}{4} \cdot e^{-\frac{R^2}{4}|t|} \qquad (5.13)$$

A more exact description, taking account of the minimum momentum transfer

$$-t^{*} \simeq m_o^{\,2} / 2|\vec{p}|$$

is given in eq. (1.10) for the diffraction dissociation model.

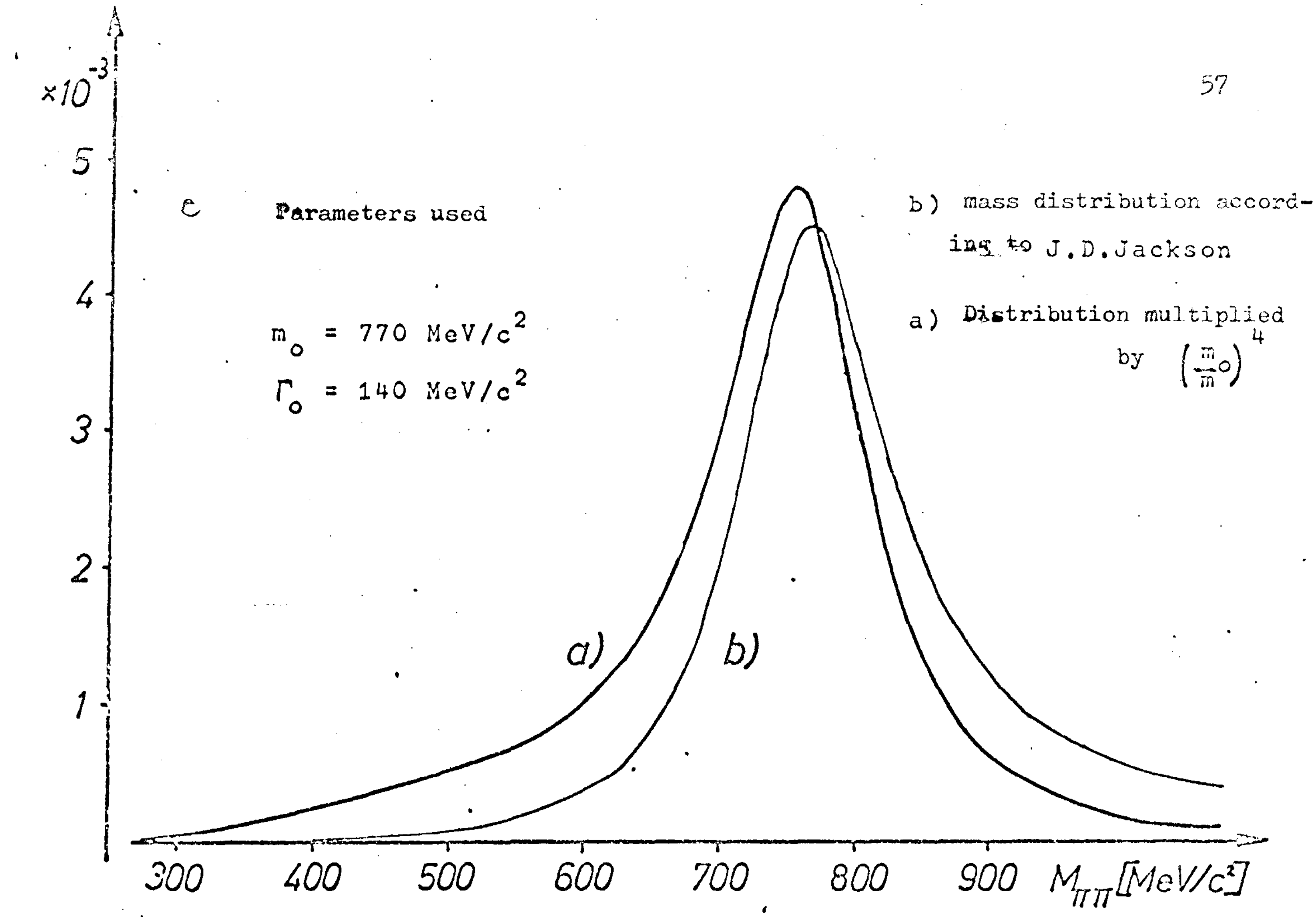

Abb.11 Vergleich der Massenverteilungen

Figure 11. Comparison of mass distributions.

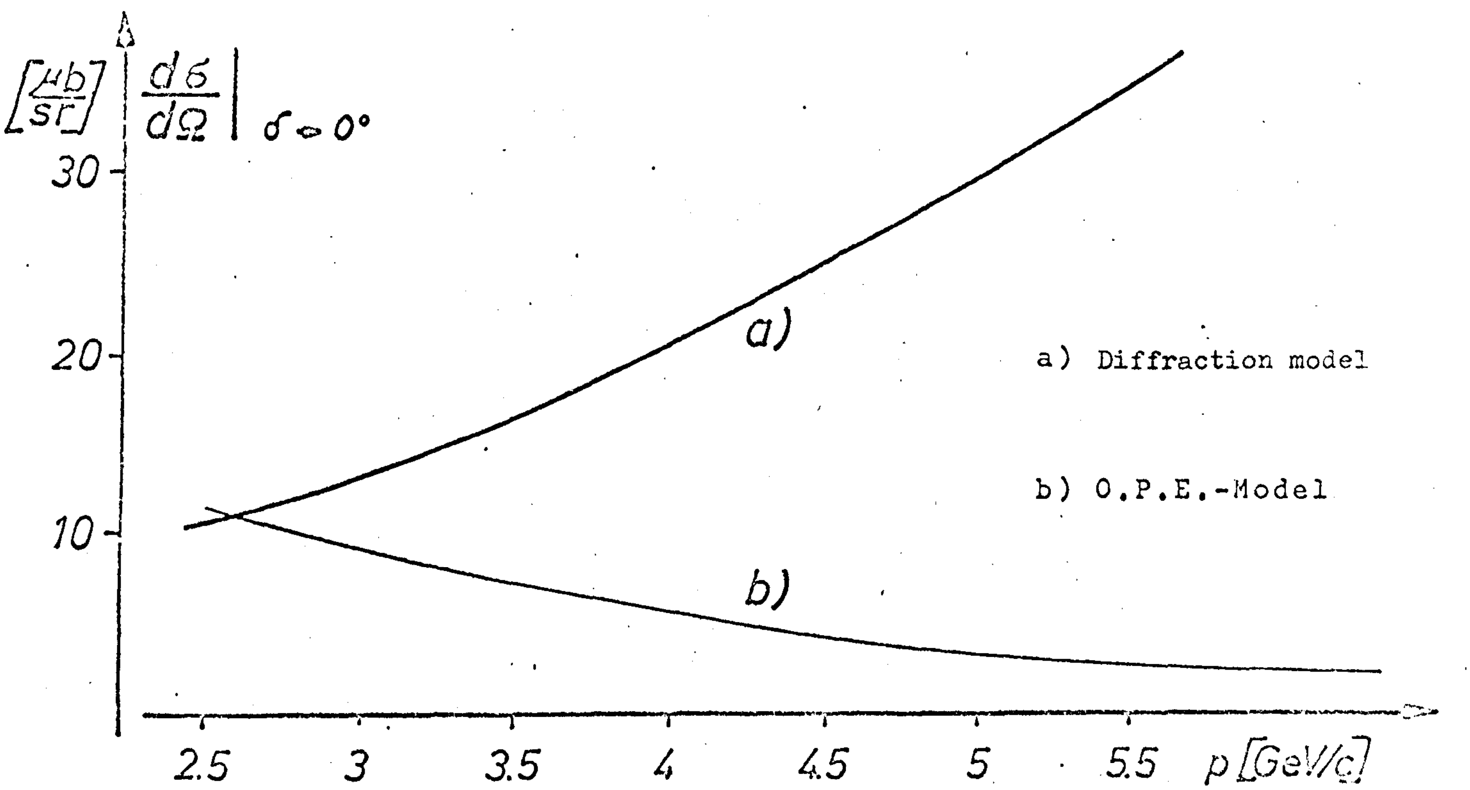

Figure 12. Qualitative comparison of the momentum dependences.

Abb.12

If one defines the function (see eq. 1.10)

$$f_T(R,t,\sigma_{\rho n}) = \left| \frac{g_T(R,t,\sigma_{\rho n})}{g_T(R,0,\sigma_{\rho n})} \right|^2 \qquad (5.14)$$

so that

$$f_T(R,0,\sigma_{\rho n}) = 1$$

then together with the two parameters r_o and $\sigma_{\rho n}$ this also describes the t-dependence for longitudinal momentum transfers. Detailed calculations which are also valid for larger transverse momentum transfers are being carried out[55].

Figure 13 shows the comparison of (5.12), (5.13), and (5.14) in lead.

Taking these altogether one obtains the following formula for the cross section

$$\frac{d^2\sigma}{d\Omega\, dm} = C(A)\cdot p^2 f'(p)\cdot f_T(R,t,\sigma_{\rho n})\cdot 2m\cdot R(m) \qquad (5.15)$$

C(A) is a normalizing constant for a constant element A. It should be noted that the amplitude g_T also describes the relative behavior in A; however, this is prevented here by the normalization condition (5.14).

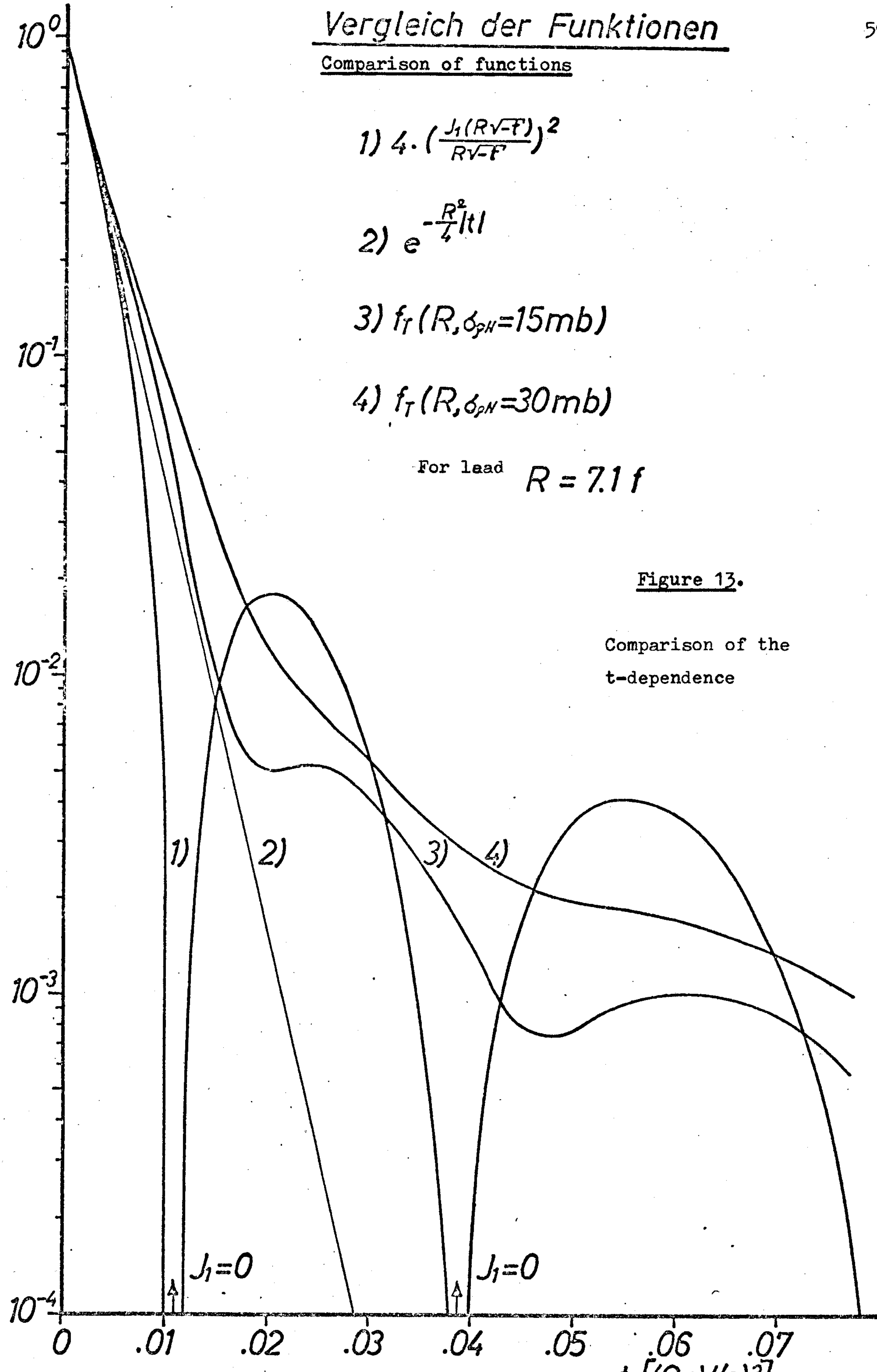

Figure 13.

Comparison of the t-dependence

Abb.13 Vergleich der t -Abhängigkeiten

5.4 Acceptance calculations

Each event is determined kinematically by angle and momentum of both decay pions. In the data these quantities appear as two triplets of hodoscope combinations (TR, QR, VR), (TL, QL, VL).

The coordination of the kinematic quantities with the hodoscope combinations is done by a relatively rapid Monte-Carlo program. This determines the

mean momentum	$\langle p_\pi \rangle$
angle in the horizontal plane	$\langle \theta \rangle$ and
azimuthal angle	$\langle \phi \rangle$

belonging to each of the 50 possible combinations of <u>one</u> spectrometer arm for the different spectrometer adjustments.

Since the other arm is mirror-symmetric, the same values hold there, so that mass, momentum and momentum transfer for each of the 50 x 50 combinations can be calculated. This program makes use of the same transport matrices, etc., as that used in the acceptance program described below.

The number N of accepted decay pion pairs of system mass m and the resultant total momentum $\vec{p}$ deriving from a resonance produced with cross-section $d^2\sigma/d\Omega\, dm$ is given by :

$$N = N_T \cdot Q_{eff} \iiiint \frac{d^2\sigma}{d\Omega\, dm}\, d\Omega\, dm\, \frac{W(\theta^*_\pi)}{4\pi}\, d\Omega^*\, A(m,\vec{p},t)\, \frac{f(k,k_0)}{k}\, dk \qquad (5.16)$$

where :

N_T is the number of target atoms per cm^2

$Q_{eff}\, \frac{f(k,k_0)}{k} dk$ is the number of γ quanta in the energy interval $(k,\ k + dk)$

$W(\theta^*_\pi)$ is the decay angle distribution according to eq. (1.3)

Ω^* is the solid angle for the π^+ in the center of mass system of the resonance

$A(m,\vec{p},\ t)$ is the acceptance function.

$A(m,\ \vec{p},\ t)$ has the value 1 if the decay pion pair of the resonance is accepted, and is otherwise 0.

Because of the large aperture displayed by the spectrometer, a relatively broad range in m and p is accepted, i.e. the estimate of the cross section $\frac{d^2\sigma(m,p,t)}{d\Omega\, dm}$ averaged over the whole aperture is too coarse because of the large change in the variables m,p,t. The variation of the cross section with p and t is described by the functions $p^2 f^1(p)$ in eq. (5.11) and f_T in eq. (5.14). According to the formula (5.15) the cross section weighted by these functions

$$\frac{1}{p^2 \cdot f'(p) \cdot f_T(R, t, \sigma_{\rho n})} \frac{d^2\sigma}{d\Omega dm} = C(A) \cdot 2\, mR(m) \qquad (5.17)$$

for a fixed target of atomic number A is dependent only on the mass m and can be used to unify the measurements from several spectrometer adjustments into a single mass spectrum.

For a small mass interval Δm the weighted cross section can be averaged over the aperture and the integration over dk in (5.16) can be transformed into an integration over dp by means of the functional determinant $\partial k / \partial p$. The pion pairs in the interval $(m, m + \Delta m)$ which are accepted are thus

$$\dot{N}(\Delta m) = N_T \cdot Q_{eff} \frac{\langle f(k, k_0) \rangle}{\langle p^2 \cdot f'(p) f_T \rangle} \left\langle \frac{d^2\sigma}{d\Omega dm} \right\rangle \iiiint_m^{m+\Delta m} p^2 f'(p) f_T \frac{W(\theta_\pi^*)}{4\pi} A\, d\Omega^* \frac{\partial k}{\partial p} \frac{dp}{k}\, d\Omega\, dm \qquad (5.8)$$

where the brems-spectrum function is likewise replaced by its mean value in its slowly varying part $f(k, k_0)$.

The integrals over the aperture are difficult to obtain analytically.

They are therefore evaluated by a Monte-Carlo method. The experiment is thus done as accurately as possible by the computer, with the difference that the cross section is constant. The acceptance for the kth mass interval m_k is then, corresponding to the basic theorem of Monte Carlo integration:

$$Acc_K(\Delta m) = \lim_{N \to \infty} \frac{M}{N} \Delta\Omega \cdot \Delta m \cdot \frac{\partial k}{\partial p} \frac{\Delta p}{k} \frac{\Delta\Omega^*}{4\pi} \frac{3}{2} \sin^2\theta_\pi^* \; p^2 \cdot f'(p) \cdot f_T \qquad (5.19)$$

N is the number of the resonances simulated by the computer in $\Delta\Omega$, Δm, Δp, for which the positive decay pion is emitted in the center of mass solid angle Ω_π^* . M gives the number of successful attempts in which both decay pions are accepted.

The Monte-Carlo integration was carried out on the IBM 360-75 computing system. The program selects a point of production $\vec{r}$ in the target volume covered by the γ-beam of (2 x 2 x thickness) cm^3 as a triplet of random numbers. Using further random numbers the resonance acquires a momentum p, a mass m and two angles from the prescribed intervals Δp, Δm, $\Delta\Omega$. Random angles from $\Delta\Omega_\pi^*$ are allotted to the positive decay pion in the center of mass system of the particle so produced. The angle and momentum of the decay pions are transformed back to the laboratory system. After transformation to a coordinate system referred to the nominal spectrometer trajectory which is suitable for the problem, the π^+ is passed through the spectrometer in accordance with the magnet transport equations. If it does not collide with any aperture boundary, i.e. it passes all triggerable counters and does not touch any screen or magnet wall, the hodoscope combination which is encountered is stored and the other decay pion is put through the spectrometer in a similar manner. If this is also accepted the functional determinants all weighting functions, and the acceptance are calculated, as well as the mass and momentum of the pair with which the hodoscope combination encountered is identified, using the quantities $\langle p_\pi \rangle$. $\langle \theta \rangle$, $\langle \varphi \rangle$ from the previously described program.

The pions may be scattered and decay during transit through the spectrometer. Hence scattering processes are simulated at particular points of the particle trajector (target, counters) by subprograms. The multiple scattering angles are assumed normally distributed with the variance

$$\langle \theta_s^2 \rangle = \left(\frac{21\ \mathrm{MeV}}{p \cdot \beta} \right)^2 \frac{X}{X_0} (1-\varepsilon)^2$$

X_o is the radiation length of the material traversed. ε is a correction quantity depending on the velocity $v = \beta . c$, and varies from 0 to 0.08.

Each pion has allotted to it a decay length by the random number generator in accordance with its Lorentz factor γ. After traversing this length the momentum and angle change in accordance with the decay kinetics of

$$\pi \rightarrow \mu + \nu$$

Since each event contains two pions which can decay independently, in the most unfavorable case 25% of the events display at least one decay. However, less than half of these are accepted.

Both processes cause a "smearing" of the mass values. The observed events in the interval $(m, m + \Delta m)$ thus contain a small contribution due to pairs of a different mass, for which the relative abundance is given by $2m.R(m)$. The probability for the occurrence of a given mass value m is allowed for by weighting each pair of original mass m_i which encounters the hodoscope combination for mean mass m_c with the factor

$$K_i = \frac{2m_i \cdot R(m_i)}{2m_c \cdot R(m_c)}$$

This has the mean value 1, if both of the disturbing effects did not exist. The mass distribution $2m.R(m)$ from eq. (5.10) with the values $m_o = 770$ MeV/c^2 and $\Gamma_o = 140$ MeV/c^2 was used. It should be emphasized that this does not represent any a priori introduction of the mass distribution. A relatively rough knowledge of the distribution is sufficient, since only the correction to the acceptance by multiple scattering and decay are calculated with its help, by replacing M in eq. (5.19) by $\sum_{i=1}^{M} K_i$.

The mass resolution was determined with the Monte-Carlo program and amounts to about 1.5%. The acceptance was hence calculated for step sizes of $\Delta m = 10\ \mathrm{MeV}/c^2$ at a time and all hodoscope combinations with mass values in the interval $(m, m + \Delta m)$ were combined. Hence one obtains finally the relation between observed pairs in the kth mass interval and the weighted cross-section:

$$\frac{1}{p^2 \cdot f'(p) \cdot f_T} \; \frac{d^2\sigma}{d\Omega\, dm} = \frac{1}{N_T \cdot Q_{eff}} \; \frac{N_K(\Delta m)}{Acc_K(\Delta m)} \qquad (5.20)$$

The calculation of the acceptance in t-intervals proceeds quite analogously allowing for the relation

$$\frac{\partial t}{\partial \Omega} = \frac{p \cdot k}{\pi}$$

which follows from eq. (5.3). The acceptance of the kth t-interval is :

$$Acc_K(\Delta t) = \lim_{N \to \infty} \frac{M'}{N} \frac{\partial t}{\partial \Omega} \Delta\Omega\, \Delta m \frac{\partial k}{\partial p} \frac{\Delta p}{k} \frac{\Delta \Omega^*}{4\pi} \frac{3}{2} \sin^2 \theta_\pi^* \cdot f'(p) \qquad (5.21)$$

In this case also the factor $3/2\ \sin^2\theta^*_\pi$ is contained in the acceptance, and makes allowance for the decay angle distribution.

In fact $M' = \sum_1^M K_i$ where the weighting factor to allow for decay and multiple scattering is in this case:

$$K_i = \frac{f_T(R, t_i, \sigma_{\rho N})}{f_T(R, t_l, \sigma_{\rho N})}$$

t_i is the original momentum transfer for an event, t_l the mean value of the interval $(t, t + \Delta t)$. The function f_T is used with the values $R = 1.2 . A^{1/3}$ [fermi] and $\sigma_{\rho N} = 31$ mb. Just as in the mass distribution function $2m.R(m)$, a rough approximation for f_T will suffice, since the correction is being applied to what is already an error quantity. Then :

$$\frac{1}{f'(p)}\ \frac{d^2\sigma}{d|t|} = \frac{1}{N_T \cdot Q_{eff}}\ \frac{N_k(\Delta t)}{Acc_k(\Delta t)} \qquad (5.22)$$

An exact knowledge of the magnet transport equations was particularly important for the Monte-Carlo integration. Because of the size of the accepted momentum range it was not possible to use transport theory either in first or second order. The transport equations were obtained by numerical integration of a bundle of 40 trajectories through the mesh of the measured magnetic field values. The coefficients of the equations are obtained by fitting to the calculated trajectories by the method of least squares. The transport equations contain all terms which are linear, bilinear and quadratic in the coordinates x, x', z, z' and $\delta p/p$, with the exception of those which are symmetrically degenerate[42], and also terms up to 4th order in

$$\frac{\delta p}{p} \quad \frac{1}{(1+\frac{\delta p}{p})}$$

These coefficients agree well with those of theory in first and second order. All deviations can be ascribed to the greater accuracy of this calculation in fourth order. In particular the focusing properties of the scattering field of the magnet are better described.

5.5 Data reduction and evaluation

At the end of each experimental run the data from all counters are printed out. The corrections introduced in the previous chapter were obtained from them and applied to the quantameter charge according to (4.1), The contents of the data tapes are transferred to the library tape in a compressed form. The program "Mass Analysis" in each case looks up the desired experimental run corresponding to the numerical code on the library tape and the appropriate sets of data cards of the kinematic quantities for the single arm Monte-Carlo program and the acceptances of the double arm program. Then the event numbers of the hodoscope combinations are read successively from the tape and their momentum, momentum transfer to target and mass are computed. The events are sorted according to the mass interval of the acceptance calculation. In order to obtain the complete mass spectrum $2m.R(m)$ the sum of all events $E(i,j,k)$ of hodoscope combination i in run j, insofar as they lie in the mass interval ($m_k \pm 5$ MeV/c^2), are divided by the appropriate acceptance summed over j so that:

$$\frac{\sum_j \sum_i E(i,j,k)}{\sum_j N_T(j)\; Q_{eff}(j)\; Acc(j,k)} = \frac{1}{\langle p^2 f'(p)\; f_T(R,t,\sigma_{\rho N})\rangle} \frac{d^2\sigma}{d\Omega dm}$$

where $Q_{eff}(j)$ already contains all the corrections. The curves for the t dependence are obtained analogously; K denotes in this case membership of an interval Δt, but the acceptance values have a different mean here in accordance with eq. (5.21).

6. MEASUREMENTS AND RESULTS

6.1 Dependence of the cross section on target nucleus

In order to investigate the dependence of ρ^o photoproduction on atomic number A of the target material the counting rate in the three symmetrical spectrometer positions:

(θ_o, P_o) = (15°, 1350 MeV/c), (11°, 1750 MeV/c), (9.5°, 2250 MeV/c)

was measured for the elements Be, C, Al, Cu, Ag, Pb. They correspond to mean ρ^o momenta of about p = 2.7; 3.5 and 4.5 GeV/c and embrace the mass interval $720 < m < 820$ MeV/c^2.

Table 6.1 gives the measured numbers of π pairs per 1 g /cm^2 and 10^{12} effective gamma quanta. Since the acceptance is the same for all targets except for multiple scattering effects amounting to less than 1%, the ratio of the numbers corresponds to the quotient of the cross sections per nucleon $(1/A)(d\sigma/d\Omega)$. These are normalized to beryllium in Table 6.1 and shown graphically in Figure 14.

The data points first increase with increasing mass number A and then fall off again. The values themselves depend very strongly on the production momentum, or more strictly on the minimum momentum transfer associated with it.

It is exactly this behavior which is described by the diffraction dissociation model in equations (1.9) and (1.10). The ratio of the effective cross sections is then given by the function

$$F_{TA}\,(R\,,\langle t\rangle,\,\sigma_{\rho N}) \quad = \quad \left|\frac{g_T(R\,,\langle t\rangle,\,\sigma_{\rho N})}{g_T(R_{Be},\langle t\rangle_{Be},\sigma_{\rho N})}\right|^2 \qquad (6.1)$$

which depends only on the parameters r_o and $\sigma_{\rho N}$. The unknown magnitude of the forward production amplitude at a nucleon $\langle f\rangle$ is not present in the quotient.

$\langle t\rangle$ is the mean value of the momentum transfer in the accepted range, weighted by the function f_T from eq. (5.14), which is different for all elements.

$$\langle t\rangle \quad = \quad \int_{t_{min}}^{t_{max}} t\cdot f_T\, dt \Big/ \int_{t_{min}}^{t_{max}} f_T\, dt$$

$\langle t\rangle$ decreases by 9% from beryllium to lead. The mean momentum transfer for the production in carbon $\langle t_c\rangle$ is introduced in Table 6.1 as the typical value.

The curves sketched in Figure 14 give the best fit of the function F_{TA} to the measured data. In all three cases the value of χ^2 is comparable with the number of degrees of freedom DF, i.e. the hypothesis F_{TA} is acceptable. The fit is sensitive to variation of the value $\sigma_{\rho N}$ and less sensitive toward r_o. Overall the best fits are

$$\sigma_{\rho N} = 31.3 \pm 2.3 \text{ mb} \quad \text{and} \quad r_o = 1.29 \pm 0.09 \text{ f.}$$

Table 6.1

Kinematic Conditions	Element	A	$\frac{\pi\text{-pairs}}{g/cm^2 \cdot 10^{12} Q_{eff}}$	$\left(\frac{1}{A}\frac{d\sigma}{d\Omega}\right) / \left(\frac{1}{9}\frac{d\sigma}{d\Omega}\right)_{Be}$
p_s = 2.7 GeV/c	Be	9.01	12.92	1.000 ± .026
$\langle t_c \rangle$ = .0129 GeV^2/c^2	C	12.01	15.25	1.181 ± .034
k_0 = 4.35 GeV	Al	26.98	19.67	1.523 ± .041
p_0 = 1350 MeV/c	Cu	63.54	18.70	1.447 ± .043
θ_0 = 15°	Ag	107.88	15.66	1.212 ± .038
	Pb	207.20	10.77	0.834 ± .037
p_s = 3.5 GeV/c	Be		41.15	1.000 ± .050
$\langle t_c \rangle$ = .0104 GeV^2/c^2	C		49.56	1.204 ± .061
k_0 = 6.02 GeV	Al		64.44	1.566 ± .078
p_0 = 1750 MeV/c	Cu		73.93	1.797 ± .090
θ_0 = 11°	Pb		63.81	1.551 ± .124
p_s = 4.5 GeV/c	Be		53.75	1.000 ± .026
$\langle t_c \rangle$ = .007 GeV^2/c^2	C		63.78	1.187 ± .030
k_0 = 6.00 GeV	Al		99.45	1.850 ± .048
p_0 = 2250 MeV/c	Cu		118.58	2.206 ± .057
θ_0 = 9.5°	Ag		121.93	2.268 ± .059
	Pb		98.06	1.824 ± .057

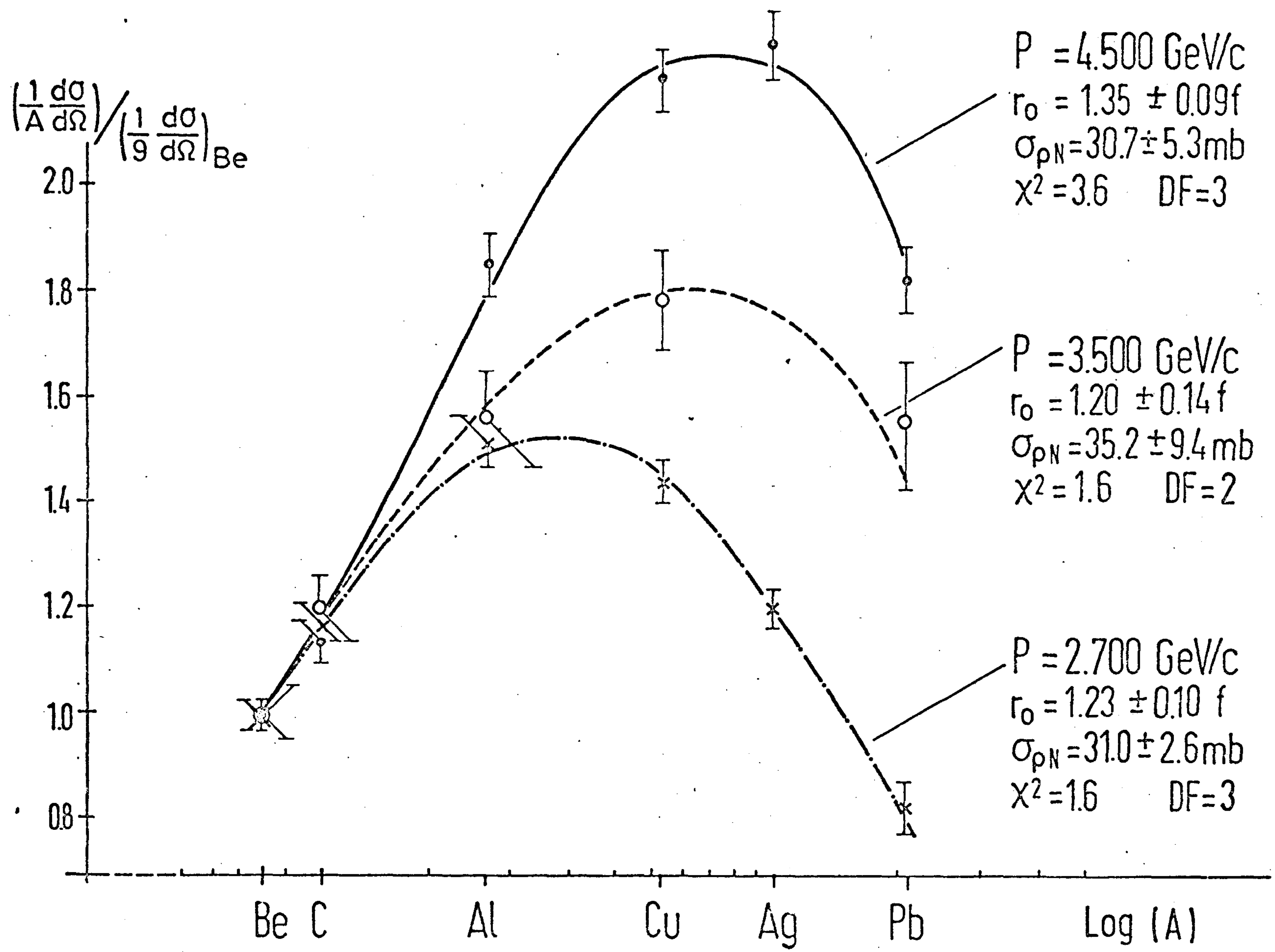

Figure 14. Relative A-dependence of ρ^0 photoproduction

Abb.14 Relative A-Abhängigkeit der ρ^0-Photoproduktion

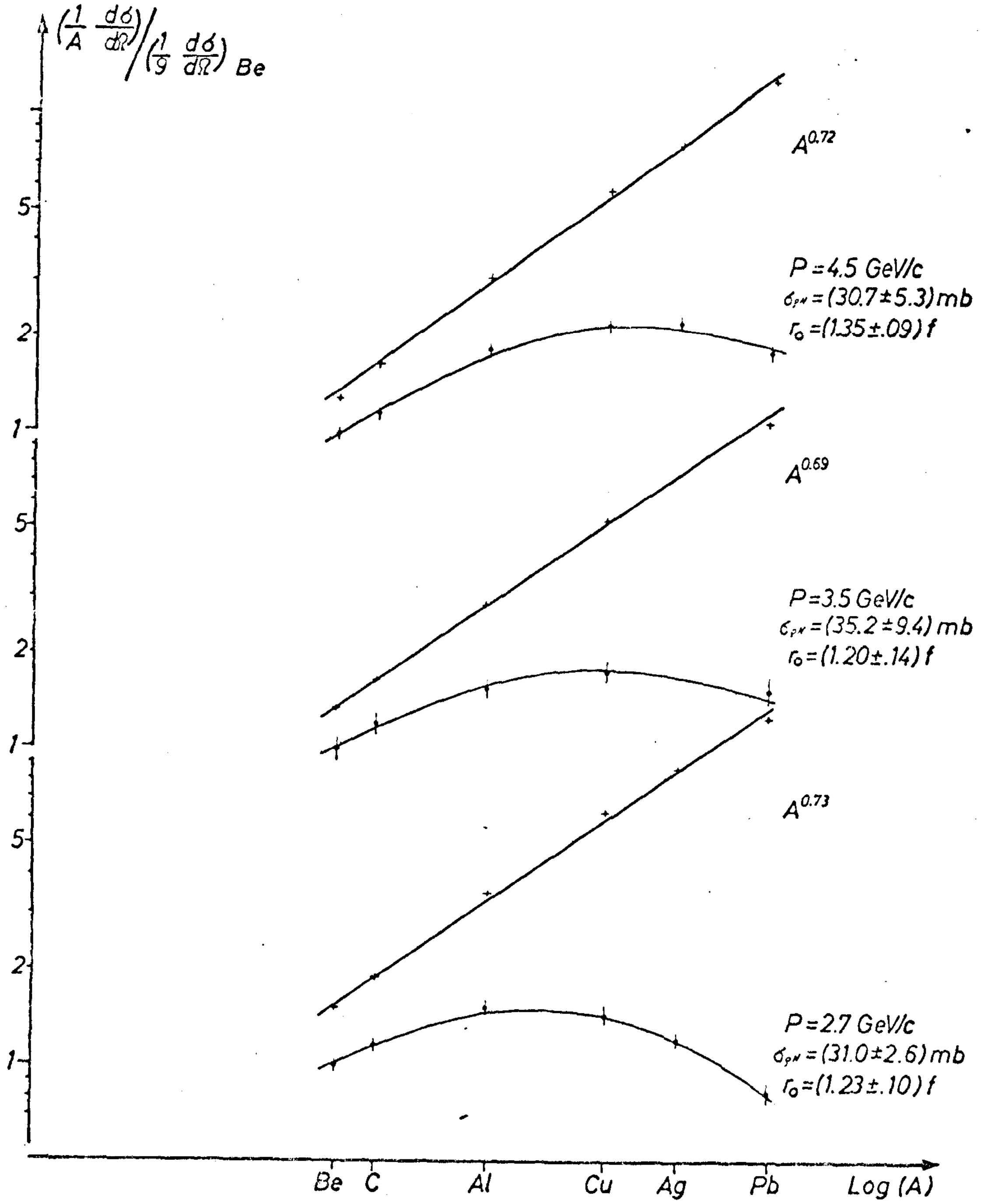

Figure 14b Relative A-dependence of ρ^0 production from Figure 14a with extrapolated behavior for $t \longrightarrow 0$

- ɸ measured values
- \+ values extrapolated to $t \longrightarrow 0$ by means of F_{TA} (R, t, $\sigma_{\rho N}$)

Let us examine the situation more closely. One would expect that according to the type of production process and the strength of the absorption the following approximate dependences on A would obtain :

Nucleus A \ Process	Coherent	Incoherent
Dense	$A^{4/3}$	$A^{2/3}$
Transparent	A^2	A

The behavior of the data points cannot be explained at all on the assumption of an incoherent production process, the cross section per nucleon would be at best constant. As the momentum increases and the minimum momentum transfer decreases as a consequence the curves become steeper and flatter. It is possible to decide upon the asymptotic behavior for $t_{min} \longrightarrow 0$, which implies production at very high momenta $p \longrightarrow \infty$, by extrapolating the fitted curves to $t = 0$ by means of $F_{TA}(R, t, \sigma_{\rho N})$. This is shown in Figure 14b. The agreement of the three extrapolations gives a further justification of the method used. The straight lines which are drawn in give the mean increase $\simeq A^{0.7}$. (Strictly speaking $F_{TA}(R, 0, \sigma_{\rho N})$ has no clear power dependence on A for finite $\sigma_{\rho N} \neq 0$). Since these values are referred to a nucleon, one obtains for production at the whole nucleus a behavior as $A^{1.7}$, which implies a coherent production process at a "gray" nucleus.

6.2 Dependence of the cross section on the momentum transfer

The behavior of the cross section as a function of the invariant momentum transfer $t = (k - p)^2$ was investigated in the elements C, Cu, Pb for a mass interval of 720-820 MeV/c. In this study use was made of the property of the spectrometer by which for an emission angle $\theta_o^{\pm} = 15^o$ for π^+ and π^- the magnet MD which is common to both particles is switched off so that the nominal momenta p_o^+ and p_o^- of both arms could be adjusted independently of one another.

Using a brems-spectrum of maximum energy $k_o = 4.35$ GeV measurements were made with θ_o fixed at 15^o and the momentum adjustments

(p_o^+/p_o^-)=(1350/1350),(1250/1450),(1100/1600),(1000/1700) MeV/c

as well as with corresponding adjustments of the opposite polarity, in which cases the accepted mass and momentum ranges remained constant. These adjustments cover in overlapping ranges production angles of $\delta = 0\text{-}6^o$ and momentum transfers t of 0.009-0.06 $(\text{GeV/c})^2$.

The smallest momentum attainable with p = 2.7 GeV/c for ρ^o mesons

$$|t_{min}| \approx \left(\frac{m_o^2}{2p}\right)^2 = 0{,}009 \quad (\text{GeV/c})^2$$

is for lead still very close to the first "diffraction minimum" at $|t_o| \cong 0.011\ (\text{GeV/c})^2$ (see Figure 13). Lower $|t|$ - values can only be obtained with higher values of the momentum p. These were measured with the symmetrical adjustment $\theta_o = 9.5^o$, $p_o = 2250$ MeV/c, which covers the same mass interval. However, the addition of these data points requires a knowledge of the p dependence of the cross section. This is obtained empirically from the data of A. Citron et al.[40] for π-scattering in the region $1 < p_\pi < 3$ GeV/c. One thus obtains an approximation for eq. (5.11)

$$f'(p_\rho) = \frac{p_\rho}{E_\rho} \left(1 + \frac{.91\ \text{GeV/c}}{p_\rho}\right)^2 \qquad (6.2)$$

Figures 15a, b, c represent the cross sections $\frac{1}{f'(p)} \frac{d\sigma}{d|t|}$ weighted by $f'(p)$ as functions of $|t|$ for C, Cu and Pb from Table 6.2. The points identified by $J_1 = 0$ would correspond to the first diffraction minimum, i.e. the null point of the Bessel function $J_1(R\sqrt{-t}) = 0$ at $R.\sqrt{-t_o} = 3.83$, for diffraction at a dense sphere of radius $R = 1.2.A^{1/3}$ [fermi].

For small momentum transfers $|t| \ll |t_o|$ eq. (5.13) holds

$$\frac{d\sigma}{d|t|} \sim e^{a(A)t}$$

The quantity a(A) was obtained by a least square error fit to the points up to $|t_o|/2$ and yielded:

$$\begin{aligned} a(C) &= (\ 47 \pm 3)(GeV/c)^{-2} \\ a(Cu) &= (139 \pm 7)(GeV/c)^{-2} \\ a(Pb) &= (290 \pm 12)(GeV/c)^{-2} \end{aligned}$$

These values are consistent with $a(A) = 9.0\ A^{2/3}$. Within the diffraction-dissociation model the function $f_T(R, t, \sigma_{\rho n})$ (eq. 5.14) describes the behavior of the $|t|$-dependence. It was further assumed that the measured data contains a small background with the $|t|$-dependence of a single nucleon $\simeq e^{10t}$. $\sigma_{\rho n} \simeq 31$ mb is already known from the previous measurement. The best fit of the function

$$D_1(A)\cdot f_T(R,t,31mb) + D_2(A)\ e^{10t}$$

to the measured values of

$$\frac{1}{f'(p)}\frac{d\sigma}{d|t|}$$

is shown in Figures 15 a, b, and c and yielded the values

$$\begin{aligned} r_o(C) &= (1.30 \pm 0.07)\ f & D_1(C) &= (\ \ 8.97 \pm 0.8)\frac{mb}{(GeV/c)^2\ Atom} \\ r_o(Cu) &= (1.30 \pm 0.08)\ f & D_1(Cu) &= (161.6 \pm 14.2)\quad '' \\ r_o(Pb) &= (1.28 \pm 0{,}08)\ f & D_1(Pb) &= (1078. \pm 121.2)\quad '' \end{aligned}$$

Table 6.2

$-t$ $[GeV/c]^2$	Cross sections : $\frac{1}{f(p)}\frac{d\sigma}{d\|t\|}$ $\left[\frac{10^{-25}\ cm^2}{GeV^2/c^2 \cdot Atom}\right]$ Carbon	Copper	Lead
.004 - .005			3.58 ± .78
.005 - .006			2.44 ± .13
.006 - .007			2.139 ± .083
.007 - .008			1.703 ± .059
.008 - .009			1.143 ± .051
.009 - .010	.0718 ± .0083	.462 ± .061	.843 ± .053
.010 - .012	.0588 ± .0020	.382 ± .015	.669 ± .025
.012 - .014	.0573 ± .0020	.298 ± .013	.487 ± .023
.014 - .016	.0469 ± .0029	.202 ± .015	.297 ± .024
.016 - .018	.0431 ± .0042	.198 ± .021	.270 ± .030
.018 - .020	.0407 ± .0042	.1566 ± .0176	.1877 ± .0250
.020 - .022	.0327 ± .0036	.0896 ± .0127	.1667 ± .0239
.022 - .024	.0327 ± .0038	.0745 ± .0116	.1679 ± .0252
.024 - .028	.0262 ± .0022	.0471 ± .0055	.1367 ± .0145
.028 - .032	.0218 ± .0020	.0443 ± .0049	.0975 ± .0115
.032 - .036	.0199 ± .0019	.0361 ± .0042	.1014 ± .0109
.036 - .040	.0152 ± .0017	.0280 ± .0036	.0566 ± .0077
.040 - .044	.0153 ± .0019	.0315 ± .0041	.0603 ± .0080
.044 - .048	.0137 ± .0023	.0386 ± .0062	.0772 ± .0120
.048 - .052	.0107 ± .0022	.0325 ± .0060	.0482 ± .0096
.052 - .056	.0069 ± .0017	.0278 ± .0054	.0401 ± .0086
.056 - .060	.0081 ± .0024	.0294 ± .0075	.0642 ± .0153
.060 - .064	.0030 ± .0014	.0149 ± .0051	.0346 ± .0105
.064 - .068	.0115 ± .0050	.0332 ± .0137	.0683 ± .0270

The values do not contain any correction for background (cf.Figure 17).
Only the statistical errors are given.

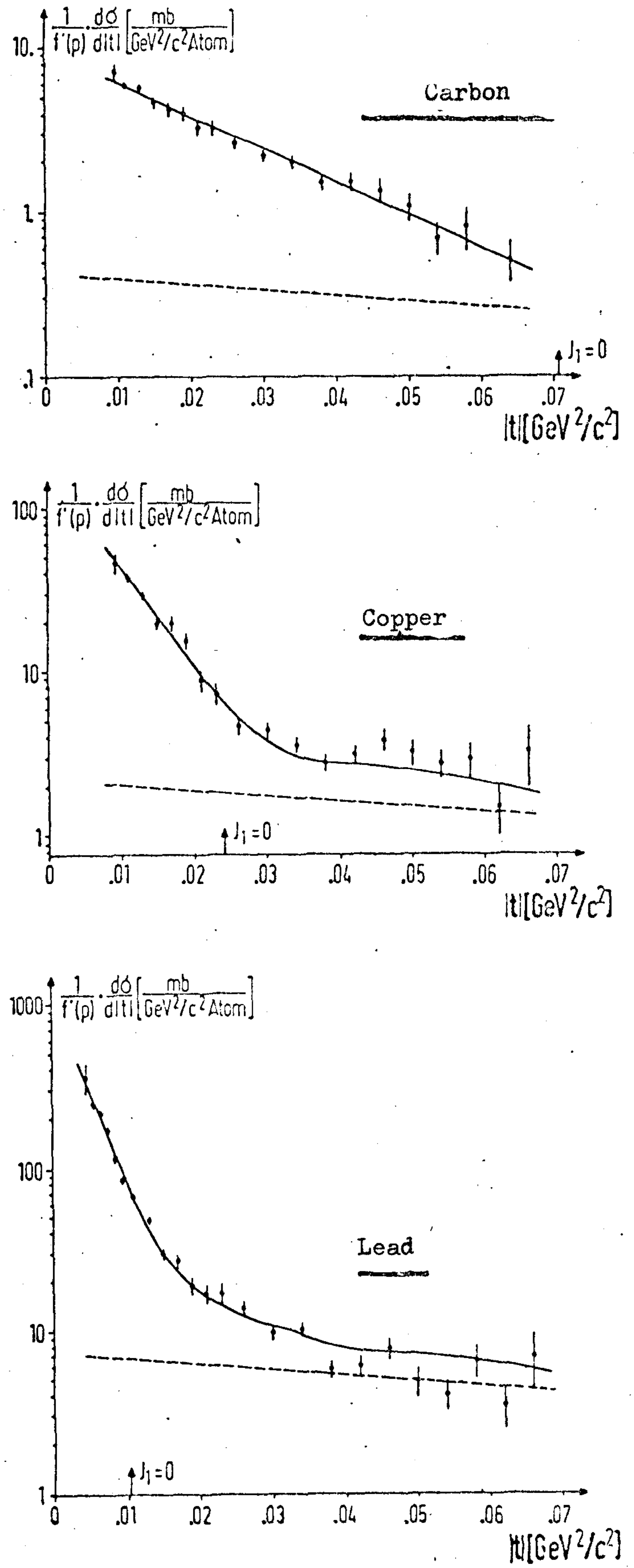

Figure 15. Differential cross section as a function of the momentum transfer $|t|$

Abb. 15 Differentieller Wirkungsquerschnitt als Funktion des Impulsübertrags $|t|$

The value $D_2(A) = 0.035.A(mb/GeV^2/c^2.Atom)$ was used simultaneously for all three curves. The value of r_o agrees well with the value found previously, so that the function $f_T(R, t, \sigma_{\rho N})$ is now completely known.

Since $f'(p)$ tends to the value 1 as the momentum increases the value $D_1(A)$ can be taken as the effective cross section for the diffractive component in the limit of very high energies.

6.3 Dependence on momentum

The momentum dependence was determined for a maximum gamma energy of $k_o = 6.00$ GeV in the following spectrometer configurations

$$(\theta_o/p_o) = (17.2^o/1200MeV/c),(15^o/1400MeV/c),(12.8^o/1579MeV/c),(11^o/2100MeV/c).$$

These cover the momentum range from 2.5 to 4.5 GeV/c. At the same time the momentum transfer changes from $0.015 > |t| > 0.006\ (GeV/c)^2$ with a knowledge of the function f_T it is possible to study the dependence of the cross section on the momentum $\vec{p}$ of the ρ^o meson.

The measurements were carried out on carbon since f_T changes very little in this case and only events from the mass interval $750 < m < 780\ MeV/c^2$ were analysed in order to exclude the effects of mass distribution.

The formula for the cross section

$$\frac{d\sigma}{d\Omega} = C(A) \cdot p^2 \cdot f'(p) \cdot f_T(R,t,\sigma_{\rho N}) \tag{6.3}$$

is verified in Figure 16 in the form

$$\frac{1}{p^2 f'(p)\ f_T(R,t,\sigma_{\rho N})}\ \frac{d\sigma}{d\Omega} = \text{Constant}$$

The same momentum dependence is found as in pion nucleon scattering.

6.4 Mass spectra

As described in Section 5.1 the mass spectra were determined with a fixed momentum configuration p_o in both arms and varying the nominal angle $\theta_o^+ = \theta_o^-$. In each case the following angle configurations were used to determine a mass spectrum :

$$\theta_o = 4^\circ,\ 5.5^\circ,\ 6.8^\circ,\ 8^\circ,\ 9.5^\circ,\ 11^\circ,\ 12{,}8^\circ,\ 15^\circ \text{ and } 17.2^\circ.$$

These are so chosen that the mass ranges overlap well (see Figure 9a).

The measured counting rate for a spectrometer adjustment corresponds to the cross section integrated over the acceptance in each case, and in accordance with eq. (5.15) we can put for this

$$\frac{d^2\sigma}{d\Omega dm} = C(A) \cdot p^2 \cdot f'(p) \cdot f(R,t,\sigma_{\rho N}) \cdot 2m \cdot R(m) \tag{6.3}$$

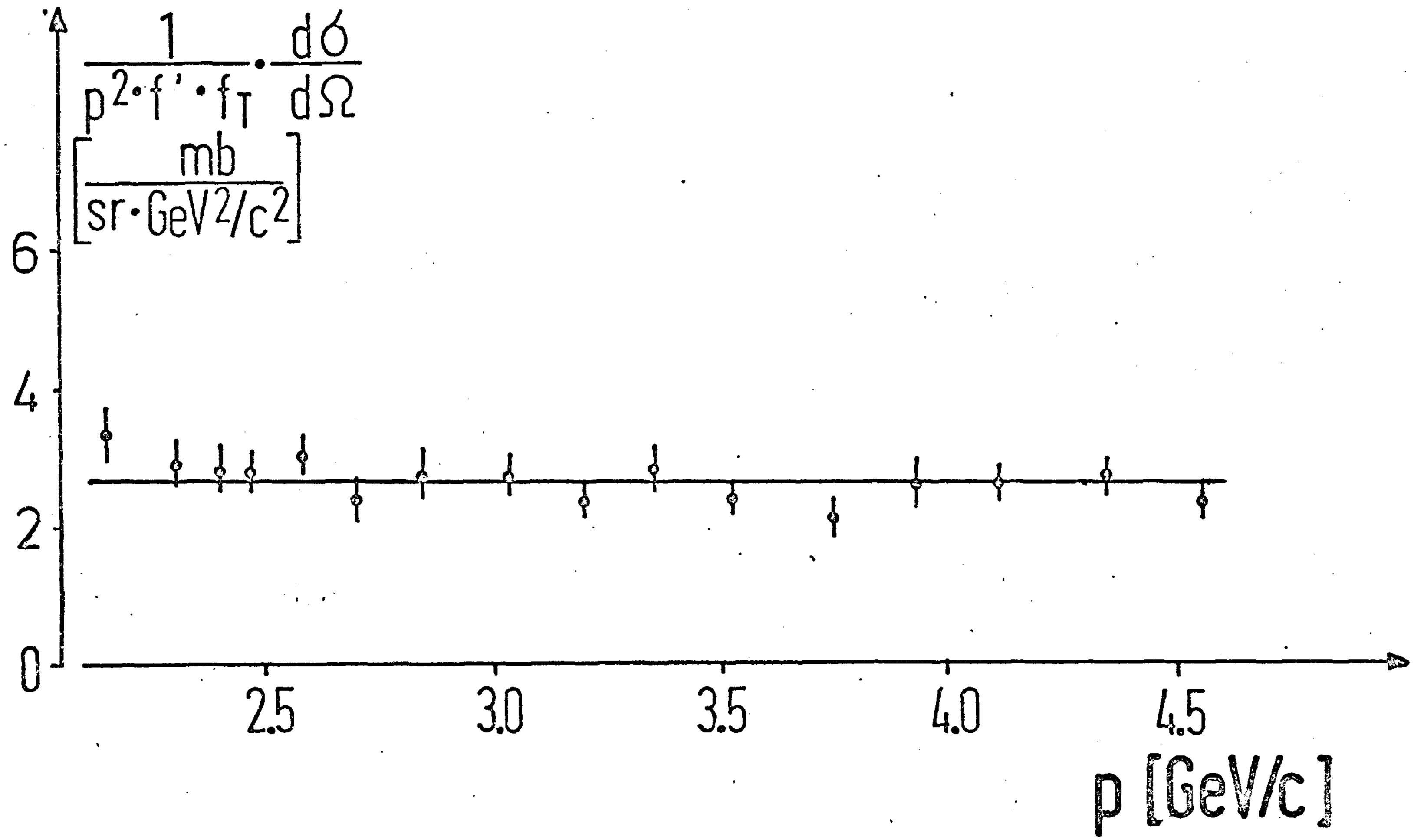

Abb.16 Verifikation der Impulsabhängigkeit

Figure 16. Verification of the momentum dependence.

Here the mass distribution function

$$R(m) = \left(\frac{m_o}{m}\right)^4 \frac{1}{\pi} \frac{m_o \, \Gamma(m)}{(m_o{}^2 - m^2)^2 + m_o{}^2 \Gamma^2(m)}$$

contains in the energy-dependent width of a resonance for a spin 1 particle decaying into two spin o particles, first proposed by J.D. Jackson[38] :

$$\Gamma(m) = \frac{m_o}{m} \cdot \Gamma_o \cdot \left[\frac{(m/2)^2 - m_\pi^2}{(m_o/2)^2 - m_\pi^2}\right]^{3/2}$$

the particle properties of interest, namely the mass m_o and width Γ_o of the ρ^o meson.

Since $f'(p)$ and $f_T(R, t, \sigma_{\rho N})$ are already known

$$\frac{1}{p^2 f'(p) f_T(R, t, \sigma_{\rho N})} \quad \frac{d\sigma}{d\Omega dm} = C(A) \cdot 2\, m \cdot R(m),$$

so that the measurements can be combined into a mass spectrum as in the case of eq. (5.20).

The spectra obtained in this way are shown in Figure 17a for carbon at $p = 3.158$ GeV/c, $k_o = 4.35$ GeV and in Figures 17b, c, d for $p = 4.500$ GeV/c $k_o = 6.00$ GeV in carbon, copper and lead. The units are

$$\left[\frac{nb}{(GeV/c)^2 \, MeV/c^2 \, sr.Atom}\right]$$

The function

$$G(m) = C_1(A) \cdot 2m\ R(m) + C_2 \cdot B(m)$$

was fitted to the measured data, minimizing χ^2 by varying the parameters m_o, Γ_o, $C_1(A)$ and C_2. $B(m)$ is a phenomenological function for the background in powers of m. This involves a certain amount of arbitrariness; it appears, however, that the fitted values of m_o, Γ_o, $C_1(A)$ depend to a very small extent on the detailed form of $B(m)$. $G(m)$ and $C_2B(m)$ are sketched in each of the Figures 17a, b, c, d. Because the ρ^o production is coherent the relative background becomes less evident as A increases and the spectra become more symmetrical. The spectrum in lead should therefore in practice be to a large extent undistorted and should represent the particle properties of the ρ^o meson best:

The mass $\quad M_o = 765 \pm 5\ \mathrm{MeV/c^2}$ and
The width $\quad \Gamma_o = 130 \pm 5\ \mathrm{MeV/c^2}$.

The cross sections for ρ^o forward production are then determined according to formula (6.3) as

$$C_1(C) = (\ 2.37 \pm .33)\ \frac{\mathrm{mb}}{\mathrm{sr}\cdot(\mathrm{GeV/c})^2}$$

$$C_1(Cu) = (\ 46.0 \pm 6.4)\ \frac{\mathrm{mb}}{\mathrm{sr}\cdot(\mathrm{GeV/c})^2}$$

$$C_1(Pb) = (287.5 \pm 48.8)\ \frac{\mathrm{mb}}{\mathrm{sr}\cdot(\mathrm{GeV/c})^2}\ ,$$

which are obtained by fitting the function $G(m)$. If (5.15) is integrated with respect to m, then one obtains from the measurements at $p = 4.5$ GeV/c and $\delta \simeq 0.5^{\circ}$ the differential cross sections

$$\frac{d\sigma}{d\Omega}(C) = (5.0 \pm .4)\ \frac{\text{mb}}{\text{sr.Nucleon}}$$

$$\frac{d\sigma}{d\Omega}(Cu) = (11.2 \pm 1.1)\ \frac{\text{mb}}{\text{sr.Nucleon}}$$

$$\frac{d\sigma}{d\Omega}(Pb) = (10.0 \pm 1.0)\ \frac{\text{mb}}{\text{sr.Nucleon}}\ .$$

The values in carbon and copper are in good agreement with the measurements done at CEA[15] of (5.17 ± 0.07) and $(10.5 \pm 0.2)\ \frac{\text{mb}}{\text{sr. Nucleon}}$ respectively.

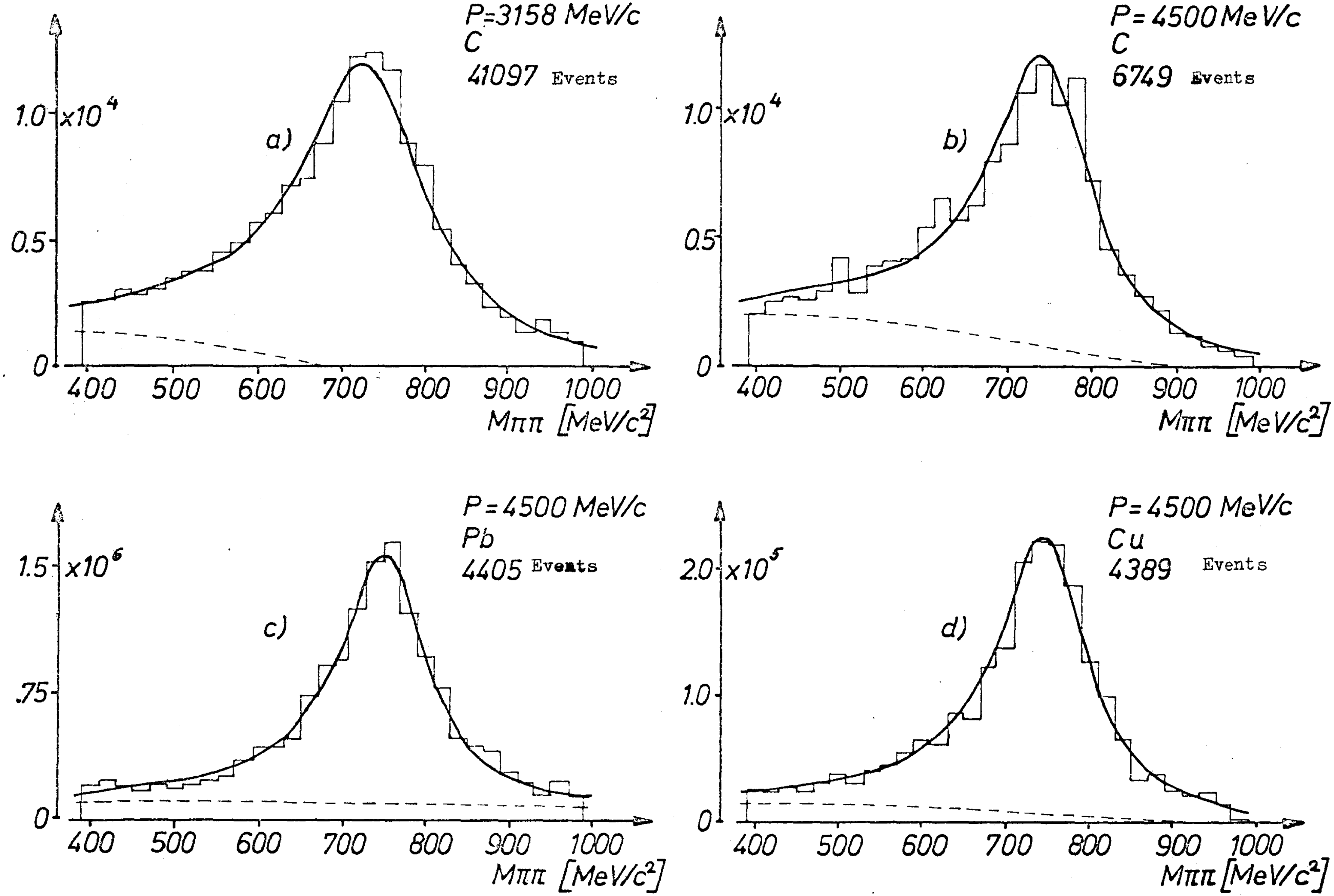

Abb.17 Massenspektren

Figure 17. Mass spectra

7. RESULTS FOR THE φ-MESON

7.1 Measurement methods and changes in the apparatus

The φ-meson was detected in the decay into two charged K-mesons

$$\phi \longrightarrow K^{+} + K^{-}$$

which according to A.H. Rosenfeld[11] occurs with a frequency of (48 $\pm$ 3)%

The symmetrical spectrometer configuration $\theta_o = 2.8^o$ and $p_o = 2600$ MeV/c covers a range of invariant masses m of K-pairs $1000 < m < 1060$ MeV/c^2. The momentum was chosen high since $K^{\pm}$ mesons decay relatively rapidly with $\tau = 12.36$ ns. It was found by a Monte-Carlo method that under these conditions (15.10 $\pm$ 0.17)% of all K-pairs reach the final counter without decaying. (2.5 $\pm$ 0.2)% are registered as pair events, in spite of decay, where the program follows the charged particles from the decays $K \longrightarrow \mu + \nu$ and $K \longrightarrow \pi + \pi^o$. Multiple scattering in target and spectrometer together with decay bring about a mass resolution for the apparatus of $\simeq 10.5$ MeV/c^2.

The essential change in the apparatus consisted in using the threshold Čerenkov counters RC and LC to suppress electrons, μ mesons and pions. For this purpose they were filled with Freon C-318 (C_4F_8)

which has a high refractive index $n = (1 + 12.85 \times 10^{-4})$ at normal pressures. The signals from these counters were combined in an "OR"-gate, the output from which acts as a veto signal on the coincidences X1, X2, Y1, Y2 (see Figure 5). If RC or LC fired, the event was not recorded. The discharge probability $(1 - \varepsilon)$ of the counter for π mesons was $> .98$. Together with the "OR" trigger condition this represents a π-suppression of $\varepsilon^2 < 4 \times 10^{-4}$. This is sufficient since the ratio of K to π pairs was 3.5×10^{-2} in unfavorable cases. K pairs which produce an impact electron with an energy > 10 MeV/c^2 in one of the Čerenkov counters are not counted. The loss was estimated at 4% in good agreement with other measurements[45].

Acceptance calculations, data evaluation experimental tests and corrections were carried out as in the case of the ρ^0 meson; the nuclear absorption was calculated on the assumption of mean cross sections $\sigma(K^+p) \simeq 18.0$ mb and $\sigma(K^-p) \simeq 27.7$ mb in the region $2.2 < p < 3.2$ GeV/c.*)

---

* No previous measurements were available on the total cross section $\sigma(KA)$ on nuclei A, so that assumptions had to be made. With $\sigma(K^+A) \simeq \sigma(K^-A) \simeq \sigma(\pi A)$ one would obtain values for the cross sections 14% higher than those given below.

7.2 Measurement of ϕ-photoproduction

1000 events were recorded in each of the target materials (Be, Al, Cu, Ag, Pb) and 8000 in C and 130 in Ta, using a fixed spectrometer adjustment of $\theta_o = 2.8^o$ and $p_o = 2600$ MeV/c.

The targets used are shown in Table 7.1.

Table 7.1

Material	Be	C	Al	Cu	Ag	Ta	Pb
Purity (%)	99.99	99.8	96.7	99.9	99.99	99.9	99.9
Thickness (mm)	15.8	15.2	4.98	1.03	1.01	.44	.53
Thickness (g/cm^2)	2.853	2.516	1.363	.910	1.056	.692	.522

Al and C were corrected as described in Section 3.3.

All events in this experiment were recorded by the subcomputing unit PDP-8 in parallel with the data tape unit and the event distribution in the individual hodoscopes was displayed on a screen as a histogram. The data are transferred into the main IBM 360-75 computer system by a recall command and analysed by means of the acceptance values stored there. The result, the mass distribution, is returned to the PDP-8 and displayed on the screen. This system allows a continuous supervision of the experiment and a preliminary analysis of the data. The function and construction are described in detail by H. Frese[41].

In the final evaluation the measurements were corrected for dead time, accidental coincidences as well as zero target measurements (< 10%) for each hodoscope combination. Table 7.2 shows the cross sections $\frac{d^2\sigma^o}{d\Omega dm}$ for the photoproduction of almost symmetrical K-pairs of different charge. The error quoted is composed of the statistical contributions from the events, Monte-Carlo tests and normalized zero-target rates.

K-pair masses of $1025 < m < 1100$ MeV/c^2 were measured in carbon, copper and lead with the configuration $\theta_o = 4^o$, $p_o = 2600$ MeV/c in order to ascertain the relative magnitude of the background. The mass spectra obtained are shown in Figure 18. They all show the ϕ meson very clearly as a peak in the spectrum at 1019 MeV/c^2, but of course the mean observed width of $\simeq$ 12 MeV/c^2 is largely due to the apparatus. If a gaussian distribution is assumed for the resolution curve with half width value 10.5 MeV/c^2 then

$$m_\phi = 1019 \pm 1 \text{ MeV}/c^2$$
$$\Gamma_\phi = 6 \pm 3 \text{ MeV}/c^2$$

Gamma energy : $4.4 < k < 6.0$ GeV

Invariant pair mass	Unweighted cross sections of the elements	$\frac{d^2\sigma}{d\Omega dm} = \frac{1}{A} \frac{\text{events}}{\text{acceptance}}$ in $\left[\frac{\mu b}{\text{sr MeV}/c^2 \text{ Nucleon}}\right]$				
m_{KK}	Be	C	Al	Cu	Ag	Pb
1003.5	1.46 ±1.05	.31 ± .18				
1006.5	.27 ± .27	.54 ± .17	.74 ± .71	.54 ± .54	.69 ± .69	.19 ± .19
1009.5	.71 ± .61	1.06 ± .13	.56 ± .56	1.29 ± .49	.91 ± .59	.81 ± .44
1012.5	1.47 ± .40	1.92 ± .12	3.16 ± .51	2.98 ± .48	3.26 ± .55	1.31 ± .35
1015.5	3.05 ± .38	4.06 ± .15	5.38 ± .58	6.77 ± .64	7.30 ± .67	4.63 ± .48
1018.5	4.00 ± .47	5.28 ± .19	6.77 ± .62	8.78 ± .68	6.72 ± .68	4.85 ± .48
1021.5	4.08 ± .54	5.19 ± .20	6.58 ± .68	7.68 ± .67	8.16 ± .78	4.62 ± .52
1024.5	2.64 ± .35	3.31 ± .12	4.99 ± .49	6.29 ± .54	5.47 ± .53	3.72 ± .38
1027.5	1.29 ± .28	1.88 ± .09	2.55 ± .37	3.26 ± .39	3.21 ± .43	2.84 ± .34
1030.5	.85 ± .19	1.18 ± .07	1.50 ± .27	1.83 ± .28	2.34 ± .34	1.39 ± .23
1033.5	.66 ± .23	.95 ± .07	1.16 ± .30	1.31 ± .30	.93 ± .30	1.46 ± .28
1036.5	.47 ± .28	.64 ± .64	.80 ± .32	1.08 ± .86	.78 ± .33	.90 ± .27
1039.5	.41 ± .23	.43 ± .06	.67 ± .30	.58 ± .27	.99 ± .36	1.07 ±1.07
1042.5	.51 ± .24	.48 ± .19	1.03 ± .35	.62 ± .62	.68 ± .32	.57 ± .57
1045.5	.50 ± .25	.34 ± .34	.70 ± .40	.50 ± .50	.27 ± .27	.87 ± .80
1048.5		.34 ± .26		1.08 ±1.08		.79 ± .36
1051.5		.27 ± .27		.0		.18 ± .18
1054.5		.36 ± .18		.38 ± .38		.20 ± .20
1057.5		.24 ± .12		.25 ± .25		.28 ± .20
1060.5		.26 ± .15		.74 ± .52		.0
1063.5		.26 ± .15		.36 ± .36		.59 ± .34
1066.5		.17 ± .10		.74 ± .43		.26 ± .19
1069.5		.37 ± .18		.0		.62 ± .36
1072.5		.27 ± .20		.58 ± .58		.31 ± .30
1075.5		.09 ± .09		.0		.0
1078.5		.32 ± .23		.68 ± .68		.0
108[illegible].5		.12 ± .12		.54 ± .54		.29 ± .29
1084.5		.0				1.10 ±1.10
1087.5		.69 ± .69				

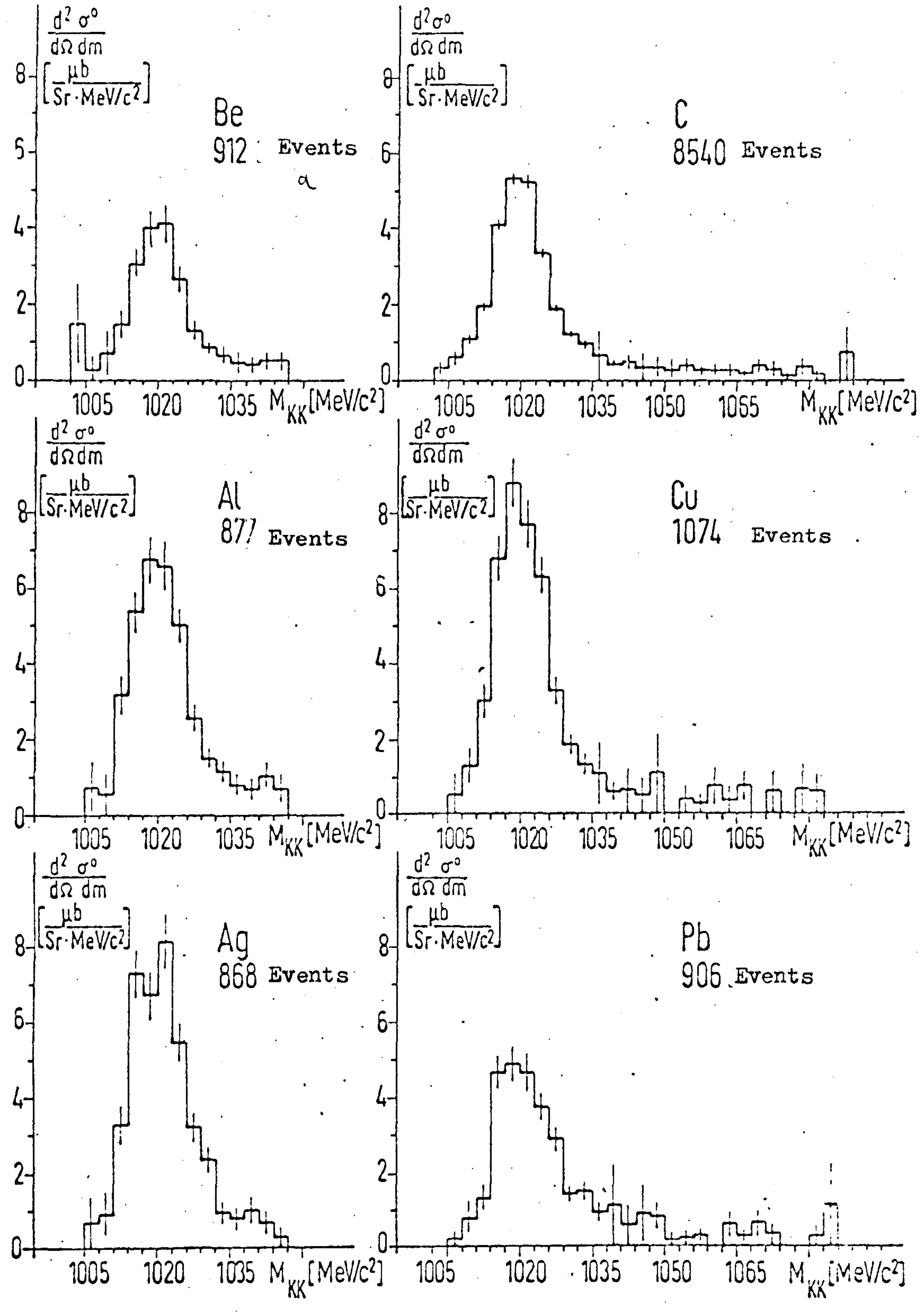

Figure 18. Differential cross section for the photoproduction of charged K-pairs as a function of the invariant pair mass.

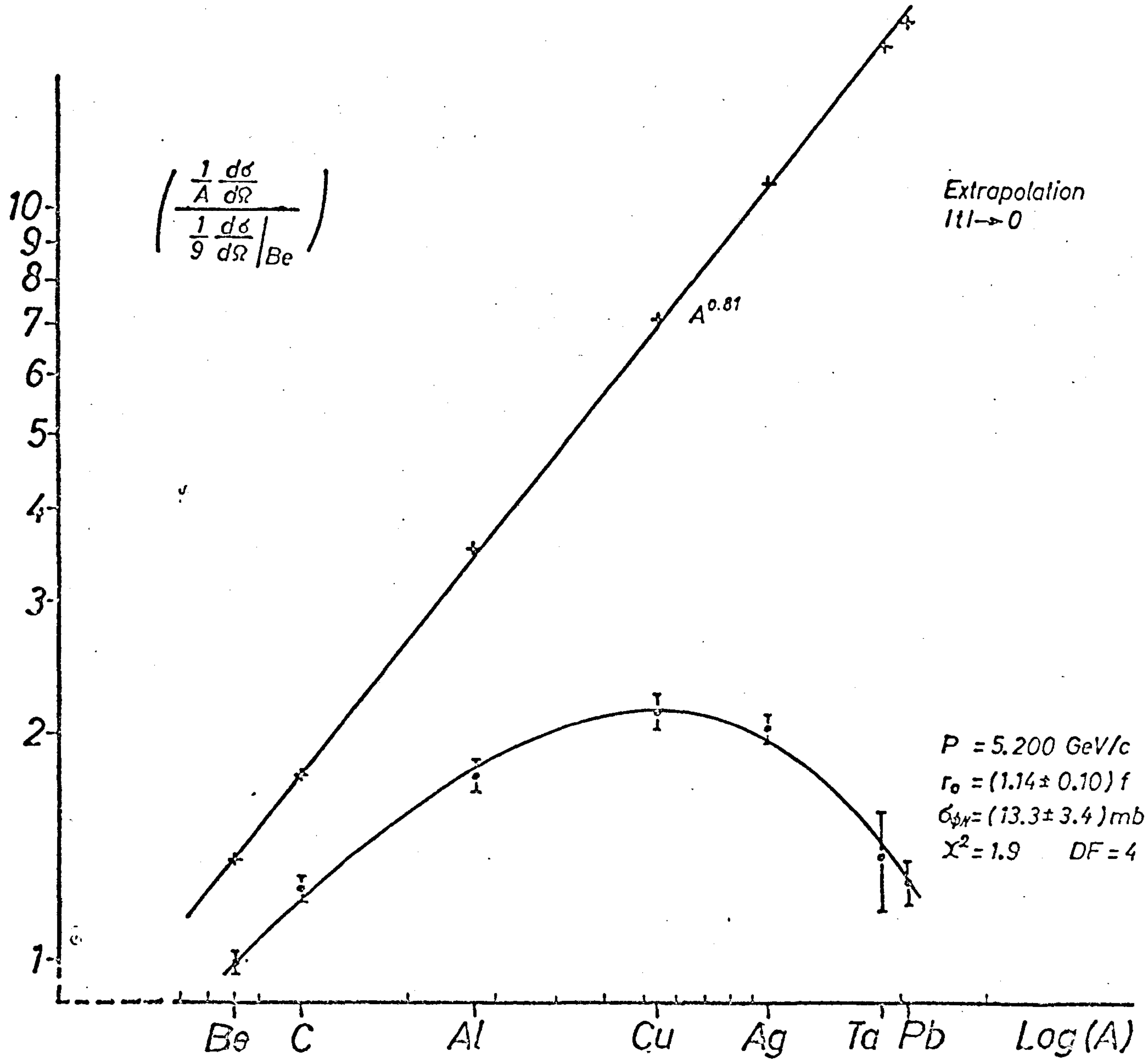

Abb. 19 Relative A-Abhängigkeit der ϕ-Photoproduktion

Figure 19. Relative A-dependence of ϕ photoproduction

7.3 Dependence of the cross section

a) On the target nucleus A

The differential cross sections $\frac{1}{A}\frac{d\sigma}{d\Omega}$ for ϕ-photoproduction at different elements A was determined in the following way: the events were divided by the branching ratio 0.48 and the acceptances weighted with the decay angle distribution, eq. (3.1). The result is the effective cross sections $\frac{1}{A}\frac{d^2\sigma}{d\Omega dm}$ which are similar to those in Figure 18 except for the weighting factor ($3/2 \sin^2 \theta_k^* \simeq 1.37$) and the branching ratio 0.48.

After subtraction of a constant background the values from the mass interval $\lfloor 1002\text{-}1038\ \mathrm{MeV}/c^2 \rfloor$ are added. The statistical errors given are produced by the events, by Monte-Carlo events and the zero-target rate.

As in ρ^o production the systematic error is 6.5% with an additional uncertainty of half the magnitude of the total background U and 6% from the branching ratio. The differential cross sections and their quotient are given in Table 7.3. t_c is the mean energy transfer for the measurement on carbon.

Table 7.3

Kinematic Conditions		Element		$\frac{1}{A}\frac{d\sigma}{d\Omega}\left[\frac{\mu b}{sr.nucl.}\right]$	U	$\left(\frac{1}{A}\frac{d\sigma}{d\Omega}\right)/\left(\frac{1}{9}\frac{d\sigma}{d\Omega}\right)_{Be}$
p	5.2 GeV/c	Be	9.01	88 ± 5	13	1.00 ± 0.06
$\lvert t_c \rvert$	= 0.113 GeV^2/c^2	C	12.01	109 ± 4	14	1.24 ± 0.04
k	= 6.2 GeV	Al	26.98	155 ± 6	16	1.77 ± 0.07
p_o	= 2600 MeV/c	Cu	63.54	189 ± 8	15	2.15 ± 0.10
θ_o	= 2.8^o	Ag	107.88	178 ± 8	15	2.03 ± 0.10
		Ta	180.9	120 ± 4	17	1.36 ± 0.20
		Pb	207.2	112 ± 6	18	1.27 ± 0.07

Figure 19 shows the values normalized to beryllium. The strong increase in the relative cross section per nucleon for small atomic numbers A again manifests the coherence of the production process. The measurements were carried out at constant momentum transfer close to t_{min}. As the nuclear radius increased the phase differences for the diffraction-dissociation process in different zones of the nucleus became noticeable and led to destructive interference (see eq. 1.9) which causes the fall-off at large A.

The curve drawn in is the best fit for the function $F_{TA}(R, \langle t\rangle, \sigma_{\phi N})$ of the diffraction dissociation model to the data. The total ϕ nucleon cross section $\sigma_{\phi N}$ and the nucleon radius r_o were varied as parameters. If the simple dissociation model describes ϕ-photoproduction one obtains as best values

$$\sigma_{\phi N} = (13.3 \pm 3.4)\,mb \quad r_o = (1.14 \pm 0.10)\,f.$$

The extrapolation to $t \longrightarrow 0$ is also drawn in. One can infer from it that at very high energies the production rate at a nucleus is proportional to $A^{1.81}$.

b) <u>On the momentum transfer</u>

Using the same data the dependence of the cross section on the invariant momentum transfer $t = (k - p_{\phi})^2$ was analysed for events in the mass interval $1017 < m < 1020$ MeV/c^2. In order to exclude the effects of the mass distribution the events in each hodoscope combination were divided by the value $2m.R(m)$ for this combination. This factor gives the probability for the occurrence of the mass m. Using a mean mass $m_o = 1018.6$ MeV/c^2 and a width $\Gamma_o = 3.6$ MeV/c^2 from the table of A.H. Rosenfeld[11] $2m.R(m)$ was calculated for each K^+K^- pair in the Monte-Carlo program before multiple scattering and decay falsify the value of the mass m, and the mean value in the counter combination was finally determined.

The decay angle distribution of K mesons in the center-of-mass system of the ϕ is again assumed to be $W(\theta_K^*) = \frac{3}{8\pi} \sin^2 \theta_K^*$.

The behavior of the differential cross section as a function of t is shown in Figure 20 for the elements carbon and lead. The steeper slope in the larger target nuclei shows unambiguously the diffractive nature of the production. The approximation $\frac{d\sigma}{d|t|} \sim e^{a(A)t}$ was fitted to the measured data points before the first diffraction minimum $(J_1 = 0)$.

It yielded the values

$$a(C) = (38 \pm 13)\ (GeV/c)^{-2}$$
$$a(Pb) = (365 \pm 80)\ (GeV/c)^{-2}$$

This exponential fall-off agrees well with the effective behavior of the function $f_T(1.14 \cdot A^{1/3}, t, 13.3 \text{ mb})$. Because the measured t interval was so small one cannot expect a more exact determination of the parameters r_o and $\sigma_{\phi N}$.

c) <u>On the momentum p</u>

The momentum dependence should be the same for all elements; however, the absolute variation of the function f_T is smaller for lower values of A and so, therefore, is the systematic error. For this reason the events for production in carbon in the mass interval $1017 < m < 1020\ MeV/c^2$, which were measured with good statistics, were analysed. Figure 21 shows the differential cross section $d\sigma/d\Omega$ from which all functional dependence on the variables p, m, t, θ^*_K have been divided out. The remaining value is according to eq. (6.3) the normalization constant for carbon:

$$C(C) = (4.35 \pm 0.38)\ \mu b/(sr \cdot GeV^2/c^2 \cdot Nucleon)$$

The behavior of the data points in Figure 21 confirms the momentum dependence f(p) corresponding to the diffraction model.

d) <u>On the helicity angle θ^*_K</u>

θ^*_K is defined as the angle made by the emergent K^+ meson with the direction of the ϕ meson in the rest system of the ϕ. The measurements in carbon were used to test the decay angle distribution. The mass distribution 2m.R(m), the momentum dependence f(p) and the function f_T were used in the Monte-Carlo program to weight the simulated ϕ mesons, on the other hand an isotropic decay angle distribution was inserted.

The values of the cross section so weighted are

$$\frac{1}{f(p) \cdot f_T(R,t,13.3mb) \cdot 2m\ R(m)} \frac{d\sigma'}{d\Omega} = C(c) \cdot 4\pi \cdot W(\theta^*_K)$$

as shown in Figure 22. An isotropic angular distribution can be excluded; on the other hand the points are consistent with the distribution already assumed

$$W\ (\theta^*_K) = \frac{3}{8\pi} \sin^2\theta^*_K$$

$\frac{d\sigma'}{d\Omega}$ would be the cross section for unpolarized ϕ mesons. The curve drawn in represents $C(C) \cdot 4\pi \cdot W(\theta^*_K)$

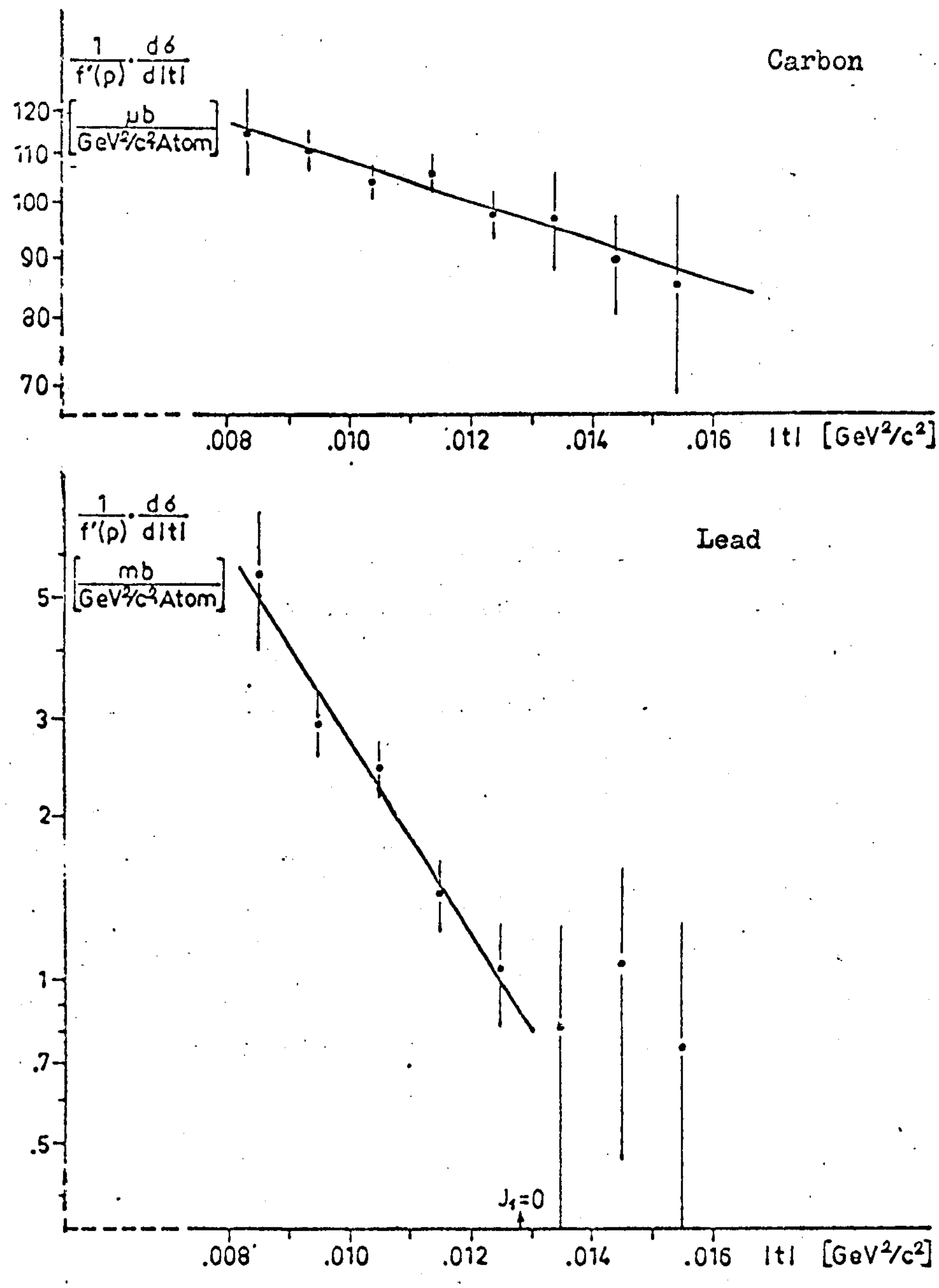

Figure 20. Cross section for o production as a function of momentum transfer t

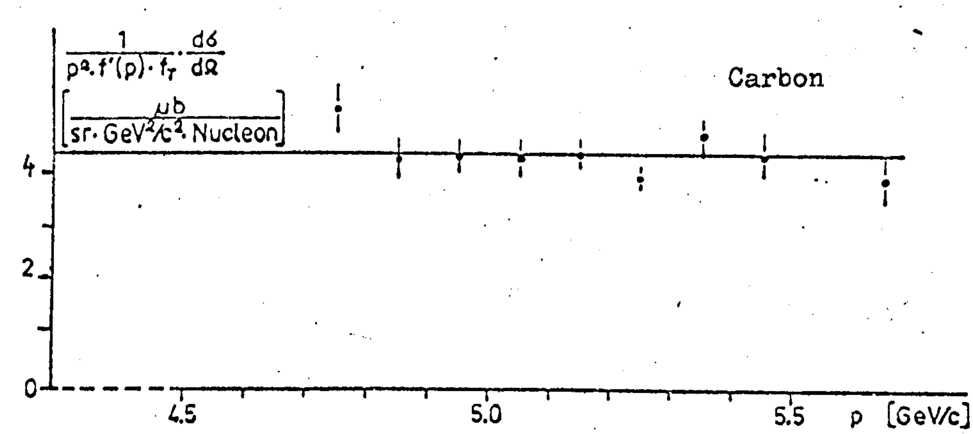

Figure 21. Verification of the momentum dependence

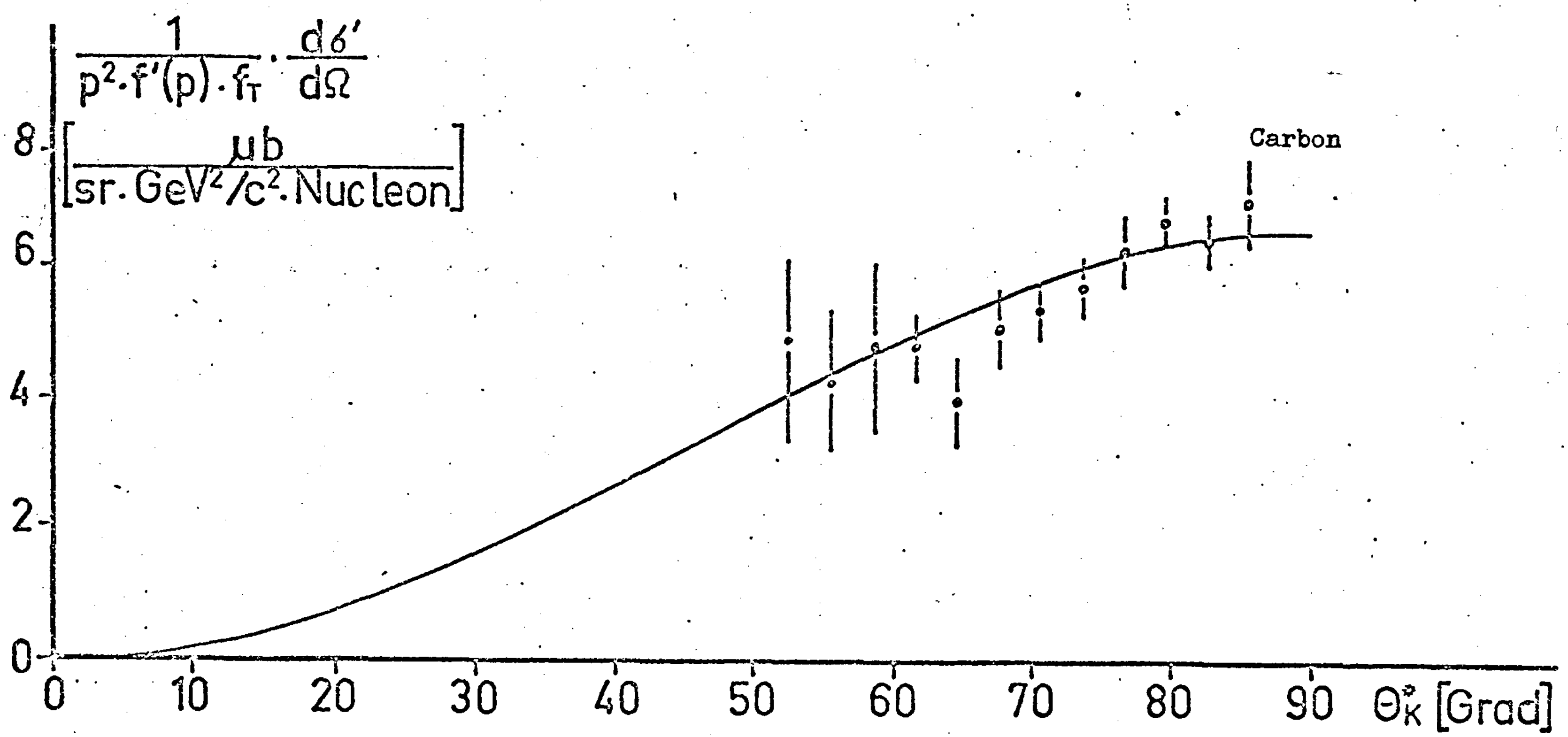

Abb.22 Abhängigkeit des Wirkungsquerschnittes vom Helizitätswinkel

Figure 22. Dependence of the cross section on the helicity angle

8. DISCUSSION OF RESULTS

8.1 Comparison of models for the production mechanism

Of the models introduced in Section 2 the one pion exchange model can be excluded, since the $\sim 1/p^2$ behavior of the differential cross section which it requires contradicts the observed $\sim p^2$ behavior and the coherent production at nuclei A cannot be explained.

The diffraction model of S.M. Berman and S.D.Drell[22] implies the multiperipheral model and was therefore only calculated for hydrogen. The inference by analogy from ρ^o photoproduction to diffraction scattering of π mesons gives a usable prediction for the momentum dependence: $f(p) = p^2 f'(p)$. It was assumed that it is applicable to all nuclei A.

In the diffraction-dissociation model[13] the γ quantum first comes into interaction with the nucleus A via the dissociation state of a vector meson; the model is therefore contained in the vector dominance model and is valid for ρ^o and ϕ mesons.

Together with a simple model of diffraction scattering in complex nuclei one obtains a consistent description of the cross section in all its variables which agrees very well with the experiments carried out.

Using the corresponding parameters from the previous section it is possible to represent all measurements by the following formula: $V = (\rho, \phi)$

$$\frac{d^2\sigma}{d\Omega dm} = C(A)\cdot p^2 f'(p)\cdot f_T(R,t,\sigma_{VN})\ 2m\cdot R(m)$$

Because of the assumptions of the model it is only valid for production in the forward direction and with very small momentum transfers.

8.2 Mass and width of the ρ^o meson

In the diffraction dissociation model of M. Ross and L. Stodolsky[13], the coupling of the γ quantum to the dissocation state of a ρ^o yields a factor $(m_o/m)^4$ which deforms the mass distribution given by J.D.Jackson[38]. Figure 23 shows the mass spectrum for production in carbon from Figure 17c. The values at higher mass are included, multiplied by 10, as measured with a configuration $\theta_o = 11.1^o$, $p_o = 2500$ MeV/c with 50,000 events.

The full curve a) represents the best fit of the function

$$C_1(A)\cdot 2m\cdot R(m) + C_2\cdot B(m)$$

with $m_o = 765$ MeV/c^2 and $\Gamma_o = 130$ MeV/c^2 to the measured data in the interval $400 < m < 940$ MeV/c^2, while the dashed curve b) represents the best fit to the mass distribution without the factor $(m_o/m)^4$ in $R(m)$. This yields $m_o = 737$ MeV/c^2 and $\Gamma_o = 104$ MeV/c^2. The extrapolation of the two fits in the region of high masses shows clearly that only solution a), which includes the factor $(m_o/m)^4$, is consistent with the data.

The interference mechanism proposed by P.Söding[12] yields another explanation for the deformation of the mass spectrum. P. Söding assumes that there is a background of nonresonantly produced pion pairs in the L=1 state in addition to the decay pions from the ρ^o meson. The interference of this amplitude with the imaginary part of the ρ^o-production amplitude leads to a component in the calculated differential cross section $d\sigma/dm_{\pi\pi}$ which varies rapidly near the resonance mass and deforms the mass distribution. The measurements made with the bubble chamber[52] can be described well by this mechanism with an assumption about the relative phase of the amplitudes and a suitable background.

One expects as a consequence of the interference a weaker fall-off in the cross section $d\sigma/d|t|$ as a function of t as the mass of the 2π system increases. Figure 24 shows a comparison for two mass regions.

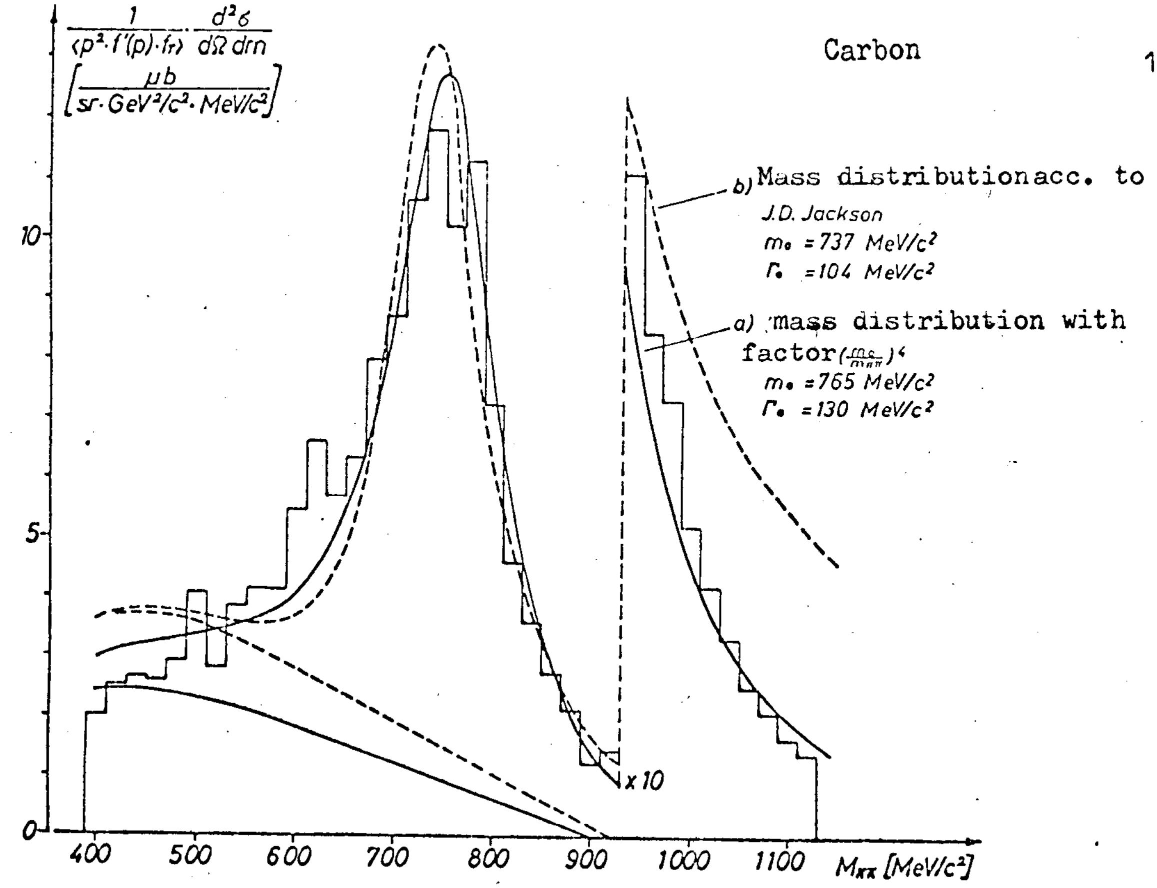

Figure 23. Comparison of the two mass distributions in the region of high pair masses

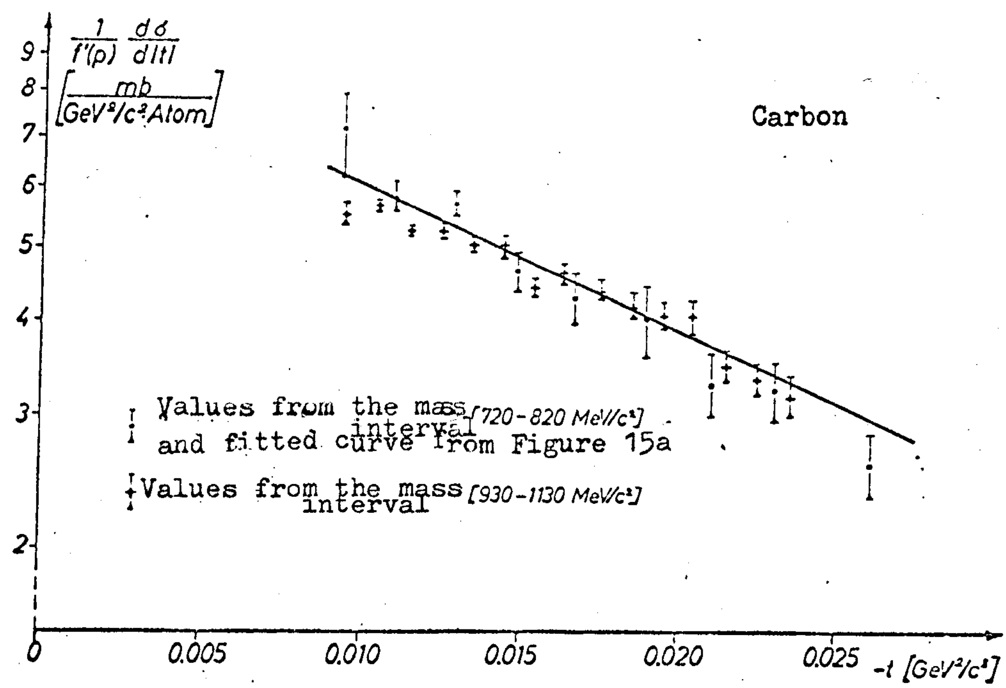

Figure 24. Comparison of the dependence on momentum transfer for events near to the ρ^0 mass and an interval of higher masses

The values were obtained by means of the relation

$$\frac{d\sigma}{d|t|} = \frac{1}{2m \cdot R(m)} \frac{d^2\sigma}{d|t|dm}$$

The relative behavior of the data points shows no significant difference for the two different mass intervals. It cannot therefore be assumed that this mechanism can explain the observed deformation of the mass spectra for production in heavy target nuclei with very small momentum transfers.

The behavior shows rather that the $\pi^+\pi^-$ spectrum is dominated by the decay of diffractively produced ρ^0 mesons even at mass values up to 1130 MeV/c^2 and this justifies the factor $(m_o/m)^4$.

The fitting of the mass distribution (a) to the measured values in lead yielded:

$$m_o = 765 \pm 5 \text{ MeV}/c^2$$
$$\Gamma_o = 130 \pm 5 \text{ MeV}/c^2.$$

With 25 degrees of freedom a value $\chi^2 = 22$ was obtained corresponding to a confidence limit for hypothesis (a) of CL = 50%, while hypothesis (b) (without $(m_o/m)^4$) only reached $\chi^2 = 36$ i.e. CL = 12%.

The quantities m_o, Γ_o are in good agreement with the values obtained by M. Roos[48] when analysing the reaction: $\pi^- + p \rightarrow \rho^0 + n$

On the other hand earlier photoproduction experiments gave $m_o' = 750$ MeV/c^2 and $\Gamma_o = 150$ MeV/c^2. Since partly different mass distributions were fitted, these mass values are not directly comparable.

7.3 Total absorption cross sections

Using sum rules which follow from the quark model, the following total absorption cross sections can be predicted :[47]

$$\sigma_{\rho p} = \sigma_{\omega p} = \frac{1}{2}(\sigma_{\pi^- p} + \sigma_{\pi^+ p})$$

$$\sigma_{\phi p} = 2 \cdot \sigma_{K^+ p} + \sigma_{\pi^- p} - 2 \cdot \sigma_{\pi^+ p}$$

The ρ^o production was investigated for momenta $2.7 < p < 5.1$ GeV/c, the ϕ-production for $4.4 < p < 6.2$ GeV/c. The cross sections $\sigma_{\pi^- p}$, $\sigma_{\pi^+ p}$ obtained in these intervals are taken from ref. 26 and $\sigma_{K^+ p}$ is taken from ref. 46, and they yield:

$$\sigma_{\rho p} = \frac{1}{2}(31.8 + 29.4) \text{ mb} \approx 30.6 \text{ mb}$$

$$\sigma_{\phi p} = (2 \cdot 18.0 + 28.8 - 2 \cdot 27.0) \text{ mb} \approx 10. \text{ mb}$$

There is good agreement with the values obtained from the A-dependence:

$$\sigma_{\rho N} = 31.3 \pm 2.3 \text{ mb}$$

$$\sigma_{\phi N} = 13.3 \pm 3.4 \text{ mb}$$

7.4 Coupling constants

In the vector dominance model the electro-magnetic current of hadrons is coupled with the vector meson field by means of the coupling constants γ_v($v = \rho, \omega, \phi$). There are various possibilities for obtaining these constants:

a) If the form factor $F(k^2)$ of the π-meson is calculated according to the graph:

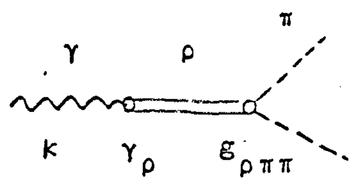

one obtains

$$F(k^2) = \frac{g_{\rho\pi\pi}}{2\gamma_\rho} \frac{m_\rho^2}{m_0^2 - k^2}$$

With the normalization condition $F(0) = 1$ there follows $g_{\rho\pi\pi} = 2\gamma_\rho$ where $g_{\rho\pi\pi}$ can be calculated from the mass $m_0 = 765$ MeV/c^2 and width $\Gamma_0 = 130$ MeV/c^2 of the ρ^0-meson:

$$\Gamma_0 = \frac{m_0}{12} \frac{g_{\rho\pi\pi}^2}{4\pi} \left(1 - \frac{4m_\pi^2}{m_0^2}\right) 3/2$$

The result is

$$\left(\frac{\gamma_\rho^2}{4\pi}\right) = 0.62 \; .$$

b) The best determination to date is obtained from the measurement of the leptonic decays of vector mesons[20]. From the branching ratio of the decay

$$BR = \frac{\Gamma(\rho^0 \to e^+ + e^-)}{(\rho^0 \to \text{alle})} = (6.5 \pm 1.4) \cdot 10^{-5}$$

one obtains[44]

$$\left(\frac{\gamma_\rho^2}{4\pi}\right) = \frac{\alpha^2}{12}\ \frac{m_o}{BR \cdot \Gamma(\rho^o \to all\ )} = 0.40 \pm {0.11 \atop 0.07}$$

A simple method of measuring the couplings consists in investigating directly the reactions

$$\begin{aligned} e^+ + e^- &\to \rho^o \\ &\to \omega \\ &\to \phi \end{aligned}$$

Because of the center-of-mass energy which is available these investigations can only be carried out at the moment with storage rings. The ρ^o production was measured on the storage rings at Novosibirsk[50] and Orsay[49] J.E. Augustin et al.[49] find, in good agreement:

$$\left(\frac{\gamma_\rho^2}{4\pi}\right) = 0.48 \pm {0.9 \atop 0.8}$$

c) A further possibility of determining the coupling constants is given by eq. (1.7)

$$\frac{d\sigma}{d\Omega}(\gamma+A \to \rho^o+A)\Big|^{\delta=0^o} = g_{\gamma\rho}{}^2\left(\frac{k}{4\pi}\right)^2\sigma_T{}^2(\ \rho^o+A\ )$$

from the work of M. Ross and L. Stodolsky[13]. This relation takes no account, compared with formula (6.3), of the dependence on the momentum transfer t_{min}, which differs according to momentum even at $\delta = 0^o$. It is therefore necessary to insert the cross section at $\delta = 0^o$ and $t = 0$; this requirement is automatically satisfied in the scattering of stable particles.

The values of $d\sigma/d\Omega$ measured at a known mean momentum transfer are extrapolated, to $t = 0$ for this purpose using the function $f_T(R, \langle t \rangle, \sigma_{VN})$, (see Figures 14b and 18), so that with $g^2_{\gamma V} = \frac{\alpha . \pi}{\gamma^2_V}$

$$\frac{\gamma_V^2}{4\pi} = \frac{\alpha}{4} \cdot \left(\frac{k}{4\pi}\right)^2 \cdot \frac{\sigma_T^2(V+A)}{\left.\frac{d\sigma}{d\Omega}\right|_{t=0}}$$

The total cross section σ_T of ρ, ϕ mesons on target nuclei A is calculated on the assumption of a homogeneous nucleon density from eq. (1.8) :

$$\sigma_T(R) = 4\pi \left\{ \frac{R^2}{2} + e^{-\sigma_{VN}\rho \cdot R} \left(\frac{R}{\sigma_{VN}\rho} + \frac{1}{(\sigma_{VN} \cdot \rho)^2} \right) - \frac{1}{(\sigma_{VN} \cdot \rho)^2} \right\}$$

The cross section for a single nucleon is already known here:

$$\begin{aligned} \sigma_{\rho N} &= 31.3 \text{ mb} \quad \text{for } \rho^o\text{-Mesons} \\ \sigma_{\phi N} &= 13.3 \text{ mb} \quad \text{for } \phi\text{ -Mesons} \end{aligned}$$

For momenta of 4.5 GeV/c one obtains from the ρ^o measurements:

Nucleus	C	Cu	Pb	
σ_T	0.26	1.11	2.90	barn
$\frac{\gamma_\rho^2}{4\pi}$	0.49 ± 0.12	0.42 ± 0.10	0.40 ± 0.10	

The error consists of the individual contributions from the uncertainty in $\sigma_{\rho N}$, r_o and $d\sigma/d\Omega$. These are treated as being uncorrelated.

On the assumption that these considerations apply in an analogous manner to the ϕ-meson, one obtains:

Nucleus	C	Cu	Pb	
σ_T	0.13	0.60	1.70	barn
$\frac{\gamma_\phi^2}{4\pi}$	7.7 ± 2.5	7.8 ± 2.8	7.8 ± 3.3	

This method of determination is not as dependent on the model as at first appears, since both $\sigma_T(R)$ and $\left.\frac{d\sigma}{d\Omega}\right|_{t=0} \sim \left| g_T(R,0,\sigma_{VN})\right|^2$ come from the same model. In the limiting case of small momentum transfers the model dependent terms vanish from the quotient

$$\lim_{t\to 0} k^2 \frac{\sigma_T^2(R)}{\left|g_T(R,0,\sigma_{VN})\right|^2} = \text{constant}$$

The coupling constants for production at three elements in each case are given as evidence of this.

The three models a), b), c) yield the same coupling constants, within the limits of error, for the ρ^o meson and thus yield a good confirmation of the vector dominance model.

Directly compared values for the coupling constant γ_ϕ do not yet exist, but may be expected soon from a measurement[51] of the leptonic decay $\phi \longrightarrow e^+ + e^-$.

According to investigations by H. Harari[54] there is at the moment no satisfactory explanation of the relative size of the measured cross section for ρ^o, ω and ϕ photoproduction. The relationship between the coupling constants is given in $SU(6)_W$ with a $\omega - \phi$ mixing angle of $\Theta = \text{arc sin } (\sqrt{1/3})$ by :

$$\frac{1}{\gamma_\rho^2} : \frac{1}{\gamma_\omega^2} \quad \frac{1}{\gamma_\phi^2} = 9 : 1 : 2$$

Compared with this prediction we find a relatively much weaker ϕ-coupling. Both spark chamber[57] and bubble-chamber[53] exhibit a strong suppression of ϕ-production.

R e f e r e n c e s

1) H. Yukawa; Proc.Phys.-Math.Soc.Japan 17, 43 (1935)

2) Lattes, Occhialini, Powell; Nature 160, 453 (1947)

3) R. Hofstadter; Revs.M.Phys. 28, 214 (1956)

4) R.G. Sachs; P.R. 87, 1101 (1952)

5) W.G.Holladay, R.G.Sachs; P.R. 98, 1155 (1955)
W.G.Holladay; P.R.101, 1198 (1956)

6) R.W.Frazer, J.R.Fulco; P.R.L.2, 365 (1959)

7) J.Bowcock, W.N.Nottingham, D.Lurie; N.C. 16, 918 (1960)

8) I.Derado; N.C. 15, 853 (1960)

9) J.J.Sakurai; Ann.Phys.(N.Y.) 2,1 (1960)
M.Gell-Mann; P.R.125, 1067 (1962)
M.Gell-Mann, D.Sharp, W.G.Wagner; P.R.L.8, 261 (1962)

10) H.Joos; P.L. 24, R 103 (1967) und Acta Physica Austriaca/Suppl.IV(1967)
N.W.Kroll, T.D.Lee, B.Zumino; P.R.157, 1376 (1967)

11) A.H.Rosenfeld et al.; Rev.Mod.Phys. (Jan. 67)

12) P.Söding; Phys.Let. 19, 702 (1965)

13) M.Ross and L.Stodolsky; Phys.Rev. 149, 1172 (1966)
L.Stodolsky; Brookhaven National Laboratory Report, BNL 11373 (1967)

14) Cambridge Bubble chamber group; P.R.146, B 4, 994 (1966)

15) L.J.Lanzerotti, R.B.Blumenthal, D.C.Ehn, W.L.Faissler, P.M.Joseph, F.M.Pipkin, J.K.Randolph, J.J.Russell, D.G.Stairs, J.Tenebaum; Phys.Rev.Letters 15, 210A (1965)

16) Aachen-Berlin-Bonn-Hamburg-Heidelberg-München Kollaboration; Nuovo Cimento 41, 270 (1966)

17) H.Blechschmidt,J.P.Dowd, B.Elsner,K.Heinloth,K.H. Höhne,S.Raither,J.Rathje D.Schmidt,J.H.Smith, J.H.Weber; Proc.of the Int.Symposium on Electron and Photon Interactions High Energies, 1965, p. 177

18) S.D.Drell and J.S.Trefil; Phys.Rev.Letters 16, 552 (1966) and ERRATUM

19) P.G.O. Freund; N.C. 44A, 411 (1966)
H.Harari; SLAC-PUB - 239 (1966)

20) J.G.Asbury,U.Becker, William K.Bertram,P.Joos, M.Rohde,A.J.S.Smith, C.L.Jordan and Samuel C.C. Ting P.R.L. 19,865 (1967)

21) H.Joos, G.Kramer; DESY 64/1 (1964)

22) S.M.Berman and S.D.Drell; Phys.Rev. 133, B 791 (1964)

23) D.Amati, S.Fubini, A.Stanghellini; N.C. 26, 896 (1962)

24) M.L.Good, W.D.Walker; P.R.120,1857 (1960)

25) J.D.Bjorken,S.D.Drell; Relativistische Quantenmechanik, (Relativistic Quantum Mechanics) 210

26) M.N.Foccacio, G.Giacomelli; CERN 66-18 (1966)

27) M.I.Longo, B.J.Moyer; P.R. 125, 701 (1962)

28) G.Belletini, G.Cocconi, A.N.Diddens, E.Lillethun, G.Matthiae,J.P.Scanlon, A.M.Wetherell; Nuc.Phys. 79, 609 (1966

29) For a definition of the terms : "Bit,Character,etc." cf . IBM-Handbook.

30) S.J.Lindenbaum; Proceed. of Dubna Conf. (1964)

31) R.Serber; Private Communication.

32) R.J.Oakes; N.C. 44A, 440 (1967)
Y.Eisenberg, E.E.Ronat,
A.Brandstetter, A.Levy,
E.Gotsman; P.L. 22, 217 and 223 (1966)
G. Kramer; DESY 67/32

33) J.G.Asbury, U.Becker, William K.Bertram, P.Joos, M.Rohde, A.J.S. Smith, S.Friedländer, C.L. Jordan, and Samuel C.C. Ting; P.R. 161, 1344 (1966)

34) R.R.Wilson; Nucl.Instr. 1, 101 (1957)

35) A.Ladage, H.Pingel; DESY 65/12 (1965) und A2/13 (1966)

36) M.Rohde; Dissertation Hamburg (1966)

37) H.W.Koch, J.W.Motz; Rev.of Mod.Phys. 31, 920 (1959)

38) J.D.Jackson N.C. 34, 1644 (1962)

39) M.L.Pearl, L.W.Jones, C.C.Ting; P.R. 132, 1252 (1963)

40) A.Citron, W.Gailbraith, T.F. Kycia, B.A.Leontić, R.H.Phillips, A.Rousset; P.R.L. 13, 205 (1964)

41) H. Fre se; Diploma Thesis

42) K.G.Steffen High Energy Beam Optics J.Wiley & Sons (1965)

43) E.Malamud; P.R. 115, 687 (1959)
J.K.Walker et al.; P.R. 114, 1126 (1966)

44) S.C.C. Ting; Stanford Conf. (1967)

45) U. Kötz; Dissertation Hamburg (1967)

46) R.L.Cool, G.Giacomelli, T.F.Kycia, B.A.Leontić, K.K. Li, A.Lundby, J.G.Teiger; Stony Brook Conf. (1965)

47) H. Joos; DESY 67/13 (1967)

48) M. Roos; CERN TH 798 (1967)

49) J.E.Augustin et al.; Orsay, Preprint (Sept.1967)

50) V.L.Auslander et al.; P.L. 25b, 433 (1967)

51) J.G.Asbury et al; The Experiment will be completed in the spring of 1968 at DESY.

52) H.Spitzer; Dissertation, Hamburg (1967) und DESY, internal report F1/4

53) Deutsche Blasenkammer-Kollaboration; DESY 66/32 see Table V

54) H.Harari; P.R.155,1565 and References cited therein.

55) H.Fleischer; Private Communication

56) S. Bose; P.R.L. 19, 1151 (1967)

57) K.H.Höhne; Dissertation Hamburg (1967)

The measurements described in the present work were carried out by Experimental Group F31 on the German electron-synchrotron, in collaboration with Columbia University, New York, and later with the Massachusetts Institute of Technology.

I wish to thank in particular Prof. P. Stähelin in suggesting this work, and for his kind support. My thanks are due also to Prof. W.Jentschke, who made these experiments possible, for his generous support. I am grateful to Prof.S.C.C. Ting for many valuable suggestions and for his tireless assistance in carrying out the experiments.

Thanks are due to Professors H. Joos and G. Weber for their keen interest. I also wish to express my gratitude to Doctors J.G. Asbury, P. Joos, W.K. Bertram, M. Binkley and A.J.S. Smith for numerous discussions and assistance in the program calculations, as well as to C.L. Jordan and Dr. M. Rohde for their help in preparing the work and for carrying out the measurements.

I am indebted to Dr. E. Lohrmann, Dr. L. Stodolsky and Prof. F. Pipkin for valuable suggestions.

I wish to thank Professors H. Joos and Dr. P. Schmüser for reading the manuscript.

My thanks are due to F. Akolk and H. Frese for setting up the data processing system, as well as to Dr. H.O. Wüster and Dr. L.Lublow for their help and for making available computing time on the IBM computers.

I should furthermore like to thank the synchrotron group for the smooth operation of the accelerator, and Miss I. Schulz for executing the drawings.

****

C u r r i c u l u m   v i t a e

I was born in Dortmund on December 17, 1938, son of Georg Becker, Head Clerk, and his wife Auguste, née Bühner.

From the fall of 1944 to Easter 1949 I attended the elementary school at Rauschenberg, with interruptions due to the war, and then until Easter 1952 the Marburg Modern High School. I then attended the Leibniz High School in Dortmund, from which I graduated at Easter 1958.

In the summer semester of 1958 I started my studies at Philipps University Marburg, passing my preliminary diploma examination on June 1, 1960. I continued my studies at Hamburg University.

In the winter term of 1961 I began work on my thesis at the Second Institute of Experimental Physics at Hamburg University, under the direction of Prof. P. Stähelin. The thesis was entitled "On the properties of spark chambers and high-voltage triggers", and I was awarded my diploma on March 2, 1964.

Since April 1, 1964 I have been doing postgraduate work on the German electron synchrotron in Hamburg-Bahrenfeld and have been working under Prof. P. Stähelin.

On April 29, 1966 I married Miss Gerda Barthel. Our daughter Katharina was born on March 3, 1967.

*****

TRANSLATION SUPPLIED BY

addis TRANSLATIONS International
Post Office Box 4097
Woodside, California 94062
Telephone: (415) 851-1040